1949

Functional renormalization group for ordinary and ghost O(N) models, with higher order gradient term

PhD thesis
Egyetemi doktori (PhD) értekezés

Zoltán Péli

Supervisor/Témavezető

Dr. Kornél Sailer

University of Debrecen
Natural Sciences and Informatics Doctoral Council
PhD School in Physics

Debreceni Egyetem
Természettudományi és Informatikai Doktori Tanács
Fizikai Tudományok Doktori Iskolája

Debrecen, 2018

Ezen értekezést a Debreceni Egyetem Természettudományi és Informatikai Doktori Tanács Fizikai Tudományok Doktori Iskolájának Részecskefizika programja keretében készítettem a Debreceni Egyetem természettudományi doktori (PhD) fokozatának elnyerése céljából. Nyilatkozom arról, hogy a tézisekben leírt eredmények nem képezik más PhD disszertáció részét.

Debrecen, 2018. október 19.

Péli Zoltán
doktorjelölt

Tanúsítom, hogy Péli Zoltán doktorjelölt 2015-2018 között a fent megnevezett Doktori Iskola Részecskefizika programjának keretében irányításommal végezte munkáját. Az értekezésben foglalt eredményekhez a jelölt önálló alkotó tevékenységével meghatározóan hozzájárult. Nyilatkozom továbbá arról, hogy a tézisekben leírt eredmények nem képezik más PhD disszertáció részét.
Az értekezés elfogadását javasolom.

Debrecen, 2018. október 19.

Dr. Sailer Kornél
témavezető

Functional renormalization group for ordinary and ghost O(N) models, with higher order gradient term

Értekezés a doktori (PhD) fokozat megszerzése érdekében
a fizika tudományágban

Írta: Péli Zoltán
okleveles fizikus

Készült a Debreceni Egyetem Fizikai Tudományok Doktori Iskolája
Részecskefizika programja keretében

Témavezető: Dr. Sailer Kornél

A doktori szigorlati bizottság:

elnök:	Dr. Schram Zsolt	.....
tagok:	Dr. Takács Gábor	.....
	Dr. Nándori István	.....

A doktori szigorlat időpontja: 2018. szeptember 21.

Az értekezés bírálói:

	Dr.	.....
	Dr.	.....

A bírálóbizottság:

elnök:	Dr.	.....
tagok:	Dr.	.....
	Dr.	.....
	Dr.	.....
	Dr.	.....

Az értekezés védésének időpontja: .....

Acknowledgements

I express my deepest gratitude to my supervisor, Kornél Sailer. His illuminating insights on physics and our fruitful discussions had a great effect on me, I would not be the young researcher I am today without him. His expert guidance has propelled me through the entire university, starting from my bachelor studies until the very end of my Ph.D.

I am also very grateful to Sándor Nagy for him readily offering and providing his experienced help.

For the last but not the least, my family, my beloved girlfriend and my friends deserve my hearty thanks for their unwavering support, care and love.

Contents

Acknowledgements **iii**

1 Background Theory **1**
1.1 Introduction . . . 1
1.2 The Renormalization Group . . . 3
1.3 Functional Renormalization Group methods . . . 4
1.3.1 Wegner and Houghton's ERGE . . . 4
1.3.2 Wetterich's ERGE . . . 6
1.4 Generic features of $O(N)$ symmetric models in FRG . . . 10

2 Critical exponents of the ordinary $O(N)$ models in the FRG approach **12**
2.1 Ansatz and derivation of the flow equations . . . 13
2.2 $O(1)$ model in continuous dimensions $2 < d < 4$ . . . 18
2.2.1 Evolution equations . . . 18
2.2.2 Crossover scaling . . . 20
2.2.3 Fixed points . . . 22
2.2.4 Numerical results . . . 23
2.3 $O(N)$ models for $N \geq 2$ and $d = 3$ . . . 28
2.3.1 Evolution equations . . . 28
2.3.2 Numerical results . . . 29
2.3.3 Asymptotic behavior for large N . . . 35

3 Phase structure of the $O(2)$ ghost model with higher-order gradient term **38**
3.1 Motivation . . . 38
3.2 Outline . . . 39
3.3 One component scalar field models . . . 41
3.3.1 Blocking transformation . . . 42
3.3.2 Polynomial potential . . . 43
3.3.3 Tree-level renormalization of the sine-Gordon model . . . 47
3.4 $O(2)$ ghost model in Case Y . . . 49
3.4.1 Application of the WH RG approach . . . 49
3.4.2 Phase structure and IR scaling laws . . . 52
3.5 $O(2)$ ghost model in Case $\tilde{Y}$ . . . 59
3.5.1 Phase diagram . . . 60
3.5.2 Phase I . . . 61
3.5.3 Phase II . . . 62

3.5.4 Phase III 64
3.5.5 On the phase transitions 66

4 Modified effective average action renormalization group method applied to the $O(1)$ ghost model with periodic condensate 69
4.1 Fourier-Wetterich renormalization group approach 71
4.1.1 Structure of the RG equation 71
4.1.2 Parameters of the periodic condensate 76
4.1.3 Strategy for solving the RG equations 76
4.2 Numerical results 77
4.2.1 On our numerical approach 77
4.2.2 The phase structure 79

5 Conclusions 83

6 Összefoglaló 87

Appendices 91

A Tree-level renormalization and the Wegner-Houghton equation 92
A.1 Tree-level renormalization of Euclidean one-component scalar field theory with polynomial potential 92
A.2 Wegner-Houghton equations for ϕ^4 models with $O(2)$ symmetry 93

B Fourier-Wetterich approach 96
B.1 Regulated full propagator 96
B.2 Traces contributing to the flow equations 98

Bibliography 99

Chapter 1

Background Theory

This chapter is dedicated to convey the ideas behind the functional renormalization group (FRG) in the Introduction and to sketch the specific methods I employed in my work in the following sections. More specifically, Wegner and Houghton's renormalization group equation and it's applicability and Wetterich's renormalization group equation along with the so called gradient expansion.

1.1 Introduction

In the current state of physics, the microscopic phenomena are well understood. The Standard Model of particle physics is a very successful theory, it describes the elementary particles and the basic interactions between them, except gravity. The symmetries present in the model enforce a beautiful simplicity in the equations. Thus, making it possible, to qualitatively and quantitatively understand many microscopic phenomena. The Standard Model along with the General Relativity are a triumph of our understanding of the laws of nature. Even though, there are a few insufficiencies, for example, the cause of neutrino masses, dark matter, dark energy and so on. In the everyday life, one may only observe electromagnetism and gravity. However, for many common observations, we have a long way to go in order to make predictions from our accessible microscopic laws of physics. Let us take the Navier - Stokes equation for example, the equation describing the flow of viscous fluids. It has not yet been proven, that three dimensional solutions always exist, in fact this is a Millennial Prize Problem. How could we derive this equation from our microscopic equations? In the macroscopic, we have powerful frameworks, such as thermodynamics and statistical physics to deal with many-body systems. This treatment makes prediction for stationary systems with large number of degrees of freedom neglecting irrelevant microscopic details. One has to bridge the gap between the known microscopic interactions and the macroscopic laws. The introduction of the article [6] summarized the main problems one has to face, when trying to formulate a method to change the scale from the simplicity of microphysics to the complexity of macrophysics: "For a thermodynamic equilibrium system of many identical microscopic degrees of

freedom, the origin of the problems on the way to complexity is threefold. First, there is often no small parameter which can be used for a systematic perturbative expansion. Second, the correlation length can be substantially larger than the characteristic distance between the microscopic objects. Collective effects become important. Finally, the relevant degrees of freedom which permit a simple formulation of the macroscopic laws may be different from the microscopic ones. A universal theoretical method for the transition from micro- to macrophysics should be able to cope with these generic features."

The scale transformations and the concept of scale invariance originates from the early days of physics. Scaling arguments were already present in the Pythagorean school and at Euclid. Scale invariance regained popularity in the 20th century. The renormalization group (RG) was first applied in particle physics. Today, its fields of applications include a wide variety of popular research areas. Originally, the goal was to treat infinities and obtain finite observables in quantum field theory. The problem of infinities was first addressed in quantum electrodynamics by Feynmann, Schwinger and Tomonaga. They were awarded the Nobel prize in 1965. They laid down the cornerstones of the perturbative renormalization.

A more refined understanding of the physical meaning of the renormalization process came from Leo P. Kadanoff. His paper [7] proposes the so-called "block-spin" renormalization group. The works of Kenneth Wilson complemented and completed this idea. The viability of Wilson's ideas for the renormalization group was demonstrated by the solution of the long-standing Kondo problem, [8]. He has also developed a method, called the ϵ-expansion in the theory of second-order phase transitions and critical phenomena [9]. He received the Nobel prize for these decisive contributions in 1982. In a microscopic, many-body system fluctuations are present. Quantum fluctuations for a quantum system and thermal fluctuations for a statistical system. Wilson said in his Nobel lecture, that: "The renormalization group approach is to integrate out the fluctuations in sequence, starting with fluctuations on an atomic scale and then moving to successively larger scales until fluctuations on all scales have been averaged out." To be exact, the renormalization group is a semi-group. The transformations can only be applied to map the Hamiltonian towards the low energy scales, since we lose microscopic information by integrating the fluctuations (however, their contributions are incorporated into the observables). In order to realize the renormalization process, one has to smoothly map the Hamiltonian H_Λ (defined in the microscopic, or high energy scale Λ), down to the macroscopic Hamiltonian H_0 (which is valid at low energy scales $k = 0$), through sufficiently small steps in the energy scale $\Lambda \to k' \to k'' \to ... \to 0$. This sequence of maps however has to leave the partition function

$$Z = \mathrm{Tr} e^{-\beta H} \tag{1.1}$$

invariant. This means, that one has to take couplings into account, which are irrelevant at the high energy scale. We may not know which degrees of freedom become relevant at lower energy scales. In the next section I am going to elaborate the idea behind the RG.

1.2 The Renormalization Group

In the field of continuous phase transitions, the success of the scaling theory in correctly predicting various critical exponent identities supported the claim, that close to the critical point, the correlation length ξ is the only important length scale and that the microscopic lengths are irrelevant. The critical behavior is governed by fluctuations, that are statistically self-similar up to the scale ξ, which diverges in the critical point, making the entire system self-similar. In fact, there are two relevant length scales of a strongly correlated system: the lattice spacing a and the correlation length ξ. In the language of particle physics, a means the typical energy scale of the underlying theory, while ξ corresponds to the Compton wavelength of the particle. When one is executing a series of RG transformations, it would be meaningless to compare, say, the correlation length at different RG steps in an extrinsic unit, like meters. It comes naturally to use the lattice spacing a as a unit of measurement. Therefore, one turns to dimensionless quantities such as $\tilde{\xi} = \xi/a$, and rescales all quantities in terms of the lattice spacing. The RG exploits the self-similarity property of continuous phase transitions. The RG flow takes place in the theory space, which is spanned by the couplings of the model. Each axis corresponds to different couplings and a given physical system corresponds to a point K here. During an RG flow - decreasing the scale k form Λ to 0 - the initial $K(\Lambda)$ point travels along a trajectory. The system is critical if the point $K(k)$ is on the (hyper)surface, where $\xi = \infty$. The different points on this hypersurface converge to a fixed point $K(k) = K(k')$ (with $k < k'$) and the system becomes completely self-similar. By linearizing the RG flow in the close vicinity of the fixed point, one can read the power law scaling of each coupling. Those scaling exponents then can be related to the critical exponents. A lot of different physical systems have identical critical exponents, which allows us to classify them into universality classes. No matter how different the microscopic theories are, they may result in the same long distance theory. This opens up the opportunity to examine simpler theories rather than more involved microscopical ones. In FRG, we derive beta functions, which describe the RG evolution of dimensionless couplings $\tilde{g}_i$ of the theory:

$$\dot{\tilde{g}}_i = \beta_{\tilde{g}_i}(\{\tilde{g}_i\}), \tag{1.2}$$

here the dot reflects the derivative with respect to the scale. When one is interested in the critical behaviour of the model, searches for fixed point solutions $\{\tilde{g}_i^*\}$ of $\beta_{\tilde{g}_i}(\{\tilde{g}_i\}) = 0$. The eigenvalues $\{\omega_i\}$ of the matrix

$$\mathcal{M}_{ij} = \left.\frac{\partial \beta_{\tilde{g}_i}}{\partial \tilde{g}_j}\right|_{\{\tilde{g}_i^*\}} \tag{1.3}$$

are the scaling exponents of the couplings near the critical point, in linear approximation of the equations. The matrix $\mathcal{M}_{ij}$ is called stability matrix.

1.3 Functional Renormalization Group methods

The FRG combines Wilson's RG with the functional methods of the quantum field theory. Actually, there are several formulations and they are called exact renormalization group equations (ERGE). Among them, one may find Wilson's ERGE, Polchinsky's ERGE, Wegner and Houghton's ERGE and Wetterich's ERGE, with no claim of being exhaustive. I'm going to talk about the latter two equations in this section.

1.3.1 Wegner and Houghton's ERGE

The paper proposing this equation is [10]. The derivation of the equation and some of the arguments made here are based on Sect. IIA of [11]. This is the simplest form of infinitesimal blocking-step RG equations. For the sake of simplicity, consider an Euclidean theory in d dimensions for a scalar field $\phi(x)$, governed by the action $S_B[\phi]$. An $O(d)$ invariant U.V. cut-off Λ is introduced in the momentum space by requiring $\tilde{\phi}_p = 0$ for $|p| > \Lambda$ to render the generating functional

$$e^{\frac{1}{\hbar}W[j]} = \int \mathcal{D}\phi \; e^{-\frac{1}{\hbar}S_B[\phi]+\frac{1}{\hbar}\phi\cdot j} \tag{1.4}$$

finite, we accommodated DeWitt's shorthand for the product of the field and current. Let us denote the moving U.V. cut-off by k. Its decreasing $k \to k - \Delta k$ results the blocking transformation of the action, which preserves (1.4). Δk serves as a new small parameter to suppress higher order loop contributions. Due to the presence of the source, this blocking introduces an explicit source dependence in the action

$$\int \mathcal{D}_k\phi \; e^{-\frac{1}{\hbar}S_k[\phi;j]+\frac{1}{\hbar}\phi\cdot j} = \int \mathcal{D}_{k-\Delta k}\phi \; e^{-\frac{1}{\hbar}S_{k-\Delta k}[\phi;j]+\frac{1}{\hbar}\phi\cdot j}, \tag{1.5}$$

where $\mathcal{D}_k\phi$ is the integration measure over the functional space $\mathcal{F}_k$, consisting of functions whose Fourier transform is non-vanishing for $|p| \leq k$. In order to avoid this complication, one usually assumes $j \in \mathcal{F}_{k-\Delta k}$. In this case, the blocking becomes a mapping $S_k[\phi] \to S_{k-\Delta k}[\phi]$ and it is enough to impose the invariance of the partition function

$$e^{-\frac{1}{\hbar}S_{k-\Delta k}[\phi]} = \int \mathcal{D}\zeta e^{-\frac{1}{\hbar}S_k[\phi+\zeta]} \tag{1.6}$$

where $\phi \in \mathcal{F}_{k-\Delta k}$ and $\zeta \in \mathcal{F}_k \backslash \mathcal{F}_{k-\Delta k}$. The evaluation of the path integral by means of the loop-expansion gives the functional RG equation,

$$S_{k-\Delta k}[\phi] = S_k[\phi+\zeta] + \frac{\hbar}{2}\mathrm{Tr}\ln\frac{\delta^2 S[\phi+\zeta']}{\delta\zeta'\delta\zeta'}\bigg|_{\zeta'=\zeta} + \mathcal{O}(\hbar^2), \tag{1.7}$$

with $\frac{\delta S[\phi+\zeta']}{\delta\zeta'}\Big|_{\zeta'=\zeta} = 0$, per definition of the loop expansion. It can be seen that (1.7) has two parts, a tree level one and the one which describes the one loop contributions ($\mathcal{O}(\hbar)$).

Let us consider a simple $\mathcal{Z}_2$ symmetric ansatz

$$S_k[\phi] = \int d^d x \Big(Z_k(\phi)(\partial_\mu \phi)^2 + U_k(\phi) \Big). \tag{1.8}$$

One cannot derive consistent flow equations for Z_k or any coupling corresponding to higher derivatives of the field variable in the WH scheme. Therefore we assume trivial wave-function renormalization, $Z_k = 1$. This is called the local potential approximation (LPA). Considering the simplest case for the background configuration $\phi = \Phi$ =const. with trivial saddle point $\zeta = 0$ and substituting (1.8) into (1.7) yields

$$U_{k-\Delta k}(\Phi) = U_k(\Phi) + \frac{\hbar}{2} \int_{k-\Delta k<|p|<k} \frac{d^d p}{(2\pi)^2} \ln\Big(p^2 + U''(\Phi) \Big) + \mathcal{O}((\hbar \Delta k)^2). \tag{1.9}$$

Each loop-integral is over the shell $k - \Delta k < |p| < k$ in momentum space. So long as the propagator is non-singular in the integration domain, the n-loop integrals will be proportional to the n-th power of the integration volume, giving a dimensionless small suppression parameter $\approx (\Delta k/k)^n$. The higher loop contributions are suppressed in the infinitesimal blocking step limit and the one-loop evolution equation turns out to be an exact functional equation. After the integration in (1.9) and taking the limit $\Delta k \to 0$, one finally acquires the flow equation for the local potential

$$\dot{U}_k(\Phi) = -k^d \frac{\hbar}{2} \frac{\Omega_d}{(2\pi)^d} \Big(k^2 + U_k''(\Phi) \Big), \tag{1.10}$$

where the dot means $k\partial_k$ and Ω_d is the d-dimensional solid angle. This is a difficult partial differential equation for U_k. This can be solved with shooting method in simpler scenarios. The most widely used tactic however, is to suppose a polynomial expansion for U_k. For example, considering

$$U_k(\Phi) = \sum_{n=1}^{M} \frac{g_{2n}}{(2n)!} \Phi^{2n} \tag{1.11}$$

with the order M for truncation. Setting $M = 2$ retains the well known ϕ^4 model, with g_2 being the running mass squared and g_4 the self-interaction coupling.

As I mentioned earlier, the Wegner-Houghton equation is restricted to the LPA. Generally, the dynamics of the field variable (and therefore information about the anomalous dimension) is taken into account by considering a field configuration, where the usual homogeneous background Φ is supplemented with an additional fluctuating field η_x with infinitesimal amplitude:

$$\phi_x = \Phi + \eta_x. \tag{1.12}$$

The equations then are expanded in powers of this fluctuating field. Naturally, the zeroth order provides the evolution equation for the local potential U_k. The second order should provide the evolution equation for the wave function renormalization Z_k. However, at $\mathcal{O}(\eta^2)$ level a new evolution equation appears for U_k, which is an obvious inconsistency.

Furthermore, for the evolution of Z_k, there is an additional problem. Either the left hand side shows up a restricted integration domain for η^2 and essentially cannot be matched to the right hand side or the radius of convergence of the gradient expansion is zero. These problems arise inherently from the integration method used to perform the momentum integrals. Namely, by the sharp, shell-by-shell integration. For further reading check [11].

It is possible for the expression $[k^2+U_k''(\zeta)]$ in the logarithms - which corresponds to the inverse propagator - to become zero at a certain scale k_s, because the matrix $\frac{\delta^2 S[\phi+\zeta]}{\delta\zeta\delta\zeta}\Big|_{\zeta=\zeta^*}$ develops zero eigenvalues. The quantity $[k^2+U_k''(\zeta)]$ is the curvature of the action at the scale k and corresponds to the restoring force against fluctuations. At this point, when the restoring force is zero, the system becomes unstable against infinitesimal fluctuations. This also means, that the mean-field approximation is no longer applicable. We have used the mean field approximation, when we set the field variable to be the homogeneous background Φ and when we assumed, that the saddle point is trivial. If the saddle point is non-trivial, then

$$S_{k-\Delta k}[\phi] = \min_{\zeta'} S_k[\phi+\zeta'] \neq S_k[\phi]. \tag{1.13}$$

This means a non-trivial RG flow for the tree level action. In general, the saddle points ζ' are difficult to find. In the case of the WH RGE, these saddle points can be considered simply as plane waves due to the simplification, that the shell-by-shell integration means. For plane waves, the tree-level WH equations takes the form

$$U_{k-\Delta k}(\Phi) = \min_{\rho_k}\left(\frac{1}{2}k^2\rho_k^2 + \frac{1}{\pi}\int_0^\pi dx U_k(\Phi+\rho_k\cos x)\right). \tag{1.14}$$

This is the blocking relation for the tree-level renormalization (TLR). I am going employ this method with some modifications in the third chapter of this work. The TLR procedure is discussed in more detail in Refs. [47, 48]

1.3.2 Wetterich's ERGE

This equation was introduced in [12]. Some arguments here are based on the second chapter of [13]. The original Wilson-Kadanoff's idea is to perform an averaging to map Hamiltonians onto other Hamiltonians at larger scales. Rather than computing this sequence of Hamiltonians, one can compute the Gibbs free energy $\Gamma[\varphi]$ of the high energy modes ($\tilde{\phi}_p$ with $|p| > k$), that have already been integrated out. The idea is to build a one parameter family of models, indexed by a scale k which fulfills the following two requirements. On one hand, when $k = \Lambda$, when no fluctuation has been integrated out, $\Gamma[\varphi]$ is equal to the microscopic/bare action:

$$\Gamma[\varphi]_{k=\Lambda} = S[\phi=\varphi]. \tag{1.15}$$

On the other hand, when $k = 0$, meaning that all fluctuations are integrated out, $\Gamma[\varphi]_{k=0}$ is the Gibbs free energy of the original model

$$\Gamma[\varphi]_{k=0} = \Gamma[\varphi]. \tag{1.16}$$

k plays the role of an infrared cut-off in the effective average action (EAA) method since Γ_k is the free energy of the rapid modes. The task is to build explicitly this one parameter family of Γ_k. The idea is to decouple the slow modes ($\tilde{\phi}_p$ with $|p| < k$) of the model in the partition function by giving them a large mass:

$$Z[j] = e^{W[j]} = \int \mathcal{D}\phi e^{-S[\phi]-\Delta S_k[\phi]+j\cdot\phi} \tag{1.17}$$

in deWitt's notation for the integration and setting $\hbar = 1$, with

$$\Delta S_k[\phi] = \frac{1}{2}\phi \cdot R_k \cdot \phi. \tag{1.18}$$

The function R_k - called the cutoff function - has to meet three requirements and apart from those, it is arbitrary. Firstly, in order to recover the original model, when all fluctuations are integrated out

$$R_{k=0} = 0 \tag{1.19}$$

has to hold. Secondly, when $k = \Lambda$,

$$R_{k=\Lambda} = \infty \tag{1.20}$$

will ensure that (1.15) holds as well. In practice it is done by setting $R_{k=\Lambda} \approx \Lambda^2$. Finally, the rapid modes (with $|p| > k$) must be almost unaffected by R_k. The Legendre transform of $W_k[j]$ ordinarily gives the effective action. However, the action that we started off with is really $S[\phi] + \frac{1}{2}\phi \cdot R_k \cdot \phi$ and so, to get the effective average action, we have to subtract this term from the Legendre transform:

$$\Gamma_k[\varphi] \stackrel{\text{def.}}{=} \left(-W[j] + j \cdot \varphi\right) - \frac{1}{2}\varphi \cdot R_k \cdot \varphi, \tag{1.21}$$

where φ is the average of the classical field

$$\varphi = \frac{\delta W[j]}{\delta j} = \langle\phi\rangle. \tag{1.22}$$

Taking the scale derivative of the EAA and conducting straightforward operations

$$\begin{aligned}
\frac{d\Gamma_k}{dk} &= -\frac{dW_k}{dk} - \frac{\delta W_k}{\delta j}\frac{dj}{dk} + \frac{dj}{dk}\cdot\varphi - \frac{1}{2}\varphi\cdot\frac{dR_k}{dk}\cdot\varphi \\
&= -\frac{dW_k}{dk} - \frac{1}{2}\varphi\cdot\frac{dR_k}{dk}\cdot\varphi \\
&= \frac{1}{2}\langle\phi\cdot\frac{dR_k}{dk}\cdot\phi\rangle - \frac{1}{2}\varphi\cdot\frac{dR_k}{dk}\cdot\varphi = \frac{1}{2}\frac{\delta^2 W_k}{\delta j\delta j}\cdot\frac{dR_k}{dk} - \frac{1}{2}\frac{\delta W_k}{\delta j}\cdot\frac{dR_k}{dk}\cdot\frac{\delta W_k}{\delta j} \\
&= \frac{1}{2}\mathrm{Tr}\left[\left(\frac{\delta j}{\delta\varphi}\right)^{-1}\cdot\frac{dR_k}{dk}\right] \\
&= \frac{1}{2}\mathrm{Tr}\left[\left(\frac{\delta^2\Gamma}{\delta\varphi\delta\varphi} + R_k\right)^{-1}\cdot\frac{dR_k}{dk}\right],
\end{aligned} \tag{1.23}$$

one arrives to Wetterich's ERGE

$$\frac{d\Gamma_k}{dk} = \frac{1}{2}\mathrm{Tr}\left[\left(\frac{\delta^2\Gamma}{\delta\varphi\delta\varphi} + R_k\right)^{-1}\cdot\frac{dR_k}{dk}\right]. \tag{1.24}$$

This ERGE has allowed to compute the anomalous dimension η in a reasonable way. It is easy to generalize this equation for multiple component fields, and to study the physics of the $O(N)$ models and many others, in all dimensions, including two. The scheme allows to retrieve very easily the one-loop results both in $4-\epsilon$ and $2+\epsilon$ dimensions and in the large N limit. This has convinced many physicists in the subject to work with this formalism.

It is worthwhile to mention here the gradient expansion. The functional methods yield exact equations, however, in order to acquire numerically computable equations, one has to truncate the functional space of the action/effective action. Γ_k can be expanded in the power series of $\nabla\varphi$ at $k > 0$. For slowly varying fields, it is expected to be well-behaved. Thus, this is a convenient way of imposing sensible truncations in the functional space of Γ_k. This is the basis of the gradient expansion that consists in proposing an ansatz for Γ_k, involving only a finite number of derivatives of the field. For example, for a $\mathcal{Z}_2$ symmetric scalar model:

$$\Gamma_k[\varphi] = \int d^dx\left(U_k(\varphi) + Z_k(\varphi)(\nabla\varphi)^2 + Y_k(\varphi)(\nabla\varphi)^4 + \mathcal{O}(\nabla^6)\right). \tag{1.25}$$

There is a simple terminology for the different orders of approximation, and I'm going to use that in the following chapters:

- $Z_k = 1$ and $Y_k = 0$, we have only a scale dependent local potential, it is called the local potential approximation (LPA),
- $Y_k = 0$ and Z_k is non-trivial, we call it next-to-leading order (NLO) approximation,
- Finally, $Y_k \neq 0$ and non-trivial, we call it next-to-next-to-leading order (NNLO) approximation.

There is one last distinction one can make. The φ-dependence of Z_k and Y_k may be neglected, this approximation is going to employed in Chapt. 2. Later this is referred to as uniform wave function renormalization.

Finally, it is in order here to elaborate the regulator functions, R_k. As it was mentioned earlier, the Wetterich ERGE in principle is independent of the choice of the regulator so long as it meets the three requirements. In order to extract tangible results, on has to truncate the exact functional equations for the RG flow. The truncation of the functional space introduces a regulator dependence to the method. This is realised in the numerical values of the universal quantities, such as the critical exponents. There are several types of the regulator functions. The stability of the universal quantities and optimisation of the RG scheme versus R_k are actively researched topics in FRG. This work is not about this type of examination, here only one kind of R_k is used, namely Litim's optimised regulator. It is proven, that it optimises the RG flow in LPA [14]. The philosophy behind Litim's regulator is to kill the loop-momentum dependence of the inverse propagator. This makes the loop integral - the momentum integral in the trace of the r.h.s. of the Wetterich equation - almost trivial, it reduces to an integral of a polynomial of the loop momentum. Thus, the flow equations for the different couplings contain no direct momentum integrals - as they can be performed analytically - and reduce to a coupled set of first order ordinary differential equations. It is not known whether Litim's regulator provides optimal results beyond LPA, however the aforementioned feature makes it a convenient choice for a regulator. The higher orders of the GE spawn more differential equations for the new couplings, that is, the usage of Litim's regulator makes the analysis of the examined system less time consuming.

1.4 Generic features of $O(N)$ symmetric models in FRG

The RG flow is believed to keep global symmetries, and thus the universality class corresponding to the given symmetry. This motivates to research different models belonging to different symmetry groups in the field of FRG. For example, the $O(1)$ models, which are actually $\mathcal{Z}_2$ symmetric, belong to the Ising universality class. Generally, the $O(N)$ symmetric models refer to vector models with an N-component field variable, $\vec{\phi}$. An ordinary, Euclidean, d dimensional, $O(N)$-symmetric model can be described via making an ansatz for its bare action at the UV scale $k = \Lambda$:

$$\Gamma_\Lambda[\vec{\phi}] = S_\Lambda[\vec{\phi}] = \int d^d x \Big(Z_\Lambda(\rho)(\nabla\vec{\phi})^2 + Y_\Lambda(\rho)(\nabla\vec{\phi})^4 + U_\Lambda(\rho) \Big), \tag{1.26}$$

where $\rho = \vec{\phi}\cdot\vec{\phi}$. The ordinary in the classification means, that the couplings in $Z_\Lambda(\rho)$ and $Y_\Lambda(\rho)$ are positive. Note that this is an NNLO level ansatz. The tools available in the FRG method allows one to *(i.)* find fixed points in the theory space of the model as well as they make it possible *(ii.)* to follow the RG flow of arbitrary trajectories with arbitrary initial conditions. By exploiting item *(i.)* one can quantitatively and qualitatively describe the characteristics of a second order phase transition, while considering item *(ii.)*, one may acquire the scaling laws (at high and low energies and at intermediate scales) of a generic trajectory in a given phase, not necessarily close to a fixed point. An FRG analysis of the $O(N)$ model generally consist of these steps.

It is well known that perturbative renormalization is only applicable in the vicinity of the trivial fixed point, the Gaussian one, where all the couplings vanish. This is a repulsive FP in the manner of lowering the momentum scale. Upon following the RG flows of different trajectories - with initial conditions close to the Gaussian fixed point (GFP) - one finds, that they emanate from the GFP. The GFP is present in the $O(N)$ models. However, another non-trivial fixed point exists there, called the Wilson-Fisher fixed point (WFFP). In some directions in the theory space it repels trajectories, in others it attracts them, therefore this is a crossover type fixed point. The WFFP drives the critical behavior of the model, the system is critical exactly in the WFFP and on the separatrix, which connects the GFP to the WFFP in the theory space. The trajectories behave differently considering where they lie compared to the separatrix. The ordinary $O(\infty > N > 0)$ models, in 3 spatial dimensions have two phases: *(a)* a symmetric one and *(b)* a symmetry broken one.

(a) The bare action may have a trivial minimum at $\vec{\phi}^* = 0$ or non-trivial ones, but the the effective action action will always have one trivial minimum. The low energy limit of the dimensionful couplings depend on the bare values of the couplings. The dimensionless couplings however scale with their tree-level scaling laws in the infrared momentum scale.

(b) The bare action exhibits non-trivial minimums at $\vec{\phi}^* \neq 0$ and the RG flow evolves these minimums towards infinities, so that the effective potential has its dimensionless non-trivial minimums at $|\vec{\phi}^*| = \infty$. At some intermediate momentum scale,

some of the positive eigenvalues of the second functional derivative matrix of the action, i.e., the propagator become zero. This phenomenon is the spinodal instability. The excitations corresponding to the zero eigenvalues require zero energy to excite and by this, they destabilize the path integral. This is remedied by the emergence of inhomogeneous saddle point(s) of the path integral, which brake spatial translational and rotational symmetries. The appearance of spinodal instability is confined inside of the region selected by the non-trivial minimums of the RG flowing potential. The dimensionful effective potential as the function of constant background field configuration flattens between the dimensionful non-trivial minimums. This flatness is referred to in the literature as Maxwell-cut, similarly to the Maxwell construction of the van der Waals equation of state. The fact that the system has non-trivial minimums, means that the ground state at a given scale is not uniquely defined. Should the system select a particular ground state, it would spontaneously break its $O(N)$ symmetry. According to Goldstone's theorem, the spontaneous violation of the $O(N)$ symmetry creates $N-1$ massless scalar particles, called Goldstone bosons. Their number is $N-1$, because this is the number of the broken symmetry group generators, which correspond to continuous symmetry. This is why, the components of the field $\vec{\phi}$ are split into two parts in the second chapter of this thesis, I refer to one component as the radial mode, and the other $N-1$ components as the transverse or Goldstone modes.

It is not a different phase, yet the most interesting, the Wilson-Fisher fixed point itself. It can be found as a solution of the fixed point equations (where all the β-functions vanish). The eigenvalue spectrum of the stability matrix in this case can be ordered in an increasing manner: $\omega_0 < \omega_1 < \dots$ The smallest eigenvalue is negative and related to the critical exponent of the correlation length $\nu = -1/\omega_0$. The other eigenvalues are positive and they give scaling corrections to ν. In LPA, the anomalous dimension is $\eta = 0$ and at higher orders of the gradient expansion one obtains an expression for η, which depends solely on the other couplings, that is, computing the WFFP is enough to acquire η, one only has to substitute the fixed point values of the couplings into the expression η. In possession of ν and η one can express all the other critical exponents. η and ν depend on the dimension of the inner space N as well as the Euclidean space d. At fixed $2 < d < 4$, ν and η are universal and the $O(N)$ models with $N = 0$, $N = 1$, $N = 2$, and $N = 3$ belong to the entangled polymers, Ising, XY-, and Heisenberg universality classes, respectively.

Chapter 2

Critical exponents of the ordinary $O(N)$ models in the FRG approach

This chapter is based on [**A**]. Chronologically, this paper was born after [**B**, **C**]. However, I believe, that this chapter would be more educative to give a brief glimpse into the applications of the FRG method and its technical tools. We are going to attune to the Wetterich's ERGE here and study in detail the critical exponent ν of the correlation length and the anomalous dimension η, characterizing the Wilson-Fisher fixed point of the $O(N)$ models in different orders of gradient expansion. The determination of these critical exponents of the $O(N)$ model is a popular subject for specialists in this field, since anomalous dimension is known to be the most susceptible among the critical exponents to the given scheme, ansatz and the regulator function as well. It became a benchmark of the employed method in FRG. In [**A**], we established a computable framework to determine ν and η of the Wilson-Fisher fixed point (WFFP) in the fourth order of the gradient expansion (NNLO) in the $O(N)$ models. I have shown, that the higher-derivative coupling (which we denoted as $\bar{Y}$) in the WFFP of the $O(1)$ model scales with $\sim \epsilon^3$ in the $4-\epsilon$ expansion. I have also studied the stability of the critical exponents against the different orders of truncation of the polynomial expansion of the model's local potential U_k. I have computed the $O(1)$ model's ν and η in continuous $2 < d < 4$ dimensions, with particular emphasis on the NNLO effect compared to the results of the second order of the gradient expansion (NLO). This is found to be in very good agreement with the literature. Finally, I have provided numerical results in NNLO for the $O(N > 1)$ models ν and η, as well as their N-dependence. I have also computed the N-dependence of the first three, rarely discussed scaling corrections $\omega_1, \omega_2, \omega_3$ to the WFFP, beyond ν. The motivation was not to achieve the numerically most precise results, but to qualitatively show the effect of the NNLO on the $O(N > 1)$ critical exponents, within our scheme.

2.1 Ansatz and derivation of the flow equations

I have contributed to the derivation of the sought flow equations. I have also written a code in a computer algebraic environment, which automatically generates the flow equations at an arbitrary order of the polynomial truncation M in LPA, NLO and NNLO. The following part of this section are quoted from [**A**], except for very slight changes in the notation of the parameters of the potential: "In order to apply the EAA RG approach to the N-component scalar field ϕ_x^a $(a = 1, 2, \ldots, N)$, one splits the EAA $\bar{\Gamma}_k[\phi] = \Gamma_k[\phi] + \Delta\Gamma_k[\phi]$ into the reduced EAA (rEAA) $\Gamma_k[\phi]$ and the regulator piece

$$\Delta\Gamma_k[\phi] \quad = \quad \frac{1}{2}\int_x \phi_x^a \mathcal{R}_{k,x,y}^{a,b}\phi_y^b, \quad \text{where} \quad \mathcal{R}_{k,x,y}^{a,b} = R_k^{a,b}(-\Box)\delta(x-y). \tag{2.1}$$

with the infrared (IR) cutoff matrix $R_k^{a,b}(u)$. Here and below the formulas are cast into the form that the differential operators act always on the index x and k denotes the running cutoff. The Wetterich equation (WE) for the rEAA Γ_k is given as

$$\dot{\Gamma}_k \quad = \quad \frac{1}{2}\mathrm{Tr}\left([\Gamma_k^{(2)} + \mathcal{R}_k]^{-1}\dot{\mathcal{R}}_k\right), \tag{2.2}$$

where the dot over the quantities indicates the scale-derivative $k\partial_k$, $\Gamma_k^{(2)}$ is a shorthand for $\Gamma_{k,x,y}^{(2)a,b} = \frac{\delta^2\Gamma_k[\phi]}{\delta\phi_x^a\delta\phi_y^b}$ $(a, b = 1, 2, \ldots, N)$. The trace is taken over a complete set of field configurations. Application of the usual GE techniques involves the split of the field $\phi_x^a = \Phi^a + \eta_x^a$ into the homogeneous background piece $\Phi^a = \Phi e^a$ and the inhomogeneous fluctuating field η_x^a (with infinitesimal amplitude), where e^a is an arbitrarily fixed unit vector in the internal space ($e^a e^a = 1$). For later convenience we introduce the projectors $\mathcal{P}_\parallel^{ab} = e^a e^b$ and $\mathcal{P}_\perp^{ab} = \delta^{ab} - e^a e^b$ acting on the N-vectors of the internal space and define the field components $\phi_{\parallel x}^a = \mathcal{P}_\parallel^{ab}\phi_x^b$ and $\phi_{\perp x}^a = \mathcal{P}_\perp^{ab}\phi_x^b$ of the radial(r-) and transverse/Goldstone(G-) modes, respectively. The Goldstone modes are absent for the case with $N = 1$. For the rEAA we make the NNLO ansatz

$$\Gamma_k[\phi] \quad = \quad \frac{1}{2}\int_{x,y} \phi_{\parallel x}^a D_{\parallel x,y}^{-1}(-\Box)\phi_{\parallel y}^a + \frac{1}{2}\int_{x,y} \phi_{\perp x}^a D_{\perp x,y}^{-1}(-\Box)\phi_{\perp y}^a + \int_x U_k(r_x) \tag{2.3}$$

with

$$D_{Ax,y}^{-1}(-\Box) \quad = \quad \mathcal{Z}_{A\ k}(-\Box)\delta_{x,y} = (-Z_{Ak}\Box + Y_{Ak}\Box^2)\delta_{x,y}, \tag{2.4}$$

where $\mathcal{Z}_{A\ k}(-\Box)$ are the momentum-dependent wave function renormalizations for the radial ($A = \parallel$) and transverse modes ($A = \perp$) and $r_x = \frac{1}{2}\phi_x^a\phi_x^a$. The r-dependence of the potential is parameterized as truncated polynomial expansion

$$U_k(r_x) \quad = \quad \sum_{n=0}^{M} \frac{u_n}{n!}(r_x - \kappa)^n, \tag{2.5}$$

where κ denotes the position of the minimum of $U_k(r_x)$, where $U_k'(r_x)|_{r_x=\kappa} = 0$. In the symmetry broken phase $u_1 = 0$ and $\kappa \neq 0$ evolves, while in the symmetric phase u_1 evolves and $\kappa = 0$. So that the potential is approximated by a polynomial of degree M of the $O(N)$-invariant variable r_x. The ansatz (2.3) treats the r- and G-modes of the field separately. This explicit breaking of $O(N)$ symmetry provides the flexibility to our RG approach that in the symmetry broken phase the dynamics may govern the system to states in which the momentum-dependent wave function renormalizations for these modes evolve differently with the gliding scale k, although one starts the evolution with the initial condition $\mathcal{Z}_{\perp\Lambda}(-\Box) = \mathcal{Z}_{\parallel\Lambda}(-\Box)$ at the ultraviolet (UV) scale Λ ensuring unbroken $O(N)$ symmetry of the bare action. In this manner spontaneous symmetry breaking may be mimicked partially by an explicit one.

The ansatz (2.3) with eqs. (2.4)-(2.5) has been inserted into the WE (2.2), then evolution equations derived for the couplings of the gradient terms and those of the local potential by using usual GE techniques. The r- and the G-modes were split as $\phi^a_{\parallel x} = \Phi e^a + \eta^a_{\parallel x}$ and $\phi^a_{\perp x} = \eta^a_{\perp x}$, respectively. Both sides of the WE have been functional Taylor-expanded in powers of the fluctuating fields $\eta^a_{\parallel x}$, $\eta^a_{\perp x}$ and the evolution equations for the local potential $U_k(r)$ and the momentum-dependent wave function renormalizations $\mathcal{Z}_{k\parallel}(Q^2)$ and $\mathcal{Z}_{k\perp}(Q^2)$ read off. The explicit evaluation of the traces on the right-hand side of the WE has been performed in the momentum representation. Denoting by Q_μ the momentum of the Fourier modes of the fluctuating field and by p_μ the loop-momentum appearing in the explicit expressions of the traces, the regulator matrix has been specified as a block-diagonal one $R_k^{a,b}(p^2) = \sum_{A=\parallel,\perp} R_{Ak}(p^2)\mathcal{P}_A^{a,b}$ choosing the regulator functions $R_{Ak}(p^2)$ in the form of Litim's optimized regulator,

$$R_{Ak}(p^2) \quad = \quad [Z_{Ak}(k^2 - p^2) + Y_{Ak}(k^4 - p^4)]\Theta(k^2 - p^2) \tag{2.6}$$

with the Heaviside function $\Theta(u)$. With this choice the loop-integrals reduce to integrals over the Euclidean sphere of radius k and can be taken analytically.

Truncating the functional Taylor-expansion at the quadratic term, the left-hand side of the WE takes the form

$$\dot{\Gamma}_k[\Phi + \eta] \quad = \quad \dot{\Gamma}_k[\Phi] + \frac{1}{2}\int_{x,y} \eta^a_x \dot{A}^{a,b}_{k,x,y}\eta^b_y, \tag{2.7}$$

while the matrix $\Gamma^{(2)a,b}_{k,x,y}[\Phi + \eta]$ can be expanded as

$$\Gamma^{(2)a,b}_{k,x,y}[\Phi + \eta] \quad = \quad A^{a,b}_{k,x,y} + (\eta B)^{a,b}_{k,x,y} + \frac{1}{2}(\eta C\eta)^{a,b}_{k,x,y}, \tag{2.8}$$

where

$$A^{a,b}_{k,x,y} = \Gamma^{(2)a,b}_{k,x,y}[\Phi], \tag{2.9}$$

$$(\eta B)^{a,b}_{k,x,y} = \int_z \eta^c_z \frac{\delta^3\Gamma_k}{\delta\phi^a_x\delta\phi^b_y\delta\phi^c_z}\bigg|_{\phi_z=\Phi}, \tag{2.10}$$

$$(\eta C\eta)^{a,b}_{k,x,y} = \int_{z,u} \eta^c_z \frac{\delta^4\Gamma_k}{\delta\phi^a_x\delta\phi^b_y\delta\phi^c_z\delta\phi^d_u}\bigg|_{\phi_z=\Phi} \eta^d_u. \tag{2.11}$$

The first-order term on the left-hand side vanishes because η_x contains no zero mode. The field-independence of the gradient terms leads to the great simplification that the third and fourth functional derivatives of the rEAA come from the derivatives of the potential alone. The functional Taylor-expansion of the trace on the right-hand side of the WE is then achieved by performing the truncated Neumann-expansion of the inverse matrix $[\Gamma^{(2)}[\phi] + \mathcal{R}_k]^{-1}$ at the IR cutoff propagator

$$G^{a,b}_{p,q} = ([\Gamma^{(2)}[\phi_B] + \mathcal{R}_k]^{-1})^{a,b}_{p,q} = \sum_{A=\parallel,\perp} G_A(p^2)\mathcal{P}^{a,b}_A, \tag{2.12}$$

where

$$G_\parallel(p^2) = [\mathcal{Z}_{\parallel\ k}(p^2) + U'_k(r) + 2rU''_k(r) + R_{\parallel\ k}(p^2)]^{-1}, \tag{2.13}$$

and

$$G_\perp(p^2) = [\mathcal{Z}_{\perp\ k}(p^2) + U'_k(r) + R_{\perp\ k}(p^2)]^{-1} \tag{2.14}$$

with $r = \frac{1}{2}\Phi^2$ are the propagators of the r- and G-modes, respectively. Here and in what follows the notation of the r-dependence of the propagators has been suppressed in order to make our formulas more transparent. The trace on the right-hand side of the WE (2.2) can then be rewritten as

$$\mathrm{Tr}\Big([\Gamma^{(2)} + \mathcal{R}_k]^{-1}\dot{\mathcal{R}}_k\Big) = T_0 + T_1 + T_{2B} + T_{2C}, \tag{2.15}$$

where

$$\begin{aligned} T_0 &= \mathrm{Tr}[G\dot{R}_k], \\ T_1 &= -\mathrm{Tr}[G\cdot(\eta B)\cdot G\dot{R}_k], \\ T_{2B} &= \mathrm{Tr}[G\cdot(\eta B)\cdot G\cdot(\eta B)\cdot G\dot{R}_k], \\ T_{2C} &= -\frac{1}{2}\mathrm{Tr}[G\cdot(\eta C\eta)\cdot G\dot{R}_k]. \end{aligned} \tag{2.16}$$

(Here the dot '$\cdot$' indicates matrix product both in the external and the internal spaces.) One finds $T_1 = 0$ because the background is homogeneous and η_x exhibits no zero mode. The other terms are given as

$$T_0 = V\sum_{A=\parallel,\perp} d_A \int_p G_A(p^2)\dot{R}_{A\ k}(p^2), \tag{2.17}$$

$$
\begin{aligned}
T_{2B} &= \int_{Q,p} 2r\Big\{\Big[[G_\parallel(p^2)]^2 G_\parallel(q^2)\delta^2(r)\dot{R}_{\parallel k}(p^2) \\
&\quad +(N-1)[G_\perp(p^2)]^2 G_\perp(q^2)\epsilon^2(r)\dot{R}_{\perp k}(p^2)\Big]_{q=Q-p}\eta_{\parallel Q}\eta_{\parallel -Q} \\
&\quad +\epsilon^2(r)\Big[[G_\parallel(p^2)]^2 G_\perp(q^2)\dot{R}_{\parallel k}(p^2)+[G_\perp(p^2)]^2 G_\parallel(q^2)\dot{R}_{\perp k}(p^2)\Big]_{q=Q-p}\eta^a_{\perp Q}\eta^a_{\perp -Q}\Big\},
\end{aligned}
\tag{2.18}
$$

$$
\begin{aligned}
T_{2C} = -\frac{1}{2}\int_{Q,p}\Big\{&\Big[[G_\parallel(p^2)]^2\gamma(r)\dot{R}_{\parallel k}(p^2)+(N-1)[G_\perp(p^2)]^2\delta(r)\dot{R}_{\perp k}(p^2)\Big]\eta_{\parallel Q}\eta_{\parallel -Q} \\
&+\Big[[G_\parallel(p^2)]^2\delta(r)\dot{R}_{\parallel k}(p^2)+(N+1)[G_\perp(p^2)]^2\epsilon(r)\dot{R}_{\perp k}(p^2)\Big]\eta^a_{\perp Q}\eta^a_{\perp -Q}\Big\}
\end{aligned}
\tag{2.19}
$$

with the degeneracies $d_\parallel = 1$ and $d_\perp = N-1$ of the r- and G-modes, respectively and

$$
\begin{aligned}
\gamma(r) &= 4r^2 U_k''''(r) + 12 r U_k'''(r) + 3U''(r), \\
\delta(r) &= 2rU_k'''(r) + U_k''(r), \\
\epsilon(r) &= U_k''(r).
\end{aligned}
\tag{2.20}
$$

The comparison of the terms of the orders $\mathcal{O}(\eta^0)$ and $\mathcal{O}(\eta^2)$ on both sides of eq. (2.15) results in the evolution equations

$$
\dot{U}_k(r) = \frac{1}{2}\sum_{A=\parallel,\perp} d_A \int_p G_A(p^2)\dot{R}_{A\ k}(p^2)
\tag{2.21}
$$

for the local potential,

$$
\begin{aligned}
\dot{\mathcal{Z}}_{\parallel k}(Q^2) &= \int_p 2r\Big\{\Big[[G_\parallel(p^2)]^2 G_\parallel(q^2)[2rU_k''' + 3U_k'']^2\dot{R}_{\parallel k}(p^2) \\
&\quad +(N-1)[G_\perp(p^2)]^2 G_\perp(q^2)[U_k'']^2\dot{R}_{\perp k}(p^2)\Big]_{q=Q-p} \\
&\quad -[G_\parallel(p^2)]^3[2rU_k''' + 3U_k'']^2\dot{R}_{\parallel k}(p^2) - (N-1)[G_\perp(p^2)]^3[U_k'']^2\dot{R}_{\perp k}(p^2)\Big\}_{r=\kappa}
\end{aligned}
\tag{2.22}
$$

for the momentum-dependent wave function renormalization of the r-mode, and

$$
\begin{aligned}
\dot{\mathcal{Z}}_{\perp k}(Q^2) &= \int_p\Big\{2r[U_k'']^2\Big[[G_\parallel(p^2)]^2 G_\perp(q^2)\dot{R}_{\parallel k}(p^2) \\
&\quad +[G_\perp(p^2)]^2 G_\parallel(q^2)\dot{R}_{\perp k}(p^2)\Big]_{q=Q-p} - [G_\perp(p^2)]^2 U_k''\dot{R}_{\perp k}(p^2)\Big\}_{r=\kappa}
\end{aligned}
\tag{2.23}
$$

for the momentum-dependent wave function renormalization of the G-modes. The right-

hand sides of eqs. (2.22) and (2.23) should be taken at the minimum of the potential $r = \kappa$ in accordance with the usage of field-independent derivative couplings. Since there are propagators in eqs. (2.22) and (2.23) taken at the momentum $p - Q$ where p is the loop-momentum, one has to Taylor-expand both sides of these equations in powers of Q_μ and make use of $O(d)$ symmetry when performing integrals of the types

$$\begin{aligned} \int_p p_\mu p_\nu f(p^2) &= d^{-1}\delta_{\mu\nu}\int p^2 f(p^2), \\ \int_p p_\mu p_\nu p_\kappa p_\lambda f(p^2) &= [d(d+2)]^{-1}\int_p (p^2)^2 f(p^2). \end{aligned} \tag{2.24}$$

Then the comparison of the terms of the orders $\mathcal{O}(Q^2)$ and $\mathcal{O}(Q^4)$ on both sides of eqs. (2.22) and (2.23) provide the evolution equations for the various couplings $Z_{A\ k}$ and $Y_{A\ k}$, respectively. The introduction of the dimensionless quantities shall be discussed below separately for the cases $N = 1$ and $N \geq 2$. The explicit forms of the evolution equations for the dimensionless couplings have been generated by a computer algebraic program. At this point one has to emphasize once again the price one has to pay for working with the simplified ansatz (2.3) instead of a one containing more complete sets of quadratic and quartic derivative terms like it is done in Refs. [6, 17] at the NLO level. In our case the introduction of the homogeneous background field Φ^a pointing into an arbitrary, but fixed direction e^a in the internal space leads necessarily to different diagonal derivative pieces for the radial $\eta^a_\parallel$ and the Goldstone $\eta^a_\perp$ modes, and finally to evolution equations of different forms even if identical momentum-dependent wave function renormalizations $\mathcal{Z}_{\parallel k}(Q^2) = \mathcal{Z}_{\perp k}(Q^2)$ (and identical cutoffs $R_{\parallel k}(p^2) = R_{\perp k}\,(p^2)$) would have been assumed. In the latter case, however, eqs. (2.22) and (2.23) would have been in contradiction. Therefore, one can not avoid the introduction of different momentum-dependent wave function renormalizations $\mathcal{Z}_{\parallel k}(Q^2) \neq \mathcal{Z}_{\perp k}(Q^2)$ for the r- and G-modes. This breaks the $O(N)$ symmetry of the rEEA explicitly, but can be considered as a kind of bookkeeping the consequences of the existence of the nontrivial minimum of the potential at $r = \kappa$ in the symmetry broken phase. Our ansatz allowing for different RG evolutions of $\mathcal{Z}_{\parallel k}(Q^2)$ and $\mathcal{Z}_{\perp k}(Q^2)$ makes the RG scheme more flexible and raises the question that starting the evolution from a symmetric initial state with $\mathcal{Z}_{\parallel\Lambda}(Q^2) = \mathcal{Z}_{\perp\Lambda}(Q^2)$ at the UV scale, whether the critical theories at the WF FP for $N \geq 2$ exhibit this symmetry or not.

The ansatz (2.3) with eq. (2.4) enables one to discuss various truncations of the GE: the LPA for $Z_{\parallel k} = Z_{\perp k} \equiv 1$, $Y_{\parallel k} = Y_{\perp k} \equiv 0$, the NLO of the GE with scale-dependent wave function renormalizations $Z_{\parallel k}$, $Z_{\perp k}$ and $Y_{\parallel k} = Y_{\perp k} \equiv 0$, whereas the running of all derivative couplings $Z_{\parallel k}$, $Z_{\perp k}$, $Y_{\parallel k}$, and $Y_{\perp k}$ corresponds to the NNLO of the GE. These truncations of the GE with given M of the truncation of the field-dependence of the local potential shall be referred to below as NLOM and NNLOM approximations. Our results are obtained with uniform wave function renormalization, i.e., field-independent derivative couplings. This will not be indicated in the notation of the approximation except of the cases when it should be emphasized with comparison of results from the literature obtained by the usage of either uniform (NLOu, NNLOu) or field-dependent (NLOf, NNLOf) derivative couplings. We have performed the numerical calculations with the polynomial truncation $M = 6$. It has been tested that our results for the exponents are stable for truncations $6 \leq M \leq 12$ in the whole investigated range of N (see more

details below). This justifies that the findings in Refs. [14, 18, 19] on the convergence of the polynomial expansions in O(N) theories, obtained in the LPA, can be applied to the NLO and NNLO approximations of the GE. The scale-derivatives of the derivative couplings have been neglected when evaluating $\dot{R}_k(p^2)$."

2.2 $O(1)$ model in continuous dimensions $2 < d < 4$

Here, I made use of my program for deriving the explicit form of evolution equations. Once it was done, I have wrote a program, for numerically integrating the evolution equations, generalized to accept the derived evolution equations for arbitrary order of the polynomial truncation M. This was used to show the behavior of the different couplings in close to critical trajectories. I have also performed the $4-\epsilon$ expansion around the Wilson-Fisher fixed point as well as computed the critical exponents ν and η in continuous dimensions $2 < d < 4$ with particular emphasis on the $d = 3$ case. The numerical integration of the flow equations employed the fourth order Runge-Kutta method. The WF FP has been located by Newton-Rhapson's method.

2.2.1 Evolution equations

Our formulas for the flow of the local potential and the wave function renormalizations contain N as a continuous parameter. Setting $N = 1$, removes eq. (2.23) for $\mathcal{Z}_\perp(Q^2)$, since in this case we have only one component of the field variable in the internal space. Therefore we work with $Z_k = Z_{\|k}$ and $Y_k = Y_{\|k}$, belonging to the r-mode. The evolution eqs. (2.21) and (2.22) reduce to

$$\dot{U}_k(r) \quad = \quad \frac{1}{2}\int_p G(p^2)\dot{R}_k(p^2) \tag{2.25}$$

for the potential $U_k(r)$ and

$$\begin{aligned}\dot{\mathcal{Z}}_k(Q^2) &= 2\kappa[2\kappa U_k'''(\kappa) + 3U''(\kappa)]^2 \\ &\times \int_p \left(G^2(p^2)[G(q^2)]_{q=Q-p} - G^3(p^2) \right) \dot{R}_k(p^2)\end{aligned} \tag{2.26}$$

for wave function renormalization $\mathcal{Z}_k(Q^2)$, where $G(p^2) = G_\|(p^2)$ and $R_k(p^2) = R_{\|k}(p^2)$.

As a next step, one turns to the dimensionless quantities (as discussed in Sec. 1.2): $\bar{r} = Z_k k^{-(d-2)} r$, $\bar{\kappa} = Z_k k^{-(d-2)}\kappa$, $\bar{u}_n = Z_k^{-n} k^{-d+n(d-2)} u_n$, and $\bar{Y}_k = Z_k^{-1} k^2 Y_k$. These definitions of the dimensionless quantities incorporating appropriate powers of the uniform wave function renormalization are advantageous, because they clear the coupling Z_k from the beta-functions. The effect of Z_k is not neglected, it affects the flow equations through the anomalous dimension.

The explicit flow equations are generated in a computer algebraic program. The evolution equations (with $\bar{\lambda} = \bar{u}_2$) in the symmetry broken phase and the approximation

scheme NNLO2 are

$$\dot{\bar{\kappa}} = -(d-2+\eta)\bar{\kappa} + a(1+2\bar{Y}_k)\bar{g}^2 \equiv \beta_{\bar{\kappa}}, \tag{2.27}$$

$$\dot{\bar{\lambda}} = (d-4+2\eta)\bar{\lambda} + b(1+2\bar{Y}_k)\bar{\lambda}^2\bar{g}^3 \equiv \beta_{\bar{\lambda}}, \tag{2.28}$$

$$\begin{aligned}\dot{\bar{Y}}_k = {} & (2+\eta)\bar{Y}_k + 18\alpha_d\bar{\kappa}\bar{\lambda}^2(1+2\bar{Y}_k)\bar{g}^4\Bigg\{\Bigg[\frac{48}{d(d+2)(d+4)} + \frac{576\bar{Y}_k}{d(d+2)(d+6)} \\ & + \frac{192}{d(d+8)}\left(\frac{1}{d}+\frac{12}{d+2}\right)\bar{Y}_k^2 + \frac{1280}{d(d+10)}\left(\frac{1}{d}+\frac{3}{d+2}\right)\bar{Y}_k^3 \\ & + \frac{1}{d(d+12)}\left(\frac{1792}{d}+\frac{6144}{d+2}\right)\bar{Y}_k^4\Bigg]\bar{g}^3 - \Bigg[\frac{12}{d(d+2)} + \frac{40}{d(d+4)}\left(3+\frac{2}{d}\right)\bar{Y}_k \\ & + \frac{160}{d(d+6)}\left(3+\frac{4}{d}\right)\bar{Y}_k^2 + \frac{192}{d(d+8)}\left(5+\frac{6}{d}+\frac{12}{d+2}\right)\bar{Y}_k^3\Bigg]\bar{g}^2 \\ & + \Bigg[\frac{1}{d} + \frac{8}{d+2}\left(1+\frac{6}{d}\right)\bar{Y}_k + \frac{24}{d+4}\left(1+\frac{12}{d}\frac{2}{d^2}+\frac{6}{d(d+2)}\right)\bar{Y}_k^2\Bigg]\bar{g} - \frac{3\bar{Y}_k}{d}\Bigg\} \equiv \beta_{\bar{Y}},\end{aligned} \tag{2.29}$$

with the anomalous dimension

$$\eta = -36\alpha_d\bar{\kappa}\bar{\lambda}^2\left(1+2\bar{Y}_k\right)\bar{g}^4\left\{\frac{4}{d}\left[\frac{1}{d+2}+\frac{8\bar{Y}_k}{d+4}+\frac{24\bar{Y}_k^2}{d+6}\right]\bar{g} - \frac{1+6\bar{Y}_k}{d}\right\} \equiv \eta(\bar{\kappa},\bar{\lambda},\bar{Y}_k) \tag{2.30}$$

and the notations

$$\bar{g} = [1+\bar{Y}_k+2\bar{\kappa}\bar{\lambda}]^{-1} \tag{2.31}$$

and $a = 6\alpha_d/d$, $b = 6a$, $\alpha_d = \frac{1}{2}\Omega_d(2\pi)^{-d}$ with the d-dimensional solid angle Ω_d. In order to acquire the RG trajectories, one has to integrate the coupled set of first order ordinary differential equations (2.27)-(2.29) for initial conditions given at the UV scale $k = \Lambda$ by using eq. (2.30) as η, and then integrate the evolution of the wave function renormalization Z_k by

$$\dot{Z}_k = -\eta Z_k. \tag{2.32}$$

Here, it is assumed that $Z_k \sim k^{-\eta}$ is satisfied close to criticality. The evolution equations for the more restrictive truncations of the GE can be obtained from the NNLO equations, as described above. In the truncation of the EAA with field-independent wave function renormalization $\mathcal{Z}_k(Q^2)$, the wave function renormalization Z_k does not evolve in the symmetric phase, it keeps its UV value $Z_k = 1$. The modification of the wave function renormalization in the symmetric phase occurs as a two-loop effect in the perturbative approach, in the FRG approach it is only present, if we account its field dependence. That is, the numerical work is concentrated on the symmetry broken phase of the model. There, the scale-dependence of Z_k may occur because of the RG flow of the non-trivial

minimum of the potential.

2.2.2 Crossover scaling

The WF crossover region has been explored numerically by integrating the RG evolution equations (2.27)-(2.29) and (2.32) (taking eqs. (2.30) and (2.31) into account) for a bunch $\mathcal{B}$ of close to critical RG trajectories running in the symmetry broken phase but in the close vicinity of the separatrix between the symmetric and symmetry broken phases. The trajectories in $\mathcal{B}$ were chosen to belong to the UV couplings $\bar{\lambda}_\Lambda = 0.1$, $Z_\Lambda = 1$, and $\bar{Y}_\Lambda = 0$, with varied $\bar{\kappa}_\Lambda$. The value $\bar{\kappa}_\Lambda^{\rm sep}$ corresponding to the separatrix was determined by fine tuning. In an ideal case, the renormalized trajectory emanated form the Gaussian FP converges to the WFFP and reaches it at $k = 0$. In our case, we can only get arbitrary close to the renormalized trajectory but not exactly on it. The system is in the vicinity of the WFFP for a given interval of the physical scale and eventually, it evolves from it as it tends to the infrared. The closer the trajectory is to the separatrix, the wider the aforementioned interval. In our case, we looked for trajectories, where the bare potential has non-trivial minimums, but in the IR the minimums become the trivial one. I fine-tuned RG trajectories, on which the vanishing of $\bar{\kappa}$ occurs at very low scales, namely at $k_{\rm c} \sim 10^{-7}$ for $\bar{\kappa}(k_{\rm c}) = 0$. The numerical investigation has been performed in various orders of truncations M, both in the NLO and NNLO. It has been established, that $M = 6$ provides stable numerical values for the exponents η and ν. The typical flow of the couplings $\bar{\kappa}$, $\bar{\lambda}$,Z_k, $\bar{Y}_k$ and the anomalous dimension η are shown in Fig. 2.1 for $d = 3$. Similar behavior was obtained for $d = 4 - \epsilon$ as well. Beyond the quite short UV scaling region, there occurs a crossover scaling region stretched over ~ 3 orders of magnitude change of the running scale k, where $\bar{\kappa}$ and $\bar{\lambda}$ keep their constant (fixed point) values $\bar{\kappa}_*$ and $\bar{\lambda}_*$. Naturally, this length of the plateaus depends on the particular fine-tuned value of $k_{\rm c}$. The function $\bar{Y}_k$ turned out to be rather flat at its minimum, with the value $\bar{Y}_*$ and that flat region is in agreement with the position of the plateaus of the functions $\bar{\kappa}(k)$ and $\bar{\lambda}(k)$. The anomalous dimension $\eta_* = \eta(\bar{\kappa}_*, \bar{\lambda}_*, \bar{Y}_*)$ is determined by means of eq. (2.30) and it turns out to be scale-independent in the very same region of the scale k. All these plateau values are independent on the particular trajectory in the bunch $\mathcal{B}$. This signals, that the trajectories in $\mathcal{B}$ are indeed get close to the WFFP, and their plateaus correspond to the fixed point values corresponding to the WF FP.

At the scale $k_{\rm c}$, the minimum of the potential is shifted to vanishing homogeneous background field, as mentioned earlier. That is, the symmetry of the vacuum state is restored in the infrared. The couplings $\bar{\lambda}$ and $\bar{Y}_k$ keep their finite non-vanishing values $\bar{\lambda}_*$ and $\sim \bar{Y}_*$, respectively, at the scale $k_{\rm c}$. This means that the theory does not become trivial. The wave function renormalization Z_k goes to infinity on the separatrix while it only reaches finite values on the various trajectories of the bunch $\mathcal{B}$. Below the scale $k_{\rm c}$, the anomalous dimension vanishes and the field-independent wave function renormalization freezes at its value $Z_{k_{\rm c}}$ reached at $k_{\rm c}$, since $\kappa(k < k_c) = 0$ and $\dot{Z}_k \sim \bar{\kappa}$. The couplings of the potential and the coupling $\bar{Y}_k$ show up tree-level scaling (see eqs. (2.27), (2.28) and (2.29) for $\bar{\kappa} = 0$) in the IR for $k < k_c$.

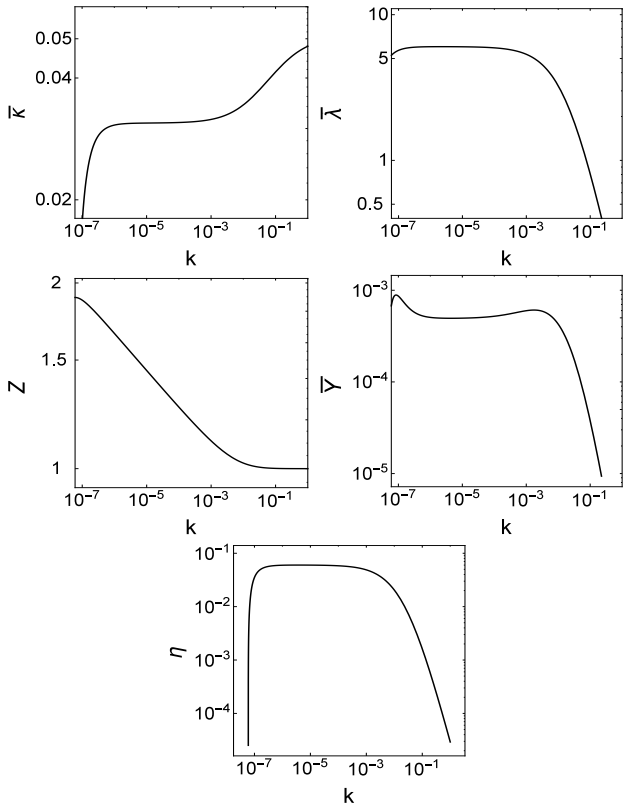

Figure 2.1: Typical scale-dependence of $\bar{\kappa}$, $\bar{\lambda}$, Z_k, $\bar{Y}_k$, and η on close to critical RG trajectories with $Z_\Lambda = 1$ and $\bar{Y}_\Lambda = 0$, determined in the approximation scheme NNLO6 for $d = 3$.

A convenient way to identify the correlation length is as the reciprocal of the scale k_c. This was signalled by the fact that the closer we got to the separatrix - where the correlation length diverges - the smaller k_c became, and wider the plateaus in the evolution of the couplings. Let the separatrix be given by the initial conditions $(\bar{\kappa}_\Lambda^{\rm sep}, \bar{\lambda}_\Lambda, Z_\Lambda = 1, \bar{Y}_\Lambda = 0)$. Then the system can be tuned to criticality by setting $\bar{\kappa}_\Lambda$ to minimise the distance $|\bar{\kappa}_\Lambda^{\rm sep} - \bar{\kappa}_\Lambda| = t^2$ of the particular RG trajectory (with $(\bar{\kappa}_\Lambda, \bar{\lambda}_\Lambda, Z_\Lambda = 1, \bar{Y}_\Lambda = 0)$) from the separatrix. This distance can be identified with the square of a kind of reduced temperature t for any given initial value $\bar{\lambda}_\Lambda$ [20]. It has been found, that the correlation length scales with the reduced temperature as $\xi \propto t^{-\nu}$, ν turned out to be constant for the bunch of the trajectories $\mathcal{B}$ (see Fig. 2.2 for that typical scaling behavior). This qualitative behavior is the same in the NLO and NNLO for dimensions $d = 3$ as well as $d = 4 - \epsilon$.

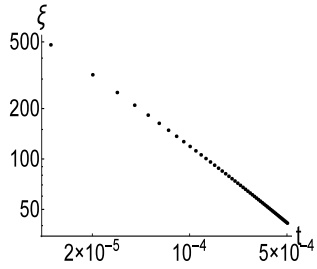

Figure 2.2: Dependence of the correlation length ξ on the reduced temperature t at the lower end of the WF crossover region in the approximation scheme NNLO6 for $d = 3$.

2.2.3 Fixed points

The fixed points $(\bar{\kappa}^*, \bar{\lambda}^*, \bar{Y}^*)$ are solutions of the equations

$$\beta_{\bar{\kappa}} = \beta_{\bar{\lambda}} = \beta_{\bar{Y}} = 0. \tag{2.33}$$

As it was discussed above, Z_k is not present in the flow equations of the couplings, $\dot{Z}_k$ completely decouples from the other equations. The fixed point equations were solved with the definition of η, which depends on the couplings $(\bar{\kappa}, \bar{\lambda}, \bar{Y})$ only. Therefore, the anomalous dimension, corresponding to the FP is $\eta^* = \eta(\bar{\kappa}^*, \bar{\lambda}^*, \bar{Y}^*)$. This work is restricted to dimensions $2 < d < 4$ and to the parameter region $Z_k > 0$, $\bar{Y}_k \geq 0$, $\bar{\lambda} \geq 0$ excluding unphysical solutions, such as the trivial fixed-point solution $Z_k = \bar{Y} = \bar{\lambda} = \bar{\kappa} = 0$ and the ones with Euclidean action unbounded from below. The fixed-point equations (2.33) have a solution with $\bar{\lambda}^*_G = 0$ and $\bar{Y}^*_G = 0$ implying $\eta^* = 0$ and $\bar{\kappa}^*_G = a$ for arbitrary fixed value of $Z_k = Z$. This represents the Gaussian FP in the LPA, when the wave function renormalization is restricted to $Z_k = 1$. In the approximation schemes, NLO and NNLO there exists a Gaussian fixed line in the theory space.

Eqs. (2.33) were solved for the WFFP in various approximation schemes with a root-finder routine, using the Newton-Rhapson method. Its advantage is that, it converges rapidly because the roots are calculated from gradients avoiding the calculation of numerical derivatives. The method works well if the initial conditions for the roots are close to the actual solution, especially, if one seeks the FP for high order of truncation M. These guesses for the initial conditions are the 'plateau' values $(\bar{\kappa}_*, \bar{\lambda}_*, \bar{Y}_*)$, exploited from the crossover scaling.

2.2.4 Numerical results

Dimension $d = 3$

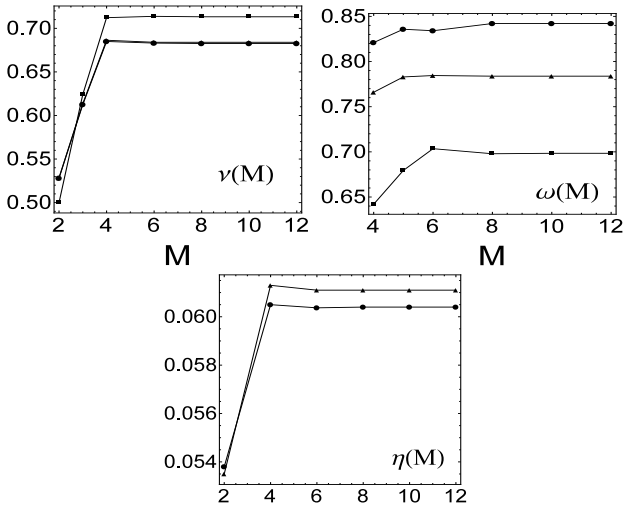

Figure 2.3: The dependence of the critical exponent ν, the subleading scaling exponent ω, and the anomalous dimension η on the order of truncation M. The LPA (rectangle) the NLO (triangle) and the NNLO (circle) results are compared. In the case of ν the NLO and NNLO results are very close, the corresponding points coincide on the diagram.

The calculations have been performed with the order of polynomial truncation $M = 6$. The dependence of the critical exponents ν, η, and the first subleading scaling exponent ω are rather stable for the truncations in the range $6 \leq M \leq 12$ in any investigated order of the gradient expansion, as shown in Fig. 2.3. The stability of the results against the particular choice of M are quantified in Table 2.1. Upon comparing the variations of the exponents investigated here - with increasing M - to the ones obtained in LPA in [14], it has to be concluded, that higher order approximations in the GE do not spoil the convergence of the polynomial expansion. Indirectly meaning, that the findings in Refs. [18] and [19] on the convergence of the polynomial expansions in O(N) theories governed by poles in the complex field plane,are applicable at the NLO and NNLO levels even in the case $N = 1$, when the RG-flow is accompanied by notable renormalization of the gradient couplings.

This work's results for the quantities, characterizing the WF FP are shown in Table 2.2 for various approximation schemes. It has been established, that the dynamically obtained (numerical integration of the equations) values $\bar{\kappa}_*$, $\bar{\lambda}_*$, etc. and the values $\bar{\kappa}^*$, $\bar{\lambda}^*$, etc. obtained as the solution of the fixed-point equations agree well in all cases. That is, we do not make any distinction between these below. It can be seen, that the WF FP is accompanied by a non-vanishing value $\bar{Y}^*$ of the higher-derivative coupling

	$\delta\nu$	$\delta\omega$	$\delta\eta$
LPA	0.071	0.730	–
NLO	0.060	0.680	0.03
NNLO	0.068	0.950	0.05

Table 2.1: The relative declination $\delta\alpha = 100 \times |\alpha_{M=12} - \alpha_{M=6}|/\alpha_{M=12}$ of the value $\alpha_{M=6}$ from the value $\alpha_{M=12}$ of the various exponents $\alpha = \nu,\ \omega, \eta$ in per cents.

Approxi-mation	$\bar{\kappa}_*$	λ_*	Y_*	η_*	ν
NLO6	0.027	6.23	–	0.057	0.615
NLOu [17]	0.041	9.25	–	0.045	0.638
NLOf [21]				$0.036\ ^{+0.008}_{-0.005}$	$0.631\ ^{+0.018}_{-0.006}$
NLOf [16]			–	0.044	0.628
NNLO6	0.031	6.02	0.0005	0.059	0.634
NNLOf [21]				$0.034\ ^{+0.005}_{-0.003}$	$0.630\ ^{+0.002}_{-0.005}$
NNLOf[15]				0.033	0.632

Table 2.2: The FP values of the various couplings, the anomalous dimension η_*, and the critical exponent ν characterizing the WF scaling region for $d = 3$, obtained in various approximation schemes. For comparison the NLO results taken from Refs. [16, 17, 21] and the NNLO results taken from Refs. [15, 21] are shown as well.

$\bar{Y}_k$. This UV irrelevant coupling becomes relevant at the WF FP. One can find similar result in [21], where the field-dependencies of the derivative couplings have been taken into account. This work's NLOu (u stands for uniform, field-independent $\mathcal{Z}_k$) results for η and ν obtained with the optimized regulator overestimate the ones obtained in [17] with the use of an exponential regulator (with similar scheme at the NLO level), thus the difference has to occur due to the use of different regulators. The results presented here in NLO6u and NNLO6u show, that the NNLO effect increases the values of η and ν by ~ 2 per cents. Comparing of the NLOu result from Ref. [17] and the NLOf (f stands for field-dependent $\mathcal{Z}_k$) ones of Ref. [16] (computed with the exponential regulator) shows, that the field-dependence of the wave function renormalization alters the values of η and ν by not more than ~ 10 and ~ 2 per cents, respectively. When the field-dependence of the derivative couplings are not neglected, the NNLO effect seems to be about ~ 6 and ~ 0.2 per cents in η and ν, respectively, according to the results in [21]. However, upon comparing the NLOf[16] and NNLOf[15] data, one can see a larger NNLO effect: ~ 30 and ~ 0.6 per cents on η and ν, respectively. This work's estimates of the NNLO effect (computed with uniform wave function renormalization) are closer to the results of [21]. Our NNLO6u values of η and ν are overestimates the ones in NNLOf [15] and NNLOf [21]. This strongly suggests, that this originates from neglecting the field-dependence of the derivative couplings, since - as the literature showed - using exponential and Litim's regulators gave results within the error bars given in Ref. [21]. In spite of their stability

against M, this work's NLO6u and NNLO6u results for the anomalous dimension overestimate the NLOf and NNLOf results of Ref. [21], while the critical exponent ν is rather close to the values found in NLOf and NNLOf.

The first few eigenvalues of the stability matrix at the WF FP [22] (see Table 2.3) have also been computed in this work. The smallest eigenvalue is negative and it corresponds to $-\nu^{-1}$, the other eigenvalues are positive and they give scaling corrections to the WF FP. It was found, that the results become stable for $M = 10$ (see $\delta\omega$ in Table 2.1). ω, ω_2, and ω_3 seem to converge with going further in the GE. This work's NNLO10 result for ω is close to the value 0.8303(18) given in [23], where it was computed by conformal bootstrap method and also close to the estimate 0.84(4) given in [24] following a thorough discussion of various approaches.

	ω	ω_2	ω_3
LPA10	0.6984	3.270	5.936
NLO10	0.7838	3.072	5.680
NNLO10	0.8421	3.061	5.675
LPA5 [22]	0.6557	3.180	5.912

Table 2.3: This work's results for the first few eigenvalues of the stability matrix at the WF FP compared to the ones given in Ref. [22].

Dimension $d = 4 - \epsilon$

The ϵ-expansion performed here has been performed at the level of truncation $M = 2$. The analytic solution of Eqs. (2.33) was sought in the form

$$\begin{aligned} \bar{\kappa}^* &= \kappa_0 + \kappa_1\epsilon + \mathcal{O}(\epsilon^2), & \bar{\lambda}^* &= \lambda_0 + \lambda_1\epsilon + +\mathcal{O}(\epsilon^2), \\ \bar{Y}^* &= \sum_{n=0}^{3} \frac{1}{n!} Y_n \epsilon^n + \mathcal{O}(\epsilon^4), & \eta^* &= \eta_0 + \eta_1\epsilon + \frac{1}{2}\eta_2\epsilon^2 + \mathcal{O}(\epsilon^3). \end{aligned} \tag{2.34}$$

The truncations of the ϵ-expansions were set in accordance with the order-by-order successive solution of the fixed-point equations. The expansion yielded

$$\begin{aligned} \bar{\kappa}^* &= \frac{3}{4}\alpha_4\left[1 + \frac{1}{2}\left(\frac{11}{3} - 2\gamma + \ln(16\pi^2)\right)\epsilon\right], \\ \bar{\lambda}^* &= \frac{16\pi^2}{9}\epsilon, \quad \bar{Y}^* = \frac{1}{6\cdot 192}\epsilon^3, \quad \eta^* = \frac{1}{36}\epsilon^2, \end{aligned} \tag{2.35}$$

where γ is the Euler-Mascheroni constant $\gamma \approx 0.577$. These analytic results are summarized in the second column of Table 2.4.

The result for $\bar{\lambda}^*$ agrees with the two-loop perturbative result in [25]. Note, that the quartic coupling $\bar{\lambda}^*_K$ in [25] is related to this work's definition via $\bar{\lambda}^*_K = 3\bar{\lambda}^*$. The two-loop result for the anomalous dimension obtained in [25] differs from the result presented here by the factor 2/3. The difference originates from that the EAA RG method sums up

Quantity	Analytic result	Numerical result
$\bar{\kappa}^*$	$0.0047 + 0.009\epsilon$	$0.0048 + 0.01\epsilon$
$\bar{\lambda}^*$	17.5ϵ	16.5ϵ
$\bar{Y}^*$	$8.7 \times 10^{-4}\epsilon^3$	$8.9 \times 10^{-4}\epsilon^3$
η^*	$0.028\epsilon^2$	$0.028\epsilon^2$
ν	$0.5 + 0.083\epsilon$[25]	$0.51 + 0.095\epsilon$

Table 2.4: Position of the WF FP in the theory space $(\bar{\kappa}, \bar{\lambda}, \bar{Y})$ as well as the corresponding η^* and ν (truncation $M = 2$) in the NNLO level of the GE for dimension $d = 4 - \epsilon$ (for $\epsilon \ll 1$). The two-loop analytical result for ν is taken from Ref. [25].

an infinite number of loop corrections in a nonperturbative way. The Eq. (2.30) for the anomalous dimension here is the NNLO generalization of the NLO Eq. (5) in [26], thus, this discrepancy is independent of specific scheme, it should be generally present in the EAA method.

It is shown in Table 2.4, that the position of the WF FP and the critical exponent ν depend linearly, the anomalous dimension η depend quadratically on ϵ in the limit $\epsilon \to 0$, in agreement with [25, 27, 28]. It is also established here, that the WF FP is characterized by a non-vanishing coupling of the $\mathcal{O}(\partial^4)$ term which is of order ϵ^3 in the ϵ-expansion. Therefore, the inclusion of $\bar{Y}_k$ into the gradient expansion does not affect the leading-order terms of $\bar{\kappa}^*$, $\bar{\lambda}^*$, and η^* in their ϵ-expansion.

The WF FP has also been found numerically for several ($\mathcal{O}(100)$) values of ϵ in the interval $[10^{-7}, 10^{-1}]$, with equal logarithmic steps in ϵ. Plotting the fixed point values of the couplings and the critical exponents on log-log plots gave linear curves, hence their power law dependence ϵ has been established. This was followed by a polynomial fitting according to Eq. (2.34). The error of the fitting has been neglected, because the point was to reinforce the analytic results. This has been successful, the analytic and numerical results agree well, as can be seen in Table 2.4.

Dependence on the continuous dimension d

The dependence of the various quantities corresponding to the WF FP are presented here as functions of the continuous dimension d in the interval $2 < d < 4$. The RG evolution equations were solved numerically for trajectories in the bunch $\mathcal{B}$ and identifying the WF crossover region. The truncation $M = 6$ was employed and the correlation length's exponent ν was computed from the derivative relation $\nu_\beta^{-1} = -\partial\beta_{\bar{\kappa}}/\partial\bar{\kappa}|_{\bar{\kappa}^*,\bar{\lambda}^*,\bar{Y}^*}$ as in Ref. [26]. It is less time consuming to calculate this, than computing the entire eigenvalue spectrum of the stability matrix. The price is that the effect of the subleading and higher order scaling corrections are neglected. The results are summarized in Fig. 2.4. The qualitative behavior of $\eta^*(d)$ and $\nu(d)$ agree with the literature. It is known from Ref. [26]. The NNLO coupling $\bar{Y}^*$ exhibits positive values for $d_0 \approx 2.7 < d < 4$ with a maximum at $d_{max} \approx 3.0$ and has a zero at d_0. It descends to negative values as the dimension d is lowered, $d_0 > d > 2$ indicating that the Euclidean action is unbounded

from below in this range in the RG scheme used here. It was found in the generalized

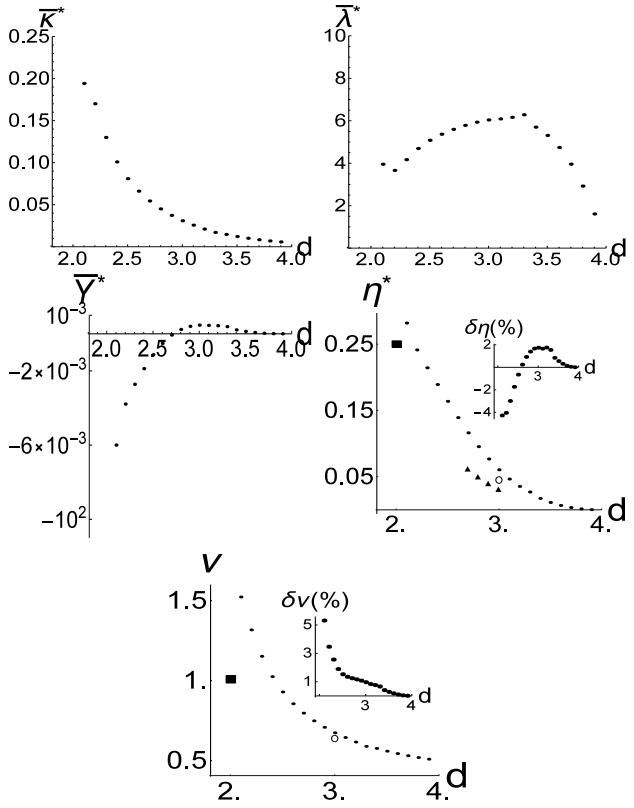

Figure 2.4: This works results for the typical quantities corresponding to WF FP plotted against the continuous dimension d in NNLO6. The values taken at $d = 4$ agree with the ϵ-expansion, eq. (2.35) for $\epsilon = 0$. The insets compare the NNLO effects to the NLO ones $\delta\eta = 100 \times (\eta^{NNLO} - \eta^{NLO})/\eta^{NNLO}$ and $\delta\nu = 100 \times (\nu^{NNLO} - \nu^{NLO})/\nu^{NNLO}$ on η and ν, respectively. For guiding the eye Onsager's exact results (full squares), the NNLOf results of [21] (full triangles), and the NLOu values taken from Table 5 of [17] (empty circles) have been shown on the plots.

proper-time RG framework, that when d decreases below $d \approx 8/3 \approx 2.67$, a competing critical point emerges in addition to the WF FP. In this scenario, the identification of the WF FP becomes numerically more involved [21]. The specific reason of the critical action becoming unbounded from below is not investigated here, it is out of the scope of the present work.

The trend of η^* obtained here shows quite a similar one as in the high-precision NNLO data in Table 5 in Ref. [21]. The insets of the plots of $\eta^*(d)$ and $\nu(d)$ in Fig. 2.4 show that the NNLO effect results in corrections not exceeding 2 per cents of the values of η and ν in the validity range $d_0 < d < 4$ of the applied RG scheme and it becomes increasingly important with decreasing dimension d in the interval $2 \leq d < d_0$. For $d = 2$, the presented results (at $d = 2.1$) deviate significantly from Onsager's exact values, but

one has to keep in mind that $d = 2$ lies out of the range of the validity of the employed RG scheme. The insets of Fig. 2.4 show also, that the NNLO effect on η^* tends to zero for dimensions $d = 4 - \epsilon$ with $\epsilon \to 0^+$, as an effect of $\mathcal{O}(\epsilon^3)$ on the quantity of $\mathcal{O}(\epsilon^2)$. Despite being small, the NNLO effects on η^* and ν may be comparable to the effect of the field-dependence of the wave function renormalization see for example, Refs. [15, 26]).

2.3 $O(N)$ models for $N \geq 2$ and $d = 3$

This section shows the reader, how the evolution equations generalize to the $O(N > 1)$ model. The numerical results contain the double-checking the stability of the polynomial expansion of the local potential as well as the analysis of the behavior of the higher derivative couplings. I also provide here the most valuable results of this chapter, the NNLO level results on the critical exponents of the $O(N > 1)$ models. Finally, I briefly examine the asymptotic behavior $N \to \infty$ of the $O(N)$ models.

2.3.1 Evolution equations

In the case of $O(N > 1)$ models, the dimensionless field-variable $\bar{r}$ is set to be defined via $\bar{r} = Z_{\perp k} k^{-(d-2)} r$. The wave function renormalization of the G-mode is chosen to be absorbed into the scale dependence of the field rather the one of the r-mode. The reason behind this is the resulting simplification of the terms in the flow equations, corresponding to the G-modes.

The flow equations are generated by my aforementioned code, from Eqs. (2.21)-(2.23). It is useful to show the evolution equations in the simple, NLO2 case,

$$\beta_{\bar{\kappa}} = -(d - 2 + \eta)\bar{\kappa} + \frac{2\alpha_d}{d}(3\hat{z}\bar{g}^2 + N - 1), \tag{2.36}$$

$$\beta_{\bar{\lambda}} = (d - 4 + 2\eta)\bar{\lambda} + \frac{2\alpha_d}{d}\bar{\lambda}^2[9\hat{z}\bar{g}^3 + 2(N - 1)], \tag{2.37}$$

$$\beta_{\hat{z}} = -\hat{z}(\bar{\eta} - \eta), \tag{2.38}$$

here $\bar{g}$ is the propagator corresponding to the radial mode $\bar{g} = (\hat{z} + 2\bar{\kappa}\bar{\lambda})^{-1}$ and the ratio $\hat{z} = Z_{\parallel k}/Z_{\perp k}$, as well as the anomalous dimensions via the relations

$$\dot{Z}_{\parallel k} = -\bar{\eta} Z_{\parallel k}, \quad \dot{Z}_{\perp k} = -\eta Z_{\perp k}, \tag{2.39}$$

where

$$\bar{\eta} = \frac{4\alpha_d}{d}\bar{\kappa}\bar{\lambda}^2\left[\frac{d-2}{d+2}\frac{N-1}{\hat{z}} + 9\hat{z}\bar{g}^4\left(1 - \frac{4\hat{z}\bar{g}}{d+2}\right)\right], \tag{2.40}$$

$$\eta = \frac{16\alpha_d}{d(d+2)}\bar{\kappa}\bar{\lambda}^2\hat{z}\bar{g}^2[d - 2\hat{z}\bar{g}]. \tag{2.41}$$

We see that assuming uniform wave function renormalization, one can work with the

single coupling $\hat{z}$ instead of the wave function renormalizations $Z_{\parallel k}$ and $Z_{\perp k}$ separately. This holds for the NNLO approximation too. However, the effect of both couplings are incorporated into $\hat{z}$. Should one take the field dependence of $\mathcal{Z}_k$ into account, it would be possible to distinguish the r- and G- modes' inverse propagator with one field dependent wave function renormalization. However, it is more intuitive, to distinguish the wave function renormalization of the radial field component and that of the transverse field components with different couplings.

2.3.2 Numerical results

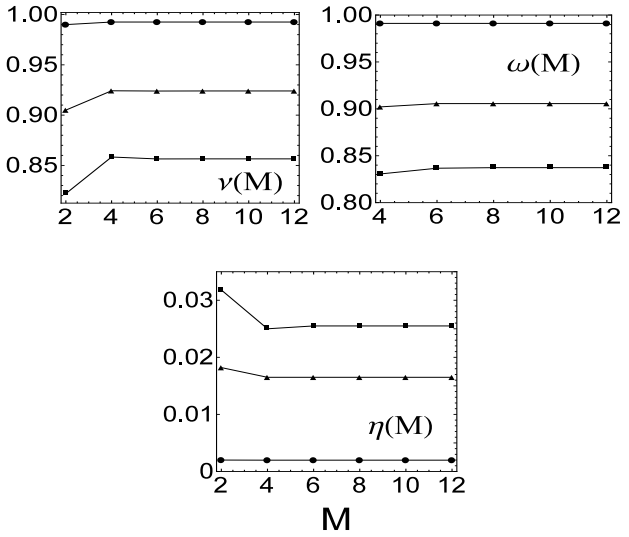

Figure 2.5: The dependence of ν, the subleading scaling exponent ω, and η on M in the NNLO approximation for the $O(5)$ (rectangle), $O(10)$ (triangle), and the $O(100)$ (circle) models.

The numerical investigation of the $O(N)$ models has been restricted to $d = 3$. The calculations have been performed with the polynomial truncation $M = 6$. The convergence of the various calculated exponents with increasing polynomial truncation M (see Fig. 2.5 and Table 2.5) have been tested. The effect of higher orders of the GE become negligible for asymptotically large N [29], and the results on the convergence of the polynomial expansion obtained at the LPA level in Refs. [14, 18, 19] get increasingly better for asymptotically large N. In the $N = \infty$ case, the LPA becomes exact.

The numerical integration of the RG flow has always been started from an $O(N)$ symmetric state, $Z_{\parallel\Lambda} = Z_{\perp\Lambda} = 1$ ($\hat{z}(\Lambda) = 1$) and with vanishing higher-derivative terms, $\bar{Y}_{\parallel\Lambda} = \bar{Y}_{\perp\Lambda} = 0$. The WF FP and computation of the corresponding quantities has been located numerically and performed by applying two different procedures: Procedure A and Procedure B. Both procedures had two steps like the one in the $O(1)$ case. Firstly, the RG evolution equations for the bunch $\mathcal{B}$ of the trajectories have been solved and thus the

	$\delta\nu$	$\delta\omega$	$\delta\eta$
$O(5)$	0.060	0.072	0.037
$O(10)$	0.001	0.022	0.0005
$O(100)$	0.0001	0.0019	0.00007

Table 2.5: The relative declination $\delta\alpha$ of the exponents $\alpha = \nu,\ \eta,\ \omega$ in per cents, with the definition in Table 2.1.

crossover region identified. Secondly, the fixed-point equations were solved. In Procedure A *(i)*, the $O(N)$ symmetry of the EAA has been enforced on the NLO level by setting $\hat{z} = 1$ at all scales, ($Z_{\parallel k} = Z_{\perp k}$) during the numerical integration of the trajectories and the FP was sought by setting $\hat{z}^* = 1$; and *(ii)* the evolution equations and the fixed-point equations have been solved by using of the explicit formulas for η and $\bar{\eta}$. The critical exponent ν has also been determined for various N values applying the same numerical procedure as in the case of the 3-dimensional $O(1)$ model. Let us emphasize, that by enforcing $\hat{z}^* = 1$, the β-function $\beta_{\hat{z}}$ decouples from the flow equations, as well as $\bar{\eta}$, the anomalous dimension of the radial mode. Only the G-mode anomalous dimension , η is present in the flow equations, hence only η affects the RG flow besides the higher derivative couplings. In Procedure B, *(i)* the ratio $\hat{z}$ has been set free to evolve, i.e., Eq. (2.38) has been included into the set of the evolution equations; and *(ii)* the fixed-point equations have been solved with setting $\hat{z}^* = \hat{z}(k_c)$, which was determined in the first step of the procedure; The scale k_c is the one for which $\bar{\kappa}(k_c) = 0$. The NNLO effect was investigated by means of both procedures.

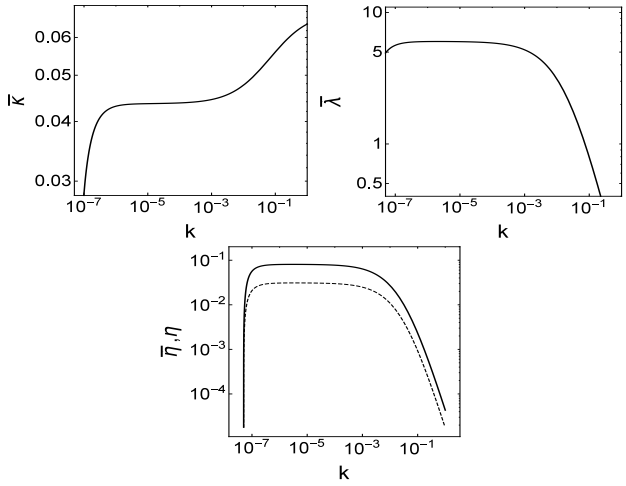

Figure 2.6: Scale-dependencies of the couplings $\bar{\kappa}$ and $\bar{\lambda}$ as well as $\bar{\eta}$ (solid black line) and η (dashed line) of the r- and G-modes, on the close-to-critical trajectories of the $O(2)$ model for dimension $d = 3$ in NNLO6 approximation, evaluated with $\hat{z}(k) = 1$.

The results of Procedure A are shown in Figs. 2.6, 2.7, 2.8, and 2.9 and the

obtained values for the characteristics of the WF FP obtained in NNLO6 are listed in Table 2.6.

N	$\bar{\kappa}^*$	λ^*	$10^4 \times Y_{\parallel}^*$	$10^4 \times Y_{\perp}^*$	$\bar{\eta}^*$	η^*	ν
0	0.014	9.40	11.0	7.0	0.045	0.0264	0.587
1	0.031	6.02	5.0	–	0.059	–	0.634
2	0.043	6.03	≈ 0.0	2.0	0.077	0.0320	0.700
3	0.057	5.35	2.0	0.4	0.085	0.0300	0.739
4	0.072	4.73	2.4	-0.6	0.088	0.0280	0.775
5	0.087	4.19	5.5	-1.0	0.090	0.0260	0.806
10	0.168	2.54	16.0	-1.6	0.095	0.0165	0.896
100	1.680	0.29	33.0	-0.3	0.099	0.0020	0.990

Table 2.6: The coupling's fixed point value at the WF FP, the critical exponent ν, and the anomalous dimensions $\bar{\eta}^*$ and η^* for the r- and G-modes, respectively, for various values of N in NNLO6 evaluated with $\hat{z} = 1$.

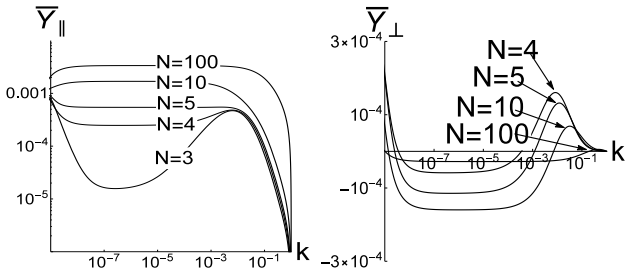

Figure 2.7: RG flow of the higher-derivative couplings $\bar{Y}_{\parallel k}$ and $\bar{Y}_{\perp k}$ for the r- and G-modes, respectively on near-critical trajextories. The different curves correspond to different values of N, all computed in the NNLO6 approximation, with $\hat{z} = 1$.

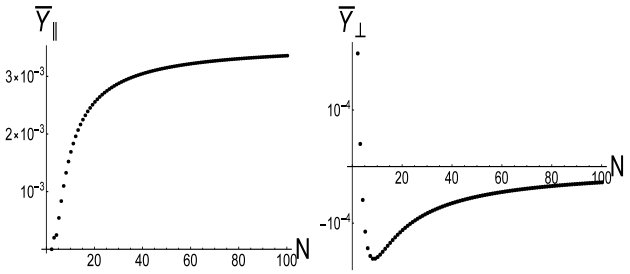

Figure 2.8: N-dependencies of the fixed point values of the higher-derivative couplings $\bar{Y}_{\parallel *}$ and $\bar{Y}_{\perp *}$ for the r- and G-modes, respectively, evaluated with $\hat{z} = 1$.

The couplings $\bar{\kappa}$, $\bar{\lambda}$ and the anomalous dimensions $\bar{\eta}$ and η show similar scale-dependencies for different N values in the region $2 \leq N \leq 100$ (see Fig. 2.6 for the typical

scaling). The trajectories at different $N > 2$, were fine-tuned to be equally close to the separatrix. It means, that we set the desired plateau width of $\bar{\kappa}$ and $\bar{\lambda}$ to be 4 orders of magnitude wide. The k_c values - which correspond to $\bar{\kappa}(k_c) = 0$ - decrease monotonically, for increasing N at a fixed plateau width. The 'plateau' values given in Table 2.6 differ from the corresponding fixed point solutions obtained by solving the fixed-point equations in the fourth digit of precision.

The crossover region is also present in the RG flow of the higher-derivative couplings $\bar{Y}_{\|k}$ and $\bar{Y}_{\perp k}$ (see Fig. 2.7). The 'plateaus' of the higher-derivative couplings are more susceptible to N. They broaden with increasing N (with the above discussed condition). Fig. 2.8 shows the N dependence of the values of the higher-derivative couplings at the WF FP. It means, that the 'plateau' values of $\bar{Y}_{\|k}$ increase monotonically and saturate, while those of $\bar{Y}_{\perp k}$ have a minimum at around $N \approx 10$ and saturate for large N too. It was found, that the higher-derivative coupling $\bar{Y}_{\perp k}$ of the G-modes exhibits negative fixed point values at the WF FP for $N > 3$ (see Figs. 2.7 and 2.8), hence the approximations used by us lead to a critical theory with action unbounded from below for $N > 3$. The origin of this problem is either the restriction to field-independence of the derivative couplings or the lack of even higher derivative terms in the EAA or the neglection of other higher derivative couplings, corresponding to independent NNLO level operators. The clarification of this problem requires further investigations in more sophisticated RG frameworks, which is out of the scope of the present work.

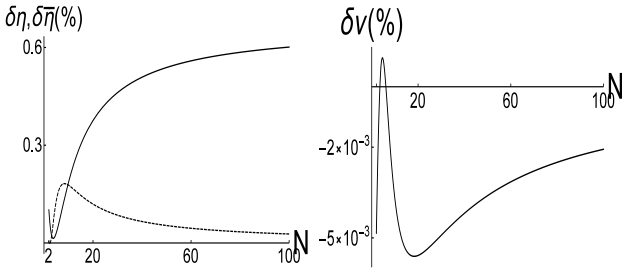

Figure 2.9: N-dependence of the NNLO effect on $\bar{\eta}^*$, η^*, and ν in the NNLO6, evaluated with $\hat{z} = 1$. The NNLO effect in per cents is given by $\delta f = 100 \times (f^{NNLO} - f^{NLO})/f^{NNLO}$ for $f = \bar{\eta}$ (solid line), $f = \eta$ (dashed line) in the left plot, and $f = \nu$ in the right plot.

Fig. 2.9 shows the NNLO effect in the $O(N)$ models with varying N. The running higher-derivative terms generally increase the values of the anomalous dimensions $\bar{\eta}^*$, η^* and decreases ν. The NNLO effect $\delta\eta$ on the anomalous dimension of the r-mode saturates for asymptotically large N values, but does not exceed 1 per cent, while the NNLO effect $\delta\bar{\eta}$ on the anomalous dimension of the G-modes dies out for large N values and never exceeds ~ 0.2 per cents. The NNLO effect $\delta\nu$, on ν dies out too with asymptotically increasing N, as LPA becomes asymptotically better approximation with increasing N.

The results presented here and obtained in Procedure A by means of the ansatz (2.3) (with eq. (2.4)) show a striking feature. The critical values of $\bar{\eta}^*$ and η^* turn out to be different, even in the NLO, despite the setting of $\hat{z} = 1$, which constraints the wave

function renormalizations for the r-mode and the G-modes to stay identical at all scales. The higher-derivative couplings $\bar{Y}_{\parallel k}$ and $\bar{Y}_{\perp k}$ for these modes differ as well, although their critical values remain 4 orders of magnitude smaller than the value $\hat{z} = 1$. A double-check to the validity of this procedure would be that the anomalous dimensions at the WF FP are identical and $\beta_{\hat{z}} = 0$ is fulfilled. However, the fixed-point equation $\beta_{\hat{z}} = 0$ is not satisfied even for $\hat{z} = 1$. When the WF FP values of $\bar{\kappa}_*$, $\bar{\lambda}_*$, $\bar{Y}_{\perp *}$, $\bar{Y}_{\parallel *}$ are inserted in the explicit formulas for $\bar{\eta}$ and η (like those in Eqs. (2.40) and (2.41)), the right-hand side of Eq. (2.38) is $\sim (\eta - \bar{\eta})$, which is $\approx -\bar{\eta}_*$ for large N. In the the presented RG framework, the critical theory preserves the $O(N)$ symmetry with the accuracy of $-\bar{\eta}$.

N	ν	ν[6]	ν 'best'	η^*	η [6]	η 'best'
0	0.587	0.589	0.5882 [25]	0.026	0.040	0.0284[25]
			0.58759700(40) [30]			
1	0.634	0.643	0.629971(4)[31]	0.059	0.044	0.0362978(20) [31]
2	0.700	0.697	0.6717(1) [32]	0.032	0.042	0.0381(2) [32]
3	0.739	0.747	0.7112(5)[33]	0.030	0.038	0.0375(5) [33]
4	0.775	0.787	0.749(2)[34]	0.028	0.034	0.0365(10)[34]
10	0.896	0.904	0.859 [35]	0.017	0.019	0.024 [35]
100	0.990	0.990	0.989[36]	0.002	0.002	0.0027[36]

Table 2.7: Comparison of this work's NNLO6u results (left columns) with LPA' results (see data ^{f} in Table 2 in Ref. [6]) of Wetterich's group (right columns), the latter computed with the usage of the exponential regulator.

Setting $\hat{z} = 1$ corresponds to an $O(N)$ symmetric ansatz for the EAA at the NLO level and allows one to make comparisons with LPA' results taken from Ref. [6]. The LPA' is also used in the literature to refer to approximation schemes, which - in hearth - are similar to the NLO approximation used here. Those LPA' results were computed without taking into account the term $(\vec{\phi}\partial\vec{\phi})^2$ in the ansatz, with different index structure so that LPA' agrees with the NLOu for $N \geq 2$ of this work. One can see in Table 2.7, that the present NNLOu results does not agree with the LPA' results of Ref. [6] although they show the same qualitative dependencies on N. For ν, the discrepancy is less than 2 per cents, while for the anomalous dimension η^* of the Goldstone modes, it is about 20 - 30%, but disappears for large N. These discrepancies are larger than the NNLO effect (see Fig. 2.9), they occur at the NLO level and are caused by the usage of different regulators. The RG results shown in Table 2.7 disagree generally with the world's best estimates without showing a monotonic dependence of these discrepancies on N. The most accurate FRG results seem to be achieved in the BMW approximation [37, 38] for the N-dependence of the scaling exponents and in NLOf and NNLOf of the GE for the critical exponents for $N = 1$ [21].

The N-dependence of the first three subleading scaling exponents have also been computed here, by diagonalizing the stability matrix at the WF FP [22]. The results are summarized in Table 2.8 and plotted in Fig. 2.10. The convergence of the calculated exponents with increasing order of polynomial truncation has been demonstrated (see $\delta\omega$ in Table 2.5). This work's LPA results show a smooth N-dependence like the LPA results of [19]. However, for $N = 1$, they spring out from the general trend of the data

at NLO and NNLO. The following explanation can be given: At NLO, thetheory space has to be extended with the wave function renormalization Z_k of the 'r-mode' for $N = 1$ and with the wave function renormalization $Z_{\perp k}$ of the G-modes for $N \geq 2$ (with the choice $\hat{z}_k = 1$). One can recognize in Table 2.6, that the anomalous dimension $\bar{\eta}^* = 0.059$ governing the flow of Z_k for $N = 1$ does not fit smoothly into the N-dependence of η governing the flow of $Z_{\perp k}$. This kind of difference of the $N = 1$ case may cause the different magnitude of the NNLO corrections for $N = 1$ and $N \geq 2$. Table 2.8 also shows that the flow of the gradient couplings affects the calculated values of ω, ω_2, and ω_3 in that order more and more significantly. Their NNLO results however tend to the LPA ones for increasing N and reproduce the correct asymptotic limits found in [19] (see Fig. 2.10).

N	ω^{LPA}	ω^{NNLO}	ω_2^{LPA}	ω_2^{NNLO}	ω_3^{LPA}	ω_3^{NNLO}
0	0.693	0.751	3.601	3.294	7.246	6.347
1	0.704	0.842	3.525	3.061	4.938	5.675
2	0.716	0.784	3.373	3.081	4.140	5.551
3	0.736	0.800	3.100	3.003	4.179	5.395
4	0.765	0.819	3.011	2.944	4.295	5.250
5	0.794	0.837	2.975	2.905	4.395	5.138
10	0.886	0.905	2.927	2.881	4.700	4.953
20	0.944	0.953	2.950	2.923	4.885	4.932
30	0.963	0.970	2.965	2.946	4.936	4.947
50	0.978	0.982	2.978	2.967	4.967	4.965
100	0.989	0.9910	2.988	2.983	4.986	4.980

Table 2.8: This work's LPA6 and NNLO6 results for the first three subleading scaling exponents.

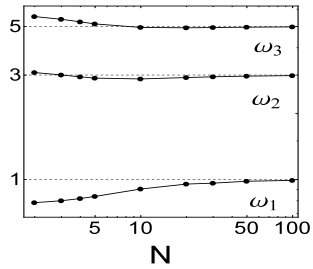

Figure 2.10: N-dependencies of the first three subleading scaling exponents at NNLO6.

It was reasonable, to repeat the analysis with Procedure B, when the ratio $\hat{z}$ also evolved, since Procedure A has shown the flaw of minimal explicit symmetry breaking. Even in Procedure B, a clear identification of the crossover scaling region in the vicinity of the WF FP can be made, independently of N. The r-mode propagators contain $\hat{z}$, which has a non-trivial scale dependence, it doesn't approach a plateau near the WF FP. It causes all the investigated quantities to exhibit a power-law scale-dependence ak^{α}

in the crossover region instead of keeping constant values. The ratio $\hat{z}$ increases strictly monotonically with decreasing scale k and evolves to the peak value $\hat{z}(k_c)$ - which is significantly larger than 1 - when the lower end of the WF crossover region is reached at the scale k_c, where $\bar{\kappa}(k_c) = 0$. The numerical values of the parameters a and α characterizing the power-law scaling of the various quantities were determined by fitting the scale-dependencies on the WF crossover region of close-to-separatrix trajectories. It has been established, that there exist WF FP solutions for fixed values of $\hat{z}^* = \hat{z}(k_c)$ for any N, where k_c belongs to the lower end of the crossover region. The fixed-point solutions reproduced the values of the corresponding parameters a with high precision. The ratio $\hat{z}$ has been found to scale as $\hat{z}(k) = \hat{z}^* k^{-[\bar{\eta}(k_c)-\eta(k_c)]}$ in the WF crossover region, in agreement with eq. (2.38).

Making use of the power-law dependencies of the various investigated quantities in the crossover scaling region, one my search for the WF FP, by using the results of the numerical integration of close to separatrix trajectories. For finding the FP, the initial conditions $\hat{z}(k_s)$, $\bar{\kappa}(k_s)$, etc. can be taken at some intermediate scale $k_s \in [k_c, k_u]$, where k_u is the scale at which the crossover region starts, i.e., the smallest value at which $\hat{z}(k_u) = 1$. It was found, on one hand, for $k_s = k_u$ these fixed-point values coincide the ones obtained in Procedure A. On the other hand, the inconsistency of the employed RG scheme, i.e., the non-vanishing of the beta-function $|\beta_{\hat{z}}(k_s)| \sim \mathcal{O}(\hat{z}(k_s)\bar{\eta}(k_s))$ is present for all scales k_s and for any $N \geq 2$. However, it is minimal at $k_s = k_u$, i.e., for Procedure A.

It can be seen that in the theory space, there is a quasi WF fixed line. The points of which can be parameterized by the values $\hat{z}^* = \hat{z}(k_s)$, the term quasi-fixed line refers to the presence of the increasing inconsistency with the choice of decreasing k_s values (which correspond to increasing values of $\hat{z}$). Holding on to the principle of minimal inconsistency, i.e., that explicit breaking of the $O(N)$ symmetry of the critical theory should be minimal, one has to identify the best estimate for the parameters of the WF FP as the ones obtained in Procedure A.

2.3.3 Asymptotic behavior for large N

	$\hat{z}_\infty = 1$		$\hat{z}_\infty = 5$	
	eq. (2.43)	NNLO6u	eq. (2.43)	NNLO6u
κ_∞	0.017	0.0168	0.017	0.019
λ_∞	29.6	29.0	29.6	30.0
$\bar{\eta}_\infty$	0.10	0.099	0.020	0.11
η_∞	0.20	0.20	0.074	0.32

Table 2.9: Comparison of the asymptotic behavior of our NNLO6u results with those evaluated on the asymptotic formulas in Eq. (2.43) for the ratios $\hat{z} = 1$ and $\hat{z} = \hat{z}^*$, at $N = 100$.

The behavior of the WF FP and the corresponding exponents have also been investigated for asymptotically large values of N. This suggests, that the critical theory

obtained in Procedure A should be favored as the physically realistic one. Neglecting the higher-derivative couplings, the trend of the data in Tab. 2.6 suggests the large N behavior

$$\bar{\kappa}^* \sim \kappa_\infty N, \quad \bar{\lambda}^* \sim \frac{\lambda_\infty}{N}, \quad \eta^* \sim \frac{\eta_\infty}{N}, \quad \bar{\eta}^* \sim \bar{\eta}_\infty, \quad \hat{z}^* = z_\infty, \tag{2.42}$$

where the star refers to the values corresponding to k_c, where the WF crossover region ends. Inserting the assumptions (2.42) into the fixed-point equations $\beta_{\bar{\kappa}} = \beta_{\bar{\lambda}} = 0$ and into (2.40) and (2.41), results in the constants

$$\begin{aligned}
\kappa_\infty &= \frac{2\alpha_d}{d(d-2)}, \quad \lambda_\infty = \frac{d(4-d)}{4\alpha_d}, \\
\bar{\eta}_\infty &= \frac{(4-d)^2}{2(d+2)z_\infty}, \quad \eta_\infty = \frac{2(4-d)^2}{d^2-4} z_\infty g_\infty^2 (d - 2z_\infty g_\infty), \\
g_\infty &= \left(z_\infty + \frac{4-d}{d-2} \right)^{-1}
\end{aligned} \tag{2.43}$$

for arbitrary value of $\hat{z}^* = \hat{z}(k_\mathrm{c}) = z_\infty$ in the leading order of N. These asymptotic relations have been checked on the base of this work's numerical NNLO results at $N = 100$ and $d = 3$ in Procedure A with $z_\infty = 1$ and in Procedure B with $z_\infty = 5$. The constants occurring in the asymptotic relations (2.42) are given in Table 2.9. The comparison shows that the Procedure A NNLO6 values for the anomalous dimensions are in agreement with the analytically predicted large N behavior, while there is discrepancy for Procedure B.

In order to locate fixed points of the $O(N)$ models for large N, the flow equations (2.21), (2.22), and (2.23) can be rewritten into

$$\dot{u}_k(\bar{r}) \quad = \quad \frac{1}{2} \int_p G_\perp(p^2) \dot{R}_{\perp k}(p^2) + \mathcal{O}(1/N), \tag{2.44}$$

$$\begin{aligned}
\dot{\mathcal{Z}}_{\parallel k}(Q^2) = \int_p \bar{r} \Big[& 2[u_k'']^2 G_\perp^2(p^2) G_\perp((Q-p)^2) \dot{R}_{\perp k}(p^2) \\
& - \Big(2u_k'' G_\perp^3(p^2) - u_k''' G_\perp^2(p^2) \Big) \dot{R}_{\perp k}(p^2) \Big] + \mathcal{O}(1/N),
\end{aligned} \tag{2.45}$$

$$\dot{\mathcal{Z}}_{\perp k}(Q^2) \quad = \quad \mathcal{O}(1/N), \tag{2.46}$$

respectively, in terms of the rescaled variable $\bar{r} = r/N$ and potential $u_k = U_k/N$. The r- and G-mode propagators keep their form given in Eqs. (2.13) and (2.14), but with $U_k(r)$ replaced by $u_k(\bar{r})$. It is easy to spot, that during the RG-flow, the momentum dependent wave function renormalization of the G-modes, $\mathcal{Z}_{\perp k}(Q^2)$ does not pick up quantum corrections, while the flow of the wave function renormalization of the r-mode decouples from the flow of the potential in the limit $N \to \infty$, because the flow equations contain only the anomalous dimension corresponding to the transverse modes and the

propagators of the transverse modes, which are independent of $\hat{z}$. In the $N \to \infty$ limit, there are infinitely many transverse modes, which suppress completely the single radial mode.

In agreement with Procedure A, the FP equations even in NLO and NNLO reduce to the single FP equation for the potential in the limit $N \to \infty$ and this provides the flow equations (2.12)-(2.14) in [39] for the couplings for the polynomial truncation $M = 3$. We can also recover the Bardeen-Moshe-Bander fixed point [40, 41] for the polynomial truncations $M \geq 3$ for $\bar{\kappa} = 1$, $\bar{\lambda} = 0$, and $\bar{g}_3 =$arbitrary (accommodating the notations of [39]). We have found, that the higher-order couplings of the potential are polynomials of $\bar{g}_3$, e.g., $\bar{g}_4 = -6\bar{g}_3^2$, $\bar{g}_5 = 60\bar{g}_3^3$, $\bar{g}_6 = -30(28\bar{g}_3^4 - \bar{g}_3^3)$, etc. The fixed points for $O(N)$ models with finite but large N has also been looked for in this work. The range from 100 to 10^5 has been scanned, by solving the flow equation (2.21), (2.22), and (2.23) as well as the corresponding fixed-point equations. The presence of the Gaussian and WF FPs have been recovered, but no other nonperturbative fixed points like those suggested in [29] have been found.

Chapter 3

Phase structure of the $O(2)$ ghost model with higher-order gradient term

This chapter is based on [**B**] and [**C**]. I talk about the motivation of this work first, which is followed by the outlining of the results. The outline is then followed by the detailed derivation and analysis of the premised results.

3.1 Motivation

Models, which contain gradient terms with alternating signs give rise to periodic ground state configurations. There are various models in solid state physics and quantum field theory, in which the ground state exhibits a periodic structure, because the periodic vacuum provides a deeper minimum of the effective action than the homogeneous one. Such cases are, for example, the Larkin-Ovchinnikov-Fulde-Ferrell type spatially inhomogeneous superconducting states [64, 65], the phase with periodically modulated chiral fields in effective chiral quark models [66, 67], the spin waves in the Heisenberg ferromagnet [68], and the charged massive Schwinger model [69] (see further examples for periodic ground states in Ref. [7] of [69]). It has been speculated that the Liouville field theory also possesses a periodic ground state [42, 43, 44]. Inhomogeneity of the ground state suggests that strongly distance-dependent interactions should be present in the system. It is reasonable to expect that for such interactions the gradient terms with sufficiently strong couplings are responsible rather than the ultralocal potential terms in the effective action. In such models, the expectation value of the kinetic-energy operator is nonvanishing, which is constructed from the derivatives of the fundamental fields. The nonvanishing expectation value arises generally due to the alternating signs of the gradient terms of various orders (see [53, 54, 55, 56] and Ref. [7] of [69]). This so-called kinetic condensation means

that quasiparticles with non-zero momentum appear and condense forming a periodic classical background field, which breaks spatial symmetries of the system spontaneously. As opposed to this, in the case of the Nambu-Goldstone type spontaneous symmetry breaking quasiparticles with vanishing momentum condense into a homogeneous classical background field.

In modern quantum gravity research much attention has been paid to the role of such ghosts, e.g. [70]-[77], [78]-[85], [86, 87, 88, 89, 90, 91]. In various cosmological scenarios close to the Planck scale and beyond it the conformal factor in the Einstein-Hilbert action makes the action unbounded from below and appears to be a ghost scalar model [45, 46]. The kinetic condensation of the conformal factor can cure the unboundedness. The kinetic condensation in the simple ghost complex scalar $U(1)$ model has some relevance in studies of the conformal degree of freedom in gravity and has been discussed in [90, 91]. There, the simplicity of the model allowed to find analytically the true ground state and to calculate the scale dependence of the EAA and therefore the scale dependence of the dressed inverse propagator by the means of the saddle-point approximation. The ground state has proven to be a family of plane waves which causes the spontaneous breaking of the $U(1)$ symmetry and also that of the rotational and translational symmetries in spacetime, because of the fixed phase and wave vector of the given ground state. They have also found, that the renormalization effects are dominated by the instability of the trivial saddle point, rather than by the quantum fluctuations. It is shown in [**B**], that in the terms of the WH RG scheme, an $U(1)$ symmetric model is equivalent with a $O(2)$ symmetric one. The goal of [**B**] and [**C**] is to pursue the investigation of the ghost condensation on a more sophisticated $O(2)$ symmetric model than in [90, 91] in the terms of the FRG.

3.2 Outline

The purpose of this chapter is to discuss the appearance and the behavior of a possible ghost condensate. The two articles both discuss the phase structure of the Euclidean, 3-dimensional $O(2)$ symmetric ghost model in two different approaches. For better transparency, they are merged here into a single chapter. Wegner and Houghton's renormalization group (WH RG) framework and the tree-level renormalization procedure (TLR) have been applied to investigate the model, with special attention to its infrared (IR) behavior. The advantage of Wegner and Houghton's scheme is the clear distinction of handling the ultraviolet (UV) and the infrared (IR) modes of the field variable. The applicability of the WH RG however, may break down at certain cases and scales (see Sect. 1.3.1), from where the RG flow is handled by the TLR procedure in order to map the deep IR behavior of the trajectories. It is also known, that the WH RG scheme is restricted to the local potential approximation (LPA). The investigated model consists of two pieces, a local $O(2)$ symmetric potential term and of course, the kinetic energy term:

$$S_k[\phi] \;=\; \frac{1}{2}\int d^3x\Big(\phi_x\Omega(-\Box)\phi_x\Big) + \int d^3x U_k(\phi^2), \tag{3.1}$$

where $\Box$ refers to the 3-dimensional Laplace operator and the bare action is defined on the UV scale $k = \Lambda$. The ordinary $O(2)$ symmetric model possesses the kinetic energy operator $\Omega(\Box) = Z(-\Box)$, with $Z = 1$. We, however modified it to

$$\Omega(\Box) = -Z\Box + Y\Box^2. \tag{3.2}$$

The usual quadratic gradient term is complemented with a quartic one. The reason of this, is that we want to study not the ordinary model, but its ghost counterpart. Throughout both [**B**] and [**C**], when the ghost (ordinary) model is discussed, the coupling Z is going to be set $Z = -1$ ($Z = +1$). This would cause the action to be unbounded from below as well as the appearance of propagators with 'wrong' sign, which are called ghosts in the quantum field theory jargon. The quartic gradient term, with $Y > 0$ is added in order to stabilize the model energetically and thus to acquire physically sensible results. I mentioned, that Z is kept constant throughout the work presented here so is the higher order gradient coupling. The natural dimension of Y corresponding to $\Box^2$ is mass^{-2}. The coupling Y is therefore UV irrelevant, i.e. perturbatively nonrenormalizable. Nevertheless, ghost condensation – when it takes place at some scale $k^2 \approx (Z/Y)$ – plays a definitively decisive role in the low energy (IR) physics of the model, that is, the coupling Y may become IR relevant. The wave function renormalization Z is dimensionless in LPA, thus it can be kept constant unambiguously. There occurs, however, an ambiguity when the couplings of higher-derivative terms are accounted for which have non-vanishing momentum dimensions. It corresponds to different approximations or RG schemes to keep either the dimensionful, or the dimensionless higher-derivative couplings constant. The difference between [**B**] and [**C**] lies in how Y is treated.

In article [**B**], the dimensionful higher order gradient coupling Y is kept on constant value. Throughout this chapter, in order to avoid discrepancy, this is going to be referred to as Case Y. In this case, the dimensionless coupling $\tilde{Y} = Yk^2$ tends to zero during the RG flow. Its interplay with the flow of the mass term of the potential severely affects the scale at which the dimensionless inverse propagator may vanish. Note, that with a dimensionful coupling in the β-functions, no fixed points can be determined. Nevertheless, the global RG flow enables one to identify the phases determining their different infrared scaling behavior and/or sensitivity to the bare parameters of the model. The massive sine-Gordon model was successfully treated in a similar approach in [52]. With this treatment, we have found a symmetric phase, where no ghost condensation occurs and a phase with restored symmetry but with a transient presence of a ghost condensate have been identified. It has also been established, that the correlation length remains finite when the phase boundary is approached in the restored symmetry phase. As opposed to this, it diverges in the symmetric phase. This discontinuity hints to a phase transition of first order. The results for the ghost model are compared with its ordinary counterpart.

In article [**C**], the dimensionless higher order gradient coupling $\tilde{Y}$ is kept on constant value. This scenario is going to be referred in the present chapter as Case $\tilde{Y}$. In this approach, the dimensionful coupling blows up in the IR, according to $Y = \tilde{Y}k^{-2}$. It is now possible, to identify fixed points. It is established here, that the addition of the higher derivative coupling provides three phases with an emergent triple point. We have also identified the types of phase transitions. Phase I is present for any values

$\tilde{Y} > 0$, it is similar to the symmetric phase of the ordinary O(2) model. Phase II is present, when $0 \leq \tilde{Y} \leq 1$. The dimensionful effective potential in phase II is quasi-universal, it depends on $\tilde{Y}$, yet it is independent of the other bare couplings. Phase II has no analogue in the ordinary O(2) model, however it has the same properties as the symmetry restored phase, found in [**B**]. Its existence is based on the ghost-condensation mechanism available in the model with $Z < 0$ and $\tilde{Y} > 0$. Phase III can be found in the range $1 < \tilde{Y} \leq 2$. Here, the dimensionful effective potential is universal, it exhibits the Maxwell cut which is accompanied with the non-vanishing amplitude of the periodic spinodal instability for scales $k \to 0$. Therefore phase III is the one in which spontaneous symmetry breaking occurs, just like in the symmetry breaking phase of the ordinary $O(2)$ model. The phase boundaries III-I and III-II intersect in a triple line. It has been found, that phase transitions II $\to$ I and III $\to$ II are of first order, while III $\to$ I is a continuous one.

The phase structure of the model turned out to be richer, when the dimensionless higher-derivative coupling $\tilde{Y}$ is kept constant along the RG flow than in the case when the dimensionful coupling Y is kept constant. Thus, it remains an open question, whether the model exhibits two or three phases. The ambiguity of keeping constant either the dimensionful or the dimensionless higher-derivative coupling is an essential feature of the LPA and it cannot be avoided in the WH RG approach [11]. Articles [**B**] and [**C**] demonstrates that such an ambiguity may affect the physical results severely when higher-derivative terms are included into the model. No such ambiguity should occur if one goes beyond the LPA in the gradient expansion.

In these works, I have contributed to the derivation of the formulas. I have written programs, one which is able to integrate the flow equations of the model, and one in which I implemented the algorithm for the tree level renormalization, both applicable to the different approaches of the two articles. I provided the numerical data and contributed to its analysis and interpretation as well as I made the plots present in the papers.

3.3 One component scalar field models

This section introduces the ghost and ordinary $O(1)$ models, the former will be straightforwardly generalized in the following section, while the latter is used as a benchmark for testing the numerical apparatus of the tree level renormalization. The two dimensional, Euclidean sine-Gordon model is also used for further testing.

3.3.1 Blocking transformation

In the LPA, the blocked action for the one-component scalar field $\phi(x)$ in 3-dimensional Euclidean space is

$$S_k[\phi] \quad = \quad \frac{1}{2}\int d^3x\Big(\phi_x\Omega(-\Box)\phi_x\Big) + \int d^3x U_k(\phi^2), \tag{3.3}$$

where k is the running cutoff, $Z = 1$ or -1, $Y \geq 0$, and $U_k(\phi)$ is the blocked potential. Note that the ordinary $O(1)$ model is retained by setting $Z = 1$ and $Y = 0$. There may be two qualitatively different situations, depending on whether the second functional derivative of the blocked action *(i)* is positive definite or *(ii)* it starts to develop zero eigenvalues. In case *(i)*, the saddle point is at $\phi' = 0$ and in the limit $\Delta k \to 0$ one arrives to the WH equation

$$k\partial_k U_k(\Phi) \quad = \quad -\alpha k^3 \ln\Big(\Omega(k^2) + \partial_\Phi^2 U_k(\Phi)\Big) \tag{3.4}$$

in the LPA, where $\Omega(k^2) = Zk^2 + Yk^4$ and $\alpha = \Omega_3/[2(2\pi)^3] = 1/(4\pi^2)$ with the solid angle $\Omega_3 = 4\pi$. In the LPA, the spatial dependence of the field variable is neglected which means, that

$$\phi_x \equiv \Phi, \quad \text{or in momentum space} \quad \tilde{\phi}_p = \Phi\delta_{p,0}, \tag{3.5}$$

where Φ is a constant with momentum dimension $[\Phi] = \frac{d-2}{2}$ in d Euclidean dimensions. Practically, Eq. (3.4) is the Eq. (1.10) taken at $d = 3$, and $\hbar = 1$ with the modified kinetic energy operator.

Given the Z_2 symmetry is unbroken, the RG trajectories can be followed up by means of Eq. (3.4) from the UV scale $k = \Lambda$ down to the IR limit $k \to 0$. In the symmetry broken phase, at some finite scale k_c the situation *(ii)* comes in effect. This is signaled by the vanishing of the argument of the logarithm in the right-hand side of Eq. (3.4). The system develops a new, non-trivial saddle point, that minimizes the blocked action. Eq. (3.4) loses its validity when $k \leq k_c$ and one has to turn to the TLR procedure and rewrite the blocking relation (1.6) into the form

$$S_{k-\Delta k}[\phi] \quad = \quad \min_{\phi'} S_k[\phi + \phi'], \tag{3.6}$$

It is convenient to reduce the functional space to one which contains plain waves as saddle-point configurations ϕ':

$$\psi_k(x) \quad = \quad 2\rho\cos(kn_\mu(k)x_\mu + \theta(k)). \tag{3.7}$$

Now, the action $S_k[\phi+\psi_k]$ becomes a function of the amplitude ρ. Here $n_\mu(k)$ is a spatial unit vector and $\theta(k)$ is a phase shift. We are going to denote the value of the amplitude of the saddle-point configuration for which the action $S_k[\phi+\psi_k]$ takes its minimum value with ρ_k. Note, that various saddle points of the system corresponding to various values of $n_\mu(k)$ and $\theta(k)$ are physically not equivalent but are expected to belong to the same

minimal value of the blocked action. Upon inserting ansatz (3.7) into (3.6) one finds

$$U_{k-\Delta k}(\Phi) \quad = \quad \min_{\{\rho\}}\left(\Omega(k^2)\rho^2 + \frac{1}{2}\int_{-1}^{1} du U_k\big(\Phi + 2\rho\cos(\pi u)\big)\right). \tag{3.8}$$

Due to spatial $O(3)$ symmetry, the expression in the braces in the right-hand side of Eq. (3.8) only depends on ρ.

3.3.2 Polynomial potential

For the local potential chosen in the Taylor-expanded form, the most commonly used expansion is Eq. (1.11). For convenience, we are going to use the following equivalent expansion

$$U_k(\Phi) \quad = \quad \sum_{n=0}^{M} \frac{v_n}{n!} r^n, \tag{3.9}$$

with $r = \frac{1}{2}\Phi^2$. The couplings from eq. (1.11) are related to the ones in (3.9) $g_{2n} = \frac{(2n)!}{n!2^n} v_n$. For truncation $M = 2$, one finds the following β-functions for the running dimensionless couplings in Case Y:

$$\begin{aligned} \beta_1^{(Z)} = k\partial_k \tilde{v}_1 &= -2\tilde{v}_1 - a\alpha \frac{\tilde{v}_2}{\tilde{v}_1 + Z + Yk^2}, \\ \beta_2^{(Z)} = k\partial_k \tilde{v}_2 &= -\tilde{v}_2 + b\alpha \frac{\tilde{v}_2^2}{(\tilde{v}_1 + Z + Yk^2)^2} \end{aligned} \tag{3.10}$$

In the other scenario, Case $\tilde{Y}$, the β-functions are

$$\begin{aligned} \beta_1^{(Z)} = k\partial_k \tilde{v}_1 &= -2\tilde{v}_1 - a\alpha \frac{\tilde{v}_2}{\tilde{v}_1 + Z + \tilde{Y}}, \\ \beta_2^{(Z)} = k\partial_k \tilde{v}_2 &= -\tilde{v}_2 + b\alpha \frac{\tilde{v}_2^2}{(\tilde{v}_1 + Z + \tilde{Y})^2} \end{aligned} \tag{3.11}$$

with $a = 1$ and $b = 3$; the upper index Z indicates the dependence of the beta-functions on the wave function renormalization Z. The dimensionless couplings $\tilde{v}_1$ and $\tilde{v}_2$ are defined by $v_1 = k^2\tilde{v}_1$ and $v_2 = k\tilde{v}_2$ through their natural dimension. The phase structure and the scaling laws in the various scaling regimes do not alter qualitatively with increasing truncation M, beyond $M = 2$. That is, we shall work with $M = 2$ when solving the WH RG equations in Case Y. However, we have improved this to $M = 10$ in Case $\tilde{Y}$ (chronologically, the investigation of Case $\tilde{Y}$ happened after Case Y). In both cases we solve the WH RG equations with fourth order Runge-Kutta method.

The RG trajectories belonging to the symmetry broken phase can be followed by the WH RG equation down to the scale k_c, where the right-hand side of Eq. (3.4) becomes singular. In order to determine the IR scaling laws in this phase, one has to exploit the tree-level renormalization. This allows to follow the RG trajectories below the

critical scale k_c down to the IR limit $k \to 0$. The same TLR procedure can be extended for ghost models with kinetic energy operator $\Omega(-\Box)$ in a straightforward manner as follows. For scales $k < k_c$, the spinodal instability occurs in Case Y, when the logarithm in the right-hand side of Eq. (3.4) satisfies the inequality

$$Z + Yk_c^2 + \tilde{v}_1(k_c) + \frac{3}{2}\tilde{v}_2(k_c)\tilde{\Phi}^2 \quad \leq \quad 0, \tag{3.12}$$

while in Case $\tilde{Y}$ it occurs, when

$$Z + \tilde{Y} + \tilde{v}_1(k_c) + \frac{3}{2}\tilde{v}_2(k_c)\tilde{\Phi}^2 \quad \leq \quad 0, \tag{3.13}$$

The last term in the left-hand side of the inequalities is positive, thus the singularity first occurs at $\Phi = 0$ with decreasing scale k, when the condition $Z + Yk_c^2 + \tilde{v}_1(k_c) = 0$ or $Z + \tilde{Y} + \tilde{v}_1(k_c) = 0$ is satisfied, respectively. For $Z = +1$ and $Y = 0$, this results $1 + \tilde{v}_1(k_c) = 0$ in both cases. Generally, there exists such a scale k_c in the symmetry broken phase. This critical scale is governed by the negative (dimensionless) mass squared in the potential. For $Z = -1$ and $Y = 0$ we find the condition $-1 + \tilde{v}_1(k_c) = 0$ for k_c in both cases again. Notice, that this condition is met with positive mass term of the potential. Straightforwardly, with $Z = -1$, $Y > 0$ the condition for occurring the singularity becomes $-1 + \tilde{v}_1(k_c) + Yk_c^2 = 0$ or $-1 + \tilde{v}_1(k_c) + \tilde{Y} = 0$ for Cases Y and $\tilde{Y}$, respectively, meaning that an interplay of the quartic gradient term and the mass term determines the scale k_c. In Case Y, supposing that $\tilde{v}_1(k_c) < 0$ holds, the critical scale is $k_c^2 = [1 - \tilde{v}_1(k_c)]/Y$ and for a small mass squared, i.e. $|\tilde{v}_1(k_c)| \ll 1$, it yields $k_c^2 \sim \mathcal{O}(1/Y)$. In such cases ghost condensation in the modes with $k < k_c$ takes place and may play a decisive role in the behavior of the phase in the deep infrared region. In Case $\tilde{Y}$, k_c is not present explicitly in (3.13), so the critical scale is determined solely through the numerical integration of the β-functions. Below k_c, an interval in Φ emerges and expands as k is further decreased. The borders of this interval are symmetric and their magnitude, the critical field value is denoted as $\Phi_c(k) = \sqrt{k}\tilde{\Phi}_c(k)$. $\tilde{\Phi}_c$ is acquired from (3.12) and (3.13) in Cases Y and $\tilde{Y}$ respectively if one replaces the inequality with equality and k_c with k. In Case Y, it is

$$\tilde{\Phi}_c(k) \quad = \quad \sqrt{2[-Z - Yk^2 - \tilde{v}_1(k)]/3\tilde{v}_2(k)}, \tag{3.14}$$

while in Case $\tilde{Y}$, it is

$$\tilde{\Phi}_c(k) \quad = \quad \sqrt{2[-Z - \tilde{Y} - \tilde{v}_1(k)]/3\tilde{v}_2(k)}, \tag{3.15}$$

The interval $|\Phi| \leq \Phi_c(k)$ survives the limit $k \to 0$ if and only if $\sqrt{k}\tilde{\Phi}_c(k)$ assumes a non-zero or infinite limit which restricts the IR scaling of the couplings $\tilde{v}_1(k)$ and $\tilde{v}_2(k)$.

For scales $k < k_c$ and background fields $\Phi \in [-\Phi_c, \Phi_c]$ one has to turn to the tree-level blocking relation (3.8). Inserting the ansatz (3.9) into it, it yields the recursion

equation in Case Y

$$U_{k-\Delta k}(\Phi) = \min_{\{\rho\}}\left(U_k(\Phi) + (Z + Yk^2)k^2\rho^2 + \sum_{n=1}^{M}\frac{\rho^{2n}}{(n!)^2}\partial_\Phi^{2n}U_k(\Phi)\right), \quad (3.16)$$

In Case $\tilde{Y}$, the recursion equation is

$$U_{k-\Delta k}(\Phi) = \min_{\{\rho\}}\left(U_k(\Phi) + (Z + \tilde{Y})k^2\rho^2 + \sum_{n=1}^{M}\frac{\rho^{2n}}{(n!)^2}\partial_\Phi^{2n}U_k(\Phi)\right), \quad (3.17)$$

for the running couplings [47]. For given scale k with given couplings $v_n(k)$ and for given homogeneous field $\Phi \in [-\Phi_c, \Phi_c]$, one determines the value $\rho_k(\Phi)$, which minimizes the right-hand side of Eq. (3.16). This minimization has to be iterated for several Φ values in the critical interval, yielding several $U_{k-\Delta k}(\Phi)$ values. Lastly, these $U_{k-\Delta k}(\Phi)$ values are fitted by the polynomial (3.9) in the critical interval, in order to read off the value of the couplings in the lower scale $v_n(k - \Delta k)$. In such an iterative manner the behavior of the RG trajectories can be investigated in the deep infrared region. This numerical procedure converges for sufficiently small values of the ratio $\Delta k/k$. The blocked potential $U_{k<k_c}(\Phi)$ outside of the interval $-\Phi_c \leq \Phi \leq \Phi_c$ should be set to be identical to $U_{k_c}(\Phi)$, because no tree-level renormalization occurs there[47]. In Sec. 3.4.1 it is argued, that the TLR of the ghost scalar field with $O(2)$ symmetry can be reduced to the case of the TLR of the real one-component ghost scalar field, when one one is looking for the non-trivial saddle-point configuration in an appropriately reduced functional space. Numerical study of that case can be found in Sec. 3.4.2.

Here, the numerical procedure for TLR is tested, by applying it to the 3-dimensional Euclidean polynomial model of the ordinary one-component scalar field with $O(1)$ symmetry ($Z = 1$, $Y = 0$). The truncation of the polynomial potential was set to $M = 10$ for the fitted potential, this way good numerical convergence was achieved when the step size $\Delta k/k = 0.001$ was used. The least square fitting method was applied with the number 60 of equidistant grid points in the interval $-\Phi_c(k) \leq \Phi \leq \Phi_c(k)$. It has been established, that the results are stable against increasing the number of grid points. Numerically, in order to get a better least square fit, the TLR procedure has been performed in a wider interval $\Phi \in [-\bar{\Phi}, \bar{\Phi}]$ (than the critical interval) with $\bar{\Phi} = \sqrt{-2v_1(k_c)/3v_2(k_c)}$. The latter approximates $\Phi_c(k)$ well for $k \ll k_c$ [47]. It has been found numerically, that the blocked potential does not pick up any tree-level correction outside of the interval of instability $\Phi \in [-\Phi_c(k), \Phi_c(k)]$.

According to this work's numerical results shown in Fig. 3.1, the dimensionful blocked potential $U_k(\Phi)$ tends to and reaches the Maxwell-construction in the limit $k \to 0$, as expected from the literature [47, 48].

Fig. 3.2 shows the numerically computed $\rho_k(\Phi)$ for the scale $k \approx 10^{-6}$, it is compared with the curve $\rho_k(\Phi) = (-\Phi + \Phi_c)/2$, from Ref. [47]. The slope of the shown $\rho_k(\Phi)$ is -0.53, which agrees with its theoretical value -0.5 very well. The dimensionful amplitude ρ_k of the spinodal instability survives the IR limit with $2\rho_{k\to 0}(\Phi = 0) \approx \Phi_c$. This means, that on vanishing background $\Phi = 0$, the instability pushes the field configuration to the homogeneous one at either $\psi_{k\to 0} = 2\rho_{k\to 0}(0) = \Phi_c$ or $-\Phi_c$, both of

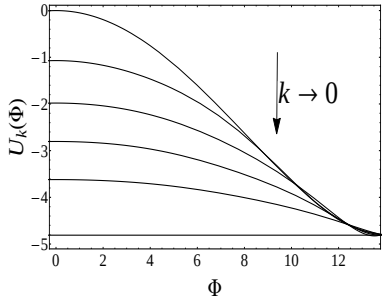

Figure 3.1: The blocked potential at various scales k.

them belonging to the same constant value of the effective potential.

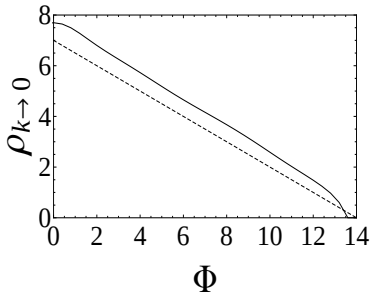

Figure 3.2: This works numerical result for $\rho_k(\Phi)$ in the IR limit $k \to 0$ (solid line) in comparison with the one shown in [47] (dashed line).

The infrared scaling of the couplings has also been established. The scaling of the dimensionless couplings $\tilde{v}_1 + 1 \sim k^{\alpha_1}$, $\tilde{v}_2 \sim k^{\alpha_2}$, and $\tilde{v}_3 \sim k^{\alpha_3}$ have been numerically determined corresponding to Φ^2, Φ^4, and Φ^6, respectively (see Fig. 3.3) yielding the following scaling exponents: $\alpha_1 = 0.08 \pm 0.08$, $\alpha_2 = 1 \pm 0.001$, and $\alpha_3 = 1.34 \pm 0.01$. The errors of α_2 and α_3 arise from the double logarithmic fit. Note, that the RG flow of $1 + \tilde{v}_1(k)$ is slowed down tremendously in the deep infrared region, that is, the numerical computation of the exponent α_1 may have an error comparable to its magnitude. However, the numerical results established, that $\Phi_c(k) \sim \sqrt{k k^{\alpha_1 - \alpha_2}}$ is infrared finite. This restricts α_1 with the equation $1 + \alpha_1 - \alpha_2 = 0$, which implies $\alpha_1 \approx 0$ with high accuracy.

It is known, that $\tilde{v}_1(k) \to -1$ and $\tilde{v}_{n>1} \to 0$ in the IR limit $k \to 0$, thus, the limit corresponds to the RG invariant effective potential $\tilde{U}_{k\to 0}(\tilde{\Phi}) = -\frac{1}{2}\tilde{\Phi}^2$ in the interval $[-\tilde{\Phi}_c, \tilde{\Phi}_c]$ [47]. In the presented numerical calculations, the coupling $\tilde{v}_1(k)$ tends to a constant value in the infrared limit, close to -1. It turned out, that this value tends to -1 linearly with decreasing step size $\Delta k/k$. The IR limit of $\tilde{v}_1(k)$ was calculated for five different step sizes, and the extrapolation to $\Delta k/k \approx 0$, shown in Fig. 3.4 resulted the extrapolated value $\tilde{v}_1^{ext}(0) = -1.005$.

This work's numerical results for the IR behavior of the ordinary $O(1)$ scalar

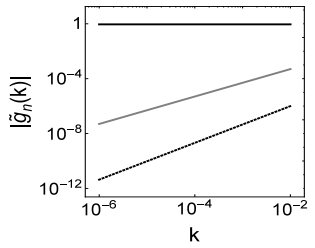

Figure 3.3: Scaling of the dimensionless couplings $\tilde{g}_2 = \tilde{v}_1$ (solid black line), $\tilde{g}_4 = 3\tilde{v}_2$ (solid gray line) and $\tilde{g}_6 = 15\tilde{v}_3$ (dashed black line).

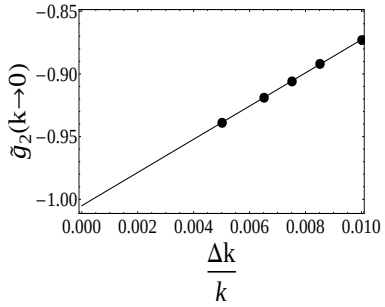

Figure 3.4: The value of $\tilde{g}_2 = \tilde{v}_1$ in the limit $k \to 0$ at effectively zero step size from extrapolation.

model is in complete agreement with the ones reported and argued for in Ref. [47].

3.3.3 Tree-level renormalization of the sine-Gordon model

A second step for the verification of our numerical apparatus for TLR is presented here. In this scenario, it has been applied to the 2-dimensional Euclidean sine-Gordon model given by the classical action

$$S[\phi] \quad = \quad \int d^2x \left[\frac{1}{2} (\partial_\mu \phi)^2 + u_1 \cos(\beta\phi) \right], \tag{3.18}$$

in the phase with spontaneously broken symmetry with $\beta^2 < 8\pi$, the so-called molecular phase. The results of the TLR of the sine-Gordon model are well known [49, 51, 50], this provides an excellent benchmark for the TLR numerical procedure. The tree-level blocking relation (3.8) for the ansatz

$$U_k(\Phi) \quad = \quad \sum_{n=0}^{M} u_n(k) \cos(n\beta\Phi) \tag{3.19}$$

is rewritten in the form of the recursion equation

$$U_{k-\Delta k}(\Phi) \quad = \quad \min_{\rho}\left[k^2\rho^2 + \sum_{n=0}^{M} u_n(k)\cos(n\beta\phi)J_0(2n\beta\rho)\right] \tag{3.20}$$

(for details, see Ref. [50]) J_0 stands for the Bessel function, M is the truncation of the potential at the M-th upper harmonic.

As for the numerical calculations, the following settings were employed: $\beta^2 = 4\pi$, $M = 10$. My numerical results match with the ones in the literature. Below the scale k_c, where the spinodal instability occurs, the amplitude $\rho(\Phi)$ of the periodic field configurations, which minimizes the action, is given by $\rho_k(\Phi) = -\frac{1}{2}(|\Phi| - \frac{2\pi}{\beta})$ [50]. As well as in the spontaneously broken phase of the one-component scalar field theory with polynomial interaction, the amplitude of the spinodal instability is IR finite. Our numerical result for $\rho_k(\Phi)$ is compared to the one obtained in Ref. [50] in Fig. 3.5.

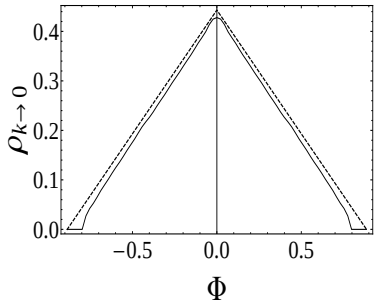

Figure 3.5: Comparison of the function $\rho_k(\Phi)$ obtained in this work numerically (solid line) to the one in Ref. [50] (dashed line) for the molecular phase of the SG model for $\beta^2 = 4\pi$.

The magnitude of the first four dimensionless couplings is plotted in Fig. 3.6. They are, in fact, renormalizable and tend to a constant value in the $k \to 0$ limit. That is, the dimensionful effective potential becomes vanishing in accordance with the requirements of convexity and periodicity [50].

This work's numerical TLR procedure, applied to compute the infrared behavior of the sine-Gordon model, produces results, which are in complete agreement with the ones obtained in Refs. [49, 51, 50].

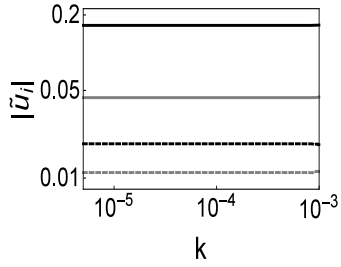

Figure 3.6: The scale-dependence of the dimensionless running couplings of the SG model in the deep IR region for $\beta^2 = 4\pi$, obtained with TLR. The solid black line corresponds to $|\tilde{u}_1|$, the solid grey line to $|\tilde{u}_2|$, the dashed black line to $|\tilde{u}_3|$ and finally, the dashed grey line to $|\tilde{u}_4|$.

3.4 $O(2)$ ghost model in Case Y

This section is going to elaborate my work on the analysis of the $O(2)$ ghost model, when the dimensionful higher derivative coupling was kept constant.

3.4.1 Application of the WH RG approach

We now turn to the main goal of [**B**], the investigation of the 3-dimensional, Euclidean, $O(2)$ symmetric ghost model with polynomial potential at the level of the LPA. The ansatz for the blocked action is

$$S_k[\underline{\phi}] \;=\; \frac{1}{2}\int d^3x \underline{\phi}^T \Omega(-\Box)\underline{\phi} + \int d^3x U_k(\underline{\phi}^T\underline{\phi}), \tag{3.21}$$

where $\underline{\phi} = \begin{pmatrix}\phi_1\\ \phi_2\end{pmatrix}$ denotes the two-component real scalar field and $U_k(\underline{\phi}^T\underline{\phi})$ is the blocked potential. For the latter, the ansatz (3.9) is applied with $r = \underline{\phi}^T\underline{\phi}$. The behavior of the model for ordinary scalar field with $Z = 1$ is also discussed here for comparison.

The phase diagram of the $O(2)$ symmetric scalar ghost model is mapped with the WH RG method. The scale dependence of the blocked potential is given by

$$k\partial_k U_k(r) \;=\; -\alpha k^3\Big[\ln[\Omega(k^2) + U_k'(r) + 2rU_k''(r)] + \ln[\Omega(k^2) + U_k'(r)]\Big], \tag{3.22}$$

with $U_k'(r) = \partial_r U_k(r)$ and $U_k''(r) = \partial_r^2 U_k(r)$. Eq. (3.22) with settings $Z = 1$, $Y = 0$ is merely the WH equation for ordinary $O(2)$ symmetric models,

$$k\partial_k U_k(\Phi) \;=\; -\alpha k^3\Big[\ln[k^2 + \partial_\Phi^2 U_k(\Phi)] + \ln[k^2 + \frac{1}{\Phi}\partial_\Phi U_k(\Phi)]^{N-1}\Big], \tag{3.23}$$

at $N = 2$, given in Ref. [47]. The agreement between Eq. (3.22) with Eq. (3.23) for

$N = 2$, is realized with the substitution $\Phi = \sqrt{2r}$.

It is worth mentioning, that the $U(1)$ symmetric ansatz

$$S_k[\phi^*, \phi] \quad = \quad \int d^d x \phi^* \Omega(-\Box)\phi + \int d^d x U_k(\phi^* \phi) \tag{3.24}$$

for the blocked action of the one-component complex scalar field $\phi = \frac{1}{\sqrt{2}}(\phi_1 + i\phi_2)$ is equivalent with the ansatz (3.21).

The WH RG equation ceases to be applicable at some scale k_c, when the argument of the logarithm on the right-hand side of Eq. (3.22) reaches zero. This happens, either due to $s_-(k) = \left[\Omega(k^2) + U_k'(r)\right] \leq 0$ or $s_+(k) = \left[\Omega(k^2) + U_k'(r) + 2rU_k''(r)\right] \leq 0$ [47]. This refers to spontaneously broken symmetry. The loop expansion is inapplicable when $k \leq k_c$. The expression $s_-(k)$ corresponds to the inverse propagator of the lightest excitations of the field, the Goldstone-bosons. In the $O(N)$ symmetric models with a homogeneous vacuum field configuration pointing into a given direction of the internal space, there are $N-1$ transverse excitations or Goldstone-bosons, as it can be seen from the power $N-1$ of the eigenvalue $s_-(k)$ under the logarithm in the right-hand side of Eq. (3.23). In the $O(1)$ case, when there are no transverse modes, the vanishing of $s_+(k)$ signals the occurrence of spinodal instability. For $N \geq 2$, the vanishing of $s_-(k)$ takes over that role, since it corresponds to the lightest excitations of the field. The critical scale k_c is given by $s_-(k_c)|_{\Phi=0} = 0$, which implies $Z + Yk_c^2 + \tilde{v}_1(k_c) = 0$, similarly to $N = 1$. In the case of local potentials, for asymptotically large values of $|\Phi|$ and for scales below k_c, the unstable interval $0 \leq |\Phi| \leq \Phi_c(k)$ (with $\Phi_c(k) = \sqrt{k}\tilde{\Phi}_c(k)$) may open up. It is determined via the vanishing of $s_-(k)$ as

$$\tilde{\Phi}_c(k) \quad = \quad \sqrt{-\frac{2[Z + Yk^2 + \tilde{v}_1(k)]}{\tilde{v}_2(k)}}. \tag{3.25}$$

Given that a non-trivial saddle point $\underline{\phi}' = \underline{\psi}_k$ appears in the integrand in the right-hand side of Eq. (A.5), the integral can be approximated by the contribution of that saddle point. This yields a tree level blocking relation, the generalization of Eq. (3.6),

$$S_{k-\Delta k}[\underline{\phi}] \quad = \quad \min_{\{\underline{\phi}'\}} S_k[\underline{\phi} + \underline{\phi}'] = S_k[\underline{\phi} + \underline{\psi}_k], \tag{3.26}$$

where $\underline{\psi}_k(x) \neq 0$ represents the non-trivial saddle-point configuration, which minimizes the action $S_k[\underline{\phi} + \underline{\phi}']$. We have to restrict ourselves to looking for non-trivial saddle-point configurations in a particular subspace of the configuration space for practical purposes. That subspace is the periodic configurations of the type given in Eq. (3.7).

In the $O(N)$ case there are more than one possible choices for the non-trivial saddle-point configuration, with various orientations in the internal space. In LPA, the background configuration should be a homogeneous one, $\underline{\phi} = \underline{\Phi} = \Phi \underline{e}$ pointing to given direction according to the unit vector $\underline{e}$ in the internal space. Generally, the non-trivial saddle-point configuration might have components both parallel and orthogonal to $\underline{e}$. The question is how to choose these components in order to minimize the value of the action.

It was argued in Ref. [47], that the TLR of ordinary $O(N)$ models for $N \geq 2$ can be reduced to the TLR of the ordinary $O(1)$ model, based on the positivity of the quadratic gradient term. The field configuration $\underline{\Phi} + \underline{\psi}_k$ can be rewritten as

$$\Phi \underline{e} + \underline{\psi}_k(x) \quad = \quad \eta_k(x) \underline{\underline{\mathcal{R}}}(x) \underline{e}, \tag{3.27}$$

without loss of generality, in terms of an appropriately chosen amplitude function $\eta_k(x)$ with the $SO(N)$ matrix $\underline{\underline{\mathcal{R}}}(x)$. The quadratic gradient term of the action assumes the form

$$\begin{aligned} &\frac{1}{2} \int d^d x \Big(\partial_\mu [\eta_k(x) \underline{\underline{\mathcal{R}}}(x) \underline{e}] \Big)^T \Big(\partial_\mu [\eta_k(x) \underline{\underline{\mathcal{R}}}(x) \underline{e}] \Big) \\ &= \frac{1}{2} \int d^d x \Big([\partial_\mu \eta_k(x)][\partial_\mu \eta_k(x)] + \eta_k^2(x) [\partial_\mu \underline{\underline{\mathcal{R}}}(x) \underline{e}]^T [\partial_\mu \underline{\underline{\mathcal{R}}}(x) \underline{e}] \Big). \end{aligned} \tag{3.28}$$

Here, the identities $[\underline{\underline{\mathcal{R}}}(x)\underline{e}]^T \underline{\underline{\mathcal{R}}}(x)\underline{e} = 1$ and $[\underline{\underline{\mathcal{R}}}(x)\underline{e}]^T \partial_\mu [\underline{\underline{\mathcal{R}}}(x)\underline{e}] = 0$ have been used. This means that any inhomogeneity of the vector $\underline{\underline{\mathcal{R}}}(x)\underline{e}$ contributes to increasing the action, that is, the non-trivial saddle point should be such that $\underline{\underline{\mathcal{R}}}(x)\underline{e}$ is homogeneous. According to this, the relation (3.27) implies that both of the vectors $\underline{\underline{\mathcal{R}}}(x)\underline{e}$ and $\underline{\psi}_k(x)$ should be parallel to $\underline{e}$, the direction of the background field. Thus, the periodic ansatz for the non-trivial saddle-point configuration (similar to Eq. (3.7)) is

$$\underline{\psi}_k(x) \quad = \quad \underline{e} 2\rho_k \cos(k n_\mu(k) x_\mu + \theta_k). \tag{3.29}$$

This is inserted into the tree-level blocking relation (3.26), which yields Eq. (3.8). This can be recast in the form of the recursion relation (3.16). Thus, TLR procedure of the ordinary $O(N)$ model indeed reduces to the one for the ordinary $O(1)$ model.

For the $O(N)$ ghost models (with $Z = -1$) the above given argumentation fails. This originates from the fact, that the terms in Eq. (3.28) acquire negative signs, therefore no conclusion can be made for the homogeneity of $\mathcal{R}\underline{e}$. Nevertheless, we shall make the ansatz (3.29) for the non-trivial saddle point. It might happen, that similar periodic saddle-point configurations with more complex orientations in the internal space give smaller value of the blocked action. When the ansatz (3.29) is applied, the TLR of the $O(2)$ ghost model reduces to the one of the $O(1)$ ghost model, except that the interval of constant background fields, where the spinodal instability occurs is now set by the critical value $\tilde{\Phi}_c(k)$ given in Eq. (3.25) instead of Eq. (A.3). The tree-level blocking relation (3.26) results in the recursion equation (3.16) for the blocked potential.

3.4.2 Phase structure and IR scaling laws

Identification of the phases

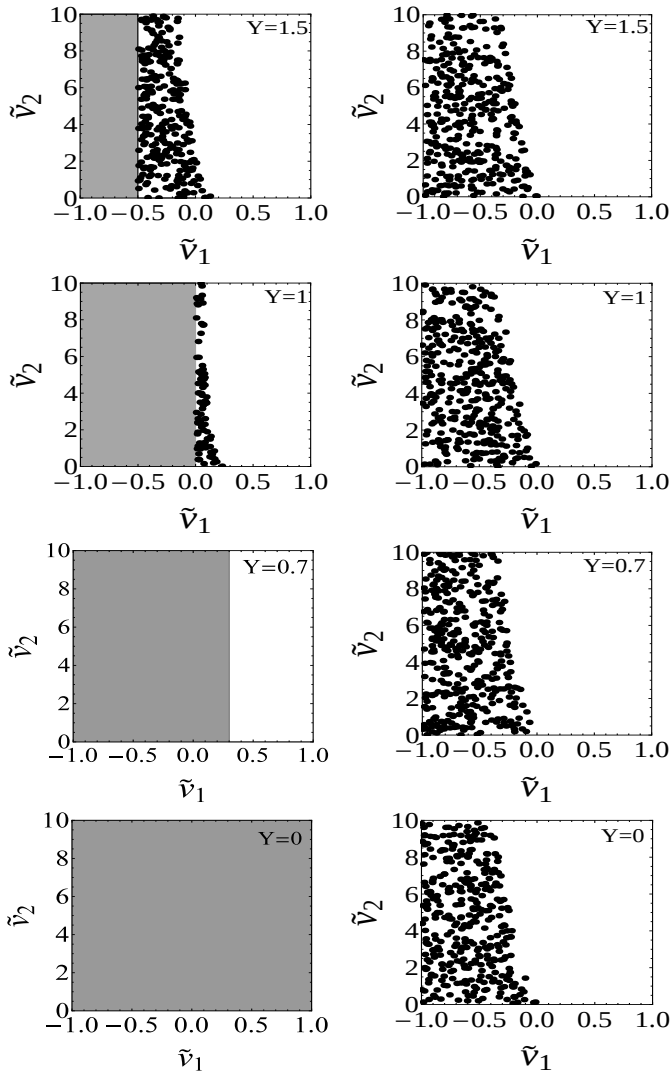

Figure 3.7: Phase diagrams in the parameter plane $(\tilde{v}_1(\Lambda), \tilde{v}_2(\Lambda))$ for several given values of Y for the ghost (left) and the ordinary (right) $O(2)$ models. The empty regions correspond to the symmetric phase I, the dotted and shadowed regions correspond to regions IIA and IIB of phase II, respectively.

The dimensionful coupling Y is kept at various given constant values during the WH RG flows. The different phases in the parameter plane $\big(\tilde{v}_1(\Lambda), \tilde{v}_2(\Lambda)\big)$ of the bare dimensionless

couplings is distinguished by considering where the global RG flow started in that plane both for the ghost and ordinary $O(2)$ models. The symmetric phase of the model (referred to as phase I here), is the region in the parameter plane, where the RG trajectories can be followed by the WH RG equation (3.22) from the UV scale down to the IR scale $k \to 0$. This is characterized by the fact, that the inverse propagator $G^{-1}(k) \equiv s_-(k)|_{\Phi=0} = Zk^2 + Yk^4 + v_1(k)$ is positive, all along those RG trajectories. In this regard, phase II is realized as the region in the parameter space, where the inverse propagator vanishes at some finite scale k_c or it is already negative in the UV ($k = \Lambda$). In order to distinguish these latter two cases, in phase II it comes handy to denote them IIA and IIB. IIA with $G^{-1}(k) > 0$ for $\Lambda \geq k > k_c > 0$ and IIB with $G^{-1}(\Lambda) = Z\Lambda^2 + Y\Lambda^4 + v_1(\Lambda) < 0$ or $-Z-Y > v_1(\Lambda)$ for $\Lambda = 1$. For the bare values satisfying the inequalities $|v_1(\Lambda)| < \Lambda^2 = 1$ and $Y > 0$, region IIB is not present for the ordinary $O(2)$ model, but it does occur for the ghost model for $v_1(\Lambda) \leq 1 - Y$ when $Y < 2$.

The first objective is to identify the regions corresponding to phases I and IIA in the parameter plane. Region IIA can be discovered by solving the WH RG equation (3.22) and detecting if the inverse propagator vanishes at a finite scale k_c. Eq. (3.22) with ansatz (3.9) reduces to the set of coupled ordinary first-order differential equations with the forms (3.10) and (3.11), with $a = 3$ and $b = 5$ for $M = 2$. Region IIA was searched for numerically. A number of 1000 random starting points of the RG trajectories have been been generated in the parameter region $\big(\tilde{v}_1(\Lambda), \tilde{v}_2(\Lambda)\big) \in [-1, 1] \otimes [0, 10]$. Fig. 3.7 shows the phase diagrams for various values of the dimensionful higher-derivative coupling Y; the empty, dotted, and shadowed regions correspond to phase I, region IIA, and region IIB, respectively.

Numerical analysis has uncovered, that phase II of the ghost model is bounded in the $\tilde{v}_1(\Lambda)$ direction, namely a trajectory in the phase space is in phase II, if $\tilde{v}_1(\Lambda) \leq \tilde{v}_u(Y, \tilde{v}_2(\Lambda))$. In the other direction, $\tilde{v}_2(\Lambda)$ in the plane $\big(\tilde{v}_1(\Lambda), \tilde{v}_2(\Lambda)\big)$, it is unbounded. For $Y \geq 1$, the phase boundary at $\tilde{v}_u > 1 - Y$ depends on Y and $\tilde{v}_2(\Lambda)$, so that region IIA is also present for $1 - Y < \tilde{v}_1(\Lambda) \leq \tilde{v}_u$, while for $Y < 1$ only region IIB appears with the boundary $\tilde{v}_u = 1 - Y$. Therefore, the symmetric phase I starts at larger and larger values of $\tilde{v}_1(\Lambda)$ in the parameter plane for decreasing Y values, For $Y \to 0$, it practically disappears. In the case of the ordinary $O(2)$ model, phase II consists of region IIA only. The phase diagrams of the ordinary and ghost models are compared in Fig. 3.7. Approximately, the phase boundary $\tilde{v}_u\big(Y, \tilde{v}_2(\Lambda)\big)$ has a linear dependence on $\tilde{v}_2(\Lambda)$, given by $\tilde{v}_u \approx -c(Y)\tilde{v}_2(\Lambda)$, where $c(Y)$ is monotonically increasing with increasing value of the higher-derivative coupling Y. Thus, the phase boundary is at $\tilde{v}_u \approx 0$ for $\tilde{v}_2(\Lambda) \ll 1$ for all values $0 \leq Y \leq 2$.

IR scaling in phase I

The IR scaling laws in phase I have been determined by means of the WH RG Eq. (3.22). Several RG trajectories were started at various 'distances' $t = \tilde{v}_1(\Lambda) - \tilde{v}_u$ and for $\tilde{v}_2(\Lambda) = 0.01,\ 0.1$ repeated for all investigated values of Y. It has been established, that the dimensionful couplings $v_n(k)$ tend to constant, finite positive values in the IR limit $k \to 0$, for both the ghost and the ordinary $O(2)$ models. Therefore, the effective potential in phase I is convex (paraboloid) for both the ghost and the ordinary models,

which is sensitive to the choice of the bare potential. In the ghost model's case the linear relation

$$v_1(0) \quad = \quad at + b(Y) \tag{3.30}$$

has been identified, where the slope a is independent of Y, while the mass squared $b(Y)$ at the phase boundary - for $t \to 0$ - monotonically decreases with the increasing values of Y (see Fig. 3.8). The coupling $v_2(0)$ decreases with decreasing coupling Y for given t and it tends to zero as the phase boundary is approached but independently of Y. In the ordinary model's case, the effective potential seems to be insensitive to the value of the higher-derivative coupling in the range $0 \leq Y < 2$, but keeps its sensitivity to the parameters of the bare potential.

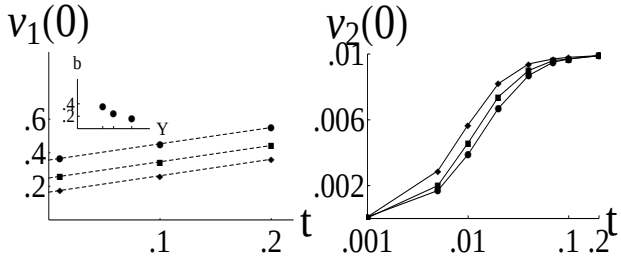

Figure 3.8: The IR values of the dimensionful couplings $v_1(0) = at + b$ (left) and $v_2(0)$ (right) vs. the 'distance' $t = \tilde{v}_1(\Lambda) - \tilde{v}_u$ from the phase boundary for $v_2(\Lambda) = 0.01$. The dots, boxes, and rhombuses correspond to $Y = 0.7,\ 1.0,\ 1.5$, respectively, the lines are only for guiding the eyes. The dependence of the coefficient b on the higher-derivative coupling Y is shown in the inset.

IR scaling laws in phase II

The RG trajectories, which belong to region IIA are tracked by the WH RG equation (3.22) from the UV scale Λ to the critical scale k_c. The scaling of the couplings in the deep IR region, i.e. below k_c are obtained by TLR which has been initiated from the potential obtained at the critical scale k_c by the solution of Eq. (3.22). In order to acquire RG trajectories in region IIB, the TLR should be started already at the UV scale. In both scenarios, the ansatz (3.9) with the order of truncation $M = 10$ has been applied for the potential(also in the TLR, and not in the WH RG method, where we used $M = 2$). As for the specifications of the TLR procedure, the scale k has been decreased from either the critical one (k_c) for region IIA or from the UV scale Λ for region IIB by 3 orders of magnitude with the step size $\Delta k/k = 0.01$. The numerical precision was set to 40 digits, the numerical minimization of $U_k(\rho, \Phi)$ with respect to ρ, at given values of Φ took maximally 500 iteration steps. The TLR procedure is quantitatively sensitive to the choice of the interval $|\Phi| \leq \bar{\Phi}$, where the minimization process of the potential $U_k(\rho, \Phi)$ and the least square fit of the blocked potential at scale $k - \Delta k$ take place. For the 'Mexican hat'-like potential $U_{k_c}(\Phi)$ in region IIA or $U_\Lambda(\Phi)$ in region IIB, the choice $\bar{\Phi} \approx 1.5\Phi_m$ was made, where $\pm\Phi_m$ are the positions of the minimums of the potential with $\Phi_m =$

$\sqrt{-2v_1(k_c)/v_2(k_c)}$ or $\Phi_m = \sqrt{-2v_1(\Lambda)/v_2(\Lambda)}$, respectively. As for convex potentials, where $v_1(k_c) > 0$ in region IIA or $v_1(\Lambda) > 0$ in region IIB, the setting $\bar{\Phi} \gtrsim 30$ has been used. In this case, no obvious region of the instability can be selected, numerically the smallest interval in Φ has been chosen given that further expanding the interval doesn't alter the result of the TLR process. It was found numerically, that the blocked potential does not acquire tree-level corrections outside of the interval $|\Phi| \leq \Phi_c$ with Φ_c given by Eq. (3.25), but the choice of a slightly wider interval makes the minimization and fitting numerically stable.

For each given value of Y and for both values $\tilde{v}_2(\Lambda) = 0.01$ and 0.1 I have computed the RG trajectories for 3 to 5 bare values of $\tilde{v}_1(\Lambda)$ distributed equidistantly in the interval $-1 < \tilde{v}_1(\Lambda) < \tilde{v}_u$. I found, that the couplings of the dimensionful blocked potential tend to constant values in the IR limit. Furthermore, it has also been observed that for any given value of Y, the effective potential is universal, it does not depend on at which point in the parameter space $(v_1(\Lambda),\ v_2(\Lambda))$ the RG trajectories have been initiated. Thus, I have computed the mean values $\overline{v_1(0)}$ and $\overline{v_2(0)}$ of the couplings $v_1(0)$ and $v_2(0)$, respectively, with their variances by averaging them over all evaluated RG trajectories belonging to a given value of Y. It has been revealed, that $\overline{v_1(0)}$ decreases strictly monotonically with increasing values of Y as shown in Fig. 3.9. As for the mean values $\overline{v_2(0)}$, they take randomly positive and negative small values with variances comparable with their magnitudes when the coupling Y is altered. Thus, we concluded that the quartic coupling of the effective potential vanishes, an averaging over all considered values of Y yields $\langle\overline{v_2(0)}\rangle = 0.004 \pm 0.01$. That is, the dimensionful effective potential is an upside facing paraboloid with a single minimum, at $\Phi = 0$ in phase II. Moreover, the nonrenormalizable, UV irrelevant coupling Y turns out to be IR relevant in phase II.

The ratio r characterizes how large part of the sum of the negative terms cancel totally or partially by the positive higher derivative term in the inverse propagator $G^{-1}(k_s)$. It is given by,

$$r \;=\; \begin{cases} \frac{Yk_s^4}{Yk_s^4+v_1(k_s)}, & \text{if} \quad v_1(k_s) \geq 0 \\ 1, & \text{if} \quad v_1(k_s) < 0 \end{cases}, \tag{3.31}$$

where $k_s = k_c$ and $k_s = \Lambda$ for regions IIA and IIB, respectively. This ratio has been evaluated for each RG trajectories computed in region II. The quantity r is a precursor of how significant is the role played by the ghost condensation in this cancellation at k_s, where TLR is started. For $v_1(k_s) < 0$, the ghost condensation is the only mechanism that can be accounted for the above mentioned cancellation. Numerical results has shown that $r \approx 1$ in most of the parameter region belonging to phase II, but it generally decreases abruptly when $\tilde{v}_1(\Lambda)$ approaches the phase boundary $\tilde{v}_u$. The IR values of the couplings in the effective potential seem, however, to be insensitive of r, i.e., of the importance of the ghost condensation at the scale k_s. The role of the ghost condensation during the global RG flow during TLR rather makes its imprint on the value of $v_1(0)$ through its dependence on Y.

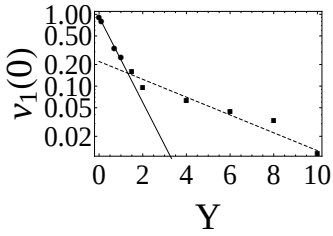

Figure 3.9: The dependence of the means $\overline{v_1(0)}$ on Y in phase II. The lines are only for guiding the eyes.

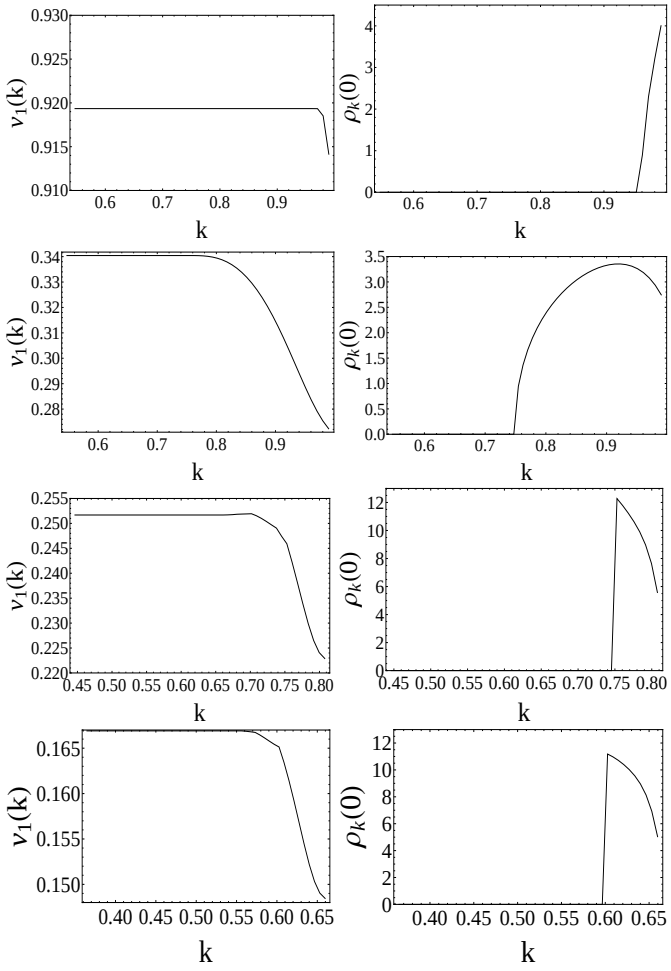

Figure 3.10: The flow of $v_1(k)$ (left column), obtained from TLR and the corresponding $\rho_k(\Phi = 0)$ for $t = \tilde{v}_2(\Lambda) = 0.1$ (right column) and $Y = 0,\ 0.7,\ 1.0$, and 1.5 (from the top to the bottom) in phase II of the ghost $O(2)$ model.

The numerical TLR procedure has revealed, that ρ_k, the amplitude of the spinodal instability suddenly acquires a large value just below the scale $k_s = \Lambda$ for region IIB as can be seen on cases $Y = 0$ and 0.7 in Fig. 3.10. This is very similar to what happens at the scale $k_s = k_c$ for region IIA as the reader can verify from cases $Y = 1.0$ and 1.5 in Fig. 3.10. However, after a small amount of (~ 30) blocking steps the condensate is rapidly washed out and does not survive the infrared limit, so it acquires zero for its amplitude. The disappearance of $\rho_k(0)$ is accompanied by the saturation of $v_1(k)$ at its IR limiting value $v_1(0)$. Generally, with regards to the running scale, a rather short scaling region (with finite, non-zero ρ_k) is followed by a long and stable IR scaling region. The plots in Fig. 3.10 belong to RG trajectories, which are characterized by the ratio $r \approx 1$. This signals, that the ghost condensation should be responsible for the existence of the finite amplitude $\rho_k(\Phi)$ of the spinodal instability when TLR is started, although, as numerical results have shown, the RG flow of the local potential starts to dominate the IR scaling after a small decrement of the scale k. Nevertheless, the presence of the condensate seems to be left behind, affecting the curvature of the effective potential through the dependence of the mass parameter $\underline{v_1(0)}$ on the higher-derivative coupling Y. Fig. 3.9 shows the exponential dependence of $\underline{v_1(0)}$ on Y changing slope at around $Y \approx 1$. Fig. 3.10 corroborates the claim, that the ghost condensation reigns the global RG flow, when the higher-derivative coupling is at around $Y \approx \mathcal{O}(\Lambda^{-2} = 1)$. Fig. 3.10 shows the reader, that the width of the k-interval, in which $\rho_k(\Phi = 0)$ is nonvanishing, increases for Y increasing from 0 towards 1, but it remains unchanged for $Y \gtrsim 1$. This can be tied to the following circumstances. The kinetic sector $\Omega(k^2)$ of the inverse propagator is an upside facing parabola with zeros at $k^2 = 0$ and $k^2 = 1/Y$ and has its minimum at $k^2 = 1/(2Y)$. Should $Y \gg \Lambda^{-2} = 1$ hold, the modes, which can give negative contributions to the action through ghost condensation, represent a small amount of the modes below the UV cutoff $\Lambda = 1$. In the extreme limit $Y \to \infty$ these modes are housed in an interval of vanishing width at zero momentum, and the instability is governed by the potential. In the other extremity, when $Y \ll \Lambda^{-2} = 1$, all modes below the UV cutoff are available for ghost condensation, however for $1/(2Y) \gg 1$ all they may give is a small negative contribution to the action and in the limit $Y \to 0$ this contribution becomes negligible. According to this naive reasoning, one may arrive to the conclusion that the ghost condensation may only play significant role at forming $v_1(0)$ when $Y \approx \mathcal{O}(\Lambda^{-2} = 1)$.

It has also been shown by numerical means, that qualitatively the range $\Phi_c(k)$ of the homogeneous background field, in which spinodal instability is present opens up gradually when the scale k decreases from k_s. Its width reaches a maximum and then abruptly falls to zero at some finite scale k_0. This means, that the amplitude ρ_k vanishes as well and the couplings $v_1(k)$ and $v_2(k)$ saturate at their IR values. The TLR does not yield any nontrivial contributes to the RG flow below k_0. This behavior is rather different of the one present in the ordinary $O(2)$ symmetric model in its symmetry broken phase.

Besides breaking the internal $O(2)$ symmetry, the ghost condensation breaks the Euclidean rotational symmetry in the 3-dimensional space as well as the translation symmetry in the x_1 direction in the Euclidean space. However, these symmetries are restored in the IR limit, since the ghost condensate dies out by then. Therefore, one has to come to the conclusion, that even phase II of the ghost model is a symmetric one. The difference between phases I and II can only be realized by considering the global RG flow: the effective potential has no sensitivity to the couplings of the bare potential in phase

II, as opposed to phase I, where such a sensitivity is essential.

Numerical effort has been made to check if in phase II of the ordinary $O(2)$ model with non-vanishing Y the TLR reproduces the Maxwell-cut for the dimensionful effective potential. The result was, that it does indeed reproduce the Maxwell-cut.

Correlation length

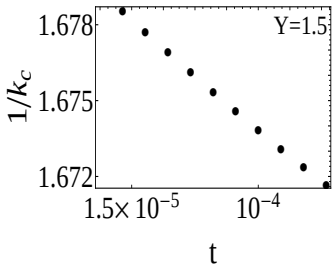

Figure 3.11: Scaling of the correlation length $\xi \sim 1/k_c$ with the reduced temperature $t = \tilde{v}_u - \tilde{v}_1(\Lambda)$ (on a lin-lin plot) at the boundary of phases I and II of the ghost $O(2)$ model for $Y = 1.5$ and $\tilde{v}_2(\Lambda) = 0.1$.

The behavior of the correlation length $\xi \sim 1/k_c$ is investigated, when one approaches the boundary of phases I and II from the side of phase II for the ghost model. This is only possible for region IIA, when k_c can be detected by solving the WH RG equation (3.22). Fig. 3.7 shows, that for a given $\tilde{v}_2(\Lambda)$, the 'distance' $\tilde{v}_u - \tilde{v}_1(\Lambda)$ measures how close an RG trajectory is to the boundary of the phases I and II. Thus, one may identify $\tilde{v}_u - \tilde{v}_1(\Lambda)$ as the reduced temperature t up to a constant factor. The dependence of the correlation length ξ on the difference $\tilde{v}_u - \tilde{v}_1(\Lambda)$, was computed by solving the WH RG equations with various initial conditions $\tilde{v}_2(\Lambda) = 0.01,\ 0.1$ and $\tilde{v}_{1i}(\Lambda) = [1 - (i/100)]\tilde{v}_u$ $(i = 1, 2, \ldots)$ for $Y = 1.0,\ 1.5,\ 2.0,\ 4.0,\ 10.0$. I have found, that the correlation length depends linearly on the reduced temperature,

$$\xi \sim 1/k_c \quad = \quad \xi_0 - \kappa[\tilde{v}_u - \tilde{v}_1(\Lambda)], \tag{3.32}$$

for any fixed values of the coupling Y, as shown in Fig. 3.11. The coefficient κ seems to rise almost linearly with increasing higher-derivative coupling Y (see Fig. 3.12).

The correlation length increases for trajectories closer and closer to the phase boundary from the side of phase II. It does not diverge however and remains finite arbitrarily close to the phase boundary. This suggests that the phase transition of the ghost $O(2)$ model is of first order, as opposed to the ordinary $O(2)$ model where the correlation length blows up according to the power law $\xi \sim t^{-\nu}$ (see for example the result for the ordinary $O(N)$ models on Fig. 2.2), when the phase boundary approached. The latter indicates a continuous phase transition, while the former most certainly not.

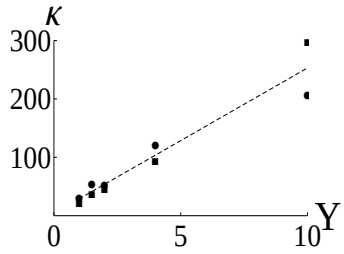

Figure 3.12: The coefficient κ in (3.32) of the correlation length against the higher-derivative coupling Y. The points correspond to various RG trajectories. The line is only for guiding the eyes.

3.5 $O(2)$ ghost model in Case $\tilde{Y}$

This analysis was conducted after Case Y. In the present section, the order of truncation of the polynomial potential (3.9) has been increased to $M = 10$ from $M = 2$ for the solution of the WH RG equations. These equations were solved with the fourth order Runge-Kutta method again. I have found that, the TLR procedure had to be refined in the means of digits of precision and the maximal iteration steps required for minimizing the potential. Generally, scale k has then been decreased from the singularity scale of the WH equations, by at least two orders of magnitude with the step size $\Delta k/k = 0.005$. The numerical precision was increased to 80 digits from 40 digits. In general, ~ 1000 iteration steps have been performed at each value of the constant background Φ for the numerical minimization of the blocked potential $U_k(\rho, \Phi)$ with respect to the amplitude ρ of the spinodal instability. The minimization process with respect to ρ in the right-hand side of Eq. (3.17) and the determination of the couplings at the lower scale $k - \Delta k$ with least-square fit are performed in the interval $0 \leq \Phi \leq \bar{\Phi}$ of the background fields which has been chosen similarly as in Case Y. For 'Mexican hat' like potential $U_{k_s}(\Phi)$, $\bar{\Phi} \approx 1.5\Phi_m$ has been set, where $\pm\Phi_m$ are the positions of the local minimums of the potential with $\Phi_m = \sqrt{-2v_1(k_s)/3v_2(k_s)}$. As for convex potentials $U_{k_s}(\Phi)$, the choice $\bar{\Phi} \gtrsim 30$ has been made similarly to the Case Y.

3.5.1 Phase diagram

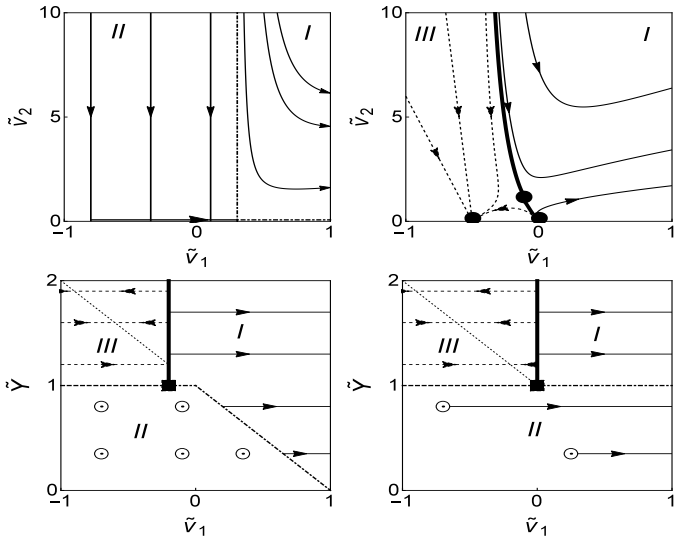

Figure 3.13: Various planar slices of the phase diagram of the ghost $O(2)$ model with a few typical RG trajectories in the parameter space $(\tilde{v}_1, \tilde{v}_2, \tilde{Y})$: the slice $(\tilde{v}_1, \tilde{v}_2)$ for $\tilde{Y} = 0.7$ (top left), the slice $(\tilde{v}_1, \tilde{v}_2)$ for $\tilde{Y} = 1.5$ (top right) with the fixed points (dots), the slice $(\tilde{v}_1, \tilde{Y})$ for $\tilde{v}_2 > 0$ (bottom left), and the slice $(\tilde{v}_1, \tilde{Y})$ for $\tilde{v}_2 = 0$ (bottom right). The phase boundaries II- I, III-I and III-II are shown by thick dashed-dotted, thick full, and dashed lines, respectively. The dotted line corresponds to a section of the straight line $\tilde{v}_1 = 1 - \tilde{Y}$, which is the IR fixed line in the slice with $\tilde{v}_2 = 0$; the full square stands for the triple point. The dotted circles represent RG trajectories flowing perpendicularly to the $\tilde{v}_2$ =const. planes.

The phase structure has been examined for RG trajectories started in the volume $[-1, +1] \otimes [0, 10] \otimes [0, 2]$ in the 3-dimensional parameter space $(\tilde{v}_1, \tilde{v}_2, \tilde{Y})$. Four slices of the phase diagram are shown in Fig. 3.13, to convey better understanding of the location of the phases and the behavior of the corresponding trajectories. The identification of the different phases was conducted with the help of the sensitivity matrix [11, 52]. The matrix $S_{n,m}$ consists of the derivatives of the running couplings with respect to the bare ones

$$S_{n,m} = \frac{\partial g_n(k)}{\partial g_m(\Lambda)}. \tag{3.33}$$

Should a singularity take place in the IR ($k \to 0$) and the UV ($\Lambda \to \infty$) limits of the elements of $S_{n,m}$, one would be able to locate different phases. In this scenario, we can find different phases in the model when the effective potential depends on different sets of bare couplings. Using this technique, we found, that there exist three phases and a triple point in all planar slices of the phase space at constant $\tilde{v}_2$. The three phases are a symmetric phase (phase I), a phase with restored symmetry (phase II), and a phase with spontaneously broken symmetry (phase III), they are going to be analyzed in detail

below. In the present WH RG approach, all the RG trajectories lie in one of the $\tilde{Y}$ =const. planes. The RG trajectories, which belong to phase II arrive perpendicularly to the plane $\tilde{v}_2 = 0$, where they take a turn with 90^o and run away to plus infinity parallel to the $\tilde{v}_1$ axis. This is due to the non-vanishing constant value of the dimensionful coupling v_1 in the IR limit $k \to 0$. Thus, the phase boundary II-I is the 2-dimensional surface $\big(\tilde{v}_1 = 1 - \tilde{Y},\ \tilde{v}_2 > 0,\ 0 < \tilde{Y} < 1\big) \cup \big(1 - \tilde{Y} < \tilde{v}_1 \leq 1,\ \tilde{v}_2 = 0,\ 0 < \tilde{Y} < 1\big)$. The Gaussian and Wilson-Fisher fixed points shown in the top-right of Fig. 3.13. These fixed points stand for fixed lines with arbitrary values of $\tilde{Y} \in [0, 2]$. The IR fixed point (line) is located in phase III and occurs only for $\tilde{Y} \in [1, 2]$. The positions of the fixed points can be calculated analytically for $M = 2$, which are summarized in Table 3.1. The inclusion of further couplings in the determination of the fixed points give quantitative numerical corrections for the Wilson-Fisher fixed point only. However, the linear and quadratic $\tilde{Y}$ dependence of the WF fixed point solution of $\tilde{v}_1$ and $\tilde{v}_2$ (respectively) would be still intact. One can see in the top-right sub-figure in Fig. 3.13, that both the Gaussian and

Fixed point	$\tilde{v}_1$	$\tilde{v}_2$
Gaussian	0	0
Wilson-Fisher	$\frac{3}{13}(1-\tilde{Y})$	$\frac{80\pi^2}{169}(1-\tilde{Y})^2$
IR	$1-\tilde{Y}$	0

Table 3.1: The fixed point couplings $\tilde{v}_1$ and $\tilde{v}_2$ for given values of $\tilde{Y}$.

Wilson-Fisher fixed points lie on the phase boundary III-I and act for the RG trajectories as cross-over points. The RG flow of trajectories in phase I is qualitatively the same independently of the value of $\tilde{Y}$ in the interval $0 < \tilde{Y} \leq 2$. In the slice $(\tilde{v}_1, \tilde{v}_2)$ for $1 < \tilde{Y} \leq 2$ the trajectories in phase III flow into the IR fixed point (line), but their evaluation gets numerically unstable in the vicinity of the fixed point. The phase boundary III-II lies in the plane $\tilde{Y} = 1$. Finally, in slices $(\tilde{v}_1, \tilde{Y})$ for constant $\tilde{v}_2 > 0$ (sub-figures at the bottom in Fig. 3.13) all the three phases can be seen, as well as the triple point. In the 3-dimensional parameter space, there is a triple line, the line of intersection of the phase boundaries III-II and III-I. The IR scaling laws have been studied in detail, revealing the symmetry properties of the various phases. They are elaborated in the following subsections.

3.5.2 Phase I

This is the symmetric phase of the model. In phase I, the RG flow of the trajectories, computed by the WH RG equation (3.22), do not acquire any singularity. As mentioned before, the RG flows of the dimensionful couplings are qualitatively the same in phase I, independently of the value of $\tilde{Y}$. They increase strictly monotonically with decreasing scale k in a short UV scaling region $\sim 0.3 < k \leq \Lambda = 1$ and then tend asymptotically to certain constant, positive values $v_n(0)$ in the IR regime. That is, the dimensionful effective potential is convex, but sensitive to the bare potential. The IR limiting values of the dimensionful couplings $v_1(0)$ and $v_2(0)$ have been computed on several RG trajectories, started at various given 'distances' $t = \tilde{v}_1(\Lambda) - \tilde{v}_u$ from the phase boundary $\tilde{v}_u$ (I-II for

$0 \leq \tilde{Y} < 1$ and I-III for $1 < \tilde{Y} \leq 2$) for given $v_2(\Lambda) = 0.01,\ 0.1$ and several $\tilde{Y}$ values. It has been established, that the IR limiting value of the dimensionful mass squared satisfies a similar linear relation as it does in Case Y

$$v_1(0) \quad = \quad at + b(\tilde{Y}), \tag{3.34}$$

with the slope $a = 1 \pm .001$. The latter, a is independent of $\tilde{Y}$, whereas, at the phase boundary ($t \to 0$),

$$b(\tilde{Y}) \quad = \quad (1 - \tilde{Y})b(0)\Theta(1 - \tilde{Y}) \tag{3.35}$$

decreases approximately linearly to zero at $\tilde{Y} = 1$ (see Fig. 3.14) and vanishes for $\tilde{Y} > 1$.

For $k \to 0$, the coupling $v_2(k)$ increases drastically with respect to its bare value $v_2(\Lambda)$, which is set to be close to the phase boundary I-II for $t \to 0$ and $0 < \tilde{Y} \ll 1$. However, it slightly acquires loop-corrections near the boundary I-III for $t \to 0$ and $1 < \tilde{Y} \leq 2$. In the latter, the behavior of $v_2(k)$ resembles to the behavior of the same type of coupling in the symmetric phase of the ordinary $O(2)$ model near the boundary of the symmetry broken phase. Far enough from the phase boundary $\tilde{v}_u$, i.e., at larger values of t, the loop-corrections are suppressed by the large values of the mass squared $v_1(0)$. That is, the coupling $v_2(k)$ as well as all higher-order couplings $v_{n>2}(k)$ stay very close to their bare values in the IR. For $t \to 0$, i.e., when approaching the phase boundary, the IR value $v_2(0)$ shows a strong dependence on $\tilde{Y}$. This relation is nonlinear and has a minimum $v_2(0) = 0$ at $\tilde{Y} = 1$ (Fig. 3.14).

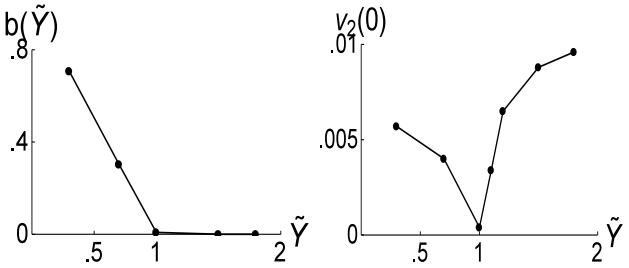

Figure 3.14: The parameters b of the IR coupling $v_1(0)$ in Eq. (3.34) (left) and the IR coupling $v_2(0)$ (right) against $\tilde{Y}$ at the 'distance' $t = \tilde{v}_1(\Lambda) - \tilde{v}_u = 0.001$ from the boundary of phase I.

3.5.3 Phase II

Phase II is present, when $0 < \tilde{Y} < 1$. Phase II is a phase with restored symmetry in the IR limit, similarly to Case Y. A periodic structure – breaking $O(2)$ symmetry as well as 3-dimensional translation and rotation symmetries – occurs below the singularity scale k_s, but it is vanishes in the limit $k \to 0$. In this phase $k_s = \Lambda$, so that the RG flow can be computed by the TLR procedure, started at the UV scale Λ. It has been established, that the couplings of the dimensionful blocked potential assume constant values along their IR scaling.

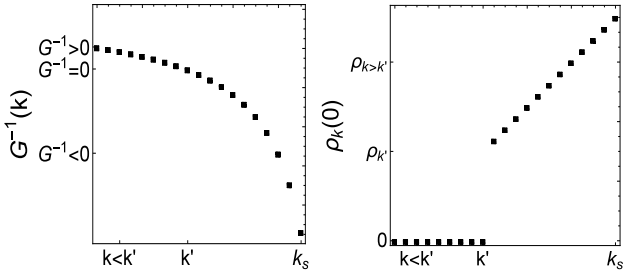

Figure 3.15: The flow of the inverse propagator $G^{-1}(k)$ (left) and the corresponding amplitude of the spinodal instability ρ_k at vanishing homogeneous background field $\Phi = 0$ (right) along the RG trajectory with $\tilde{Y} = 0.7$, $\tilde{v}_1(\Lambda) = -0.1$, $\tilde{v}_2(\Lambda) = 0.01$ and the step size $\Delta k/k = 5 \cdot 10^{-5}$.

The typical behavior of the inverse propagator $G^{-1} = (-1 + \tilde{Y})k^2 + v_1(k)$ and the corresponding amplitude of the spinodal instability $\rho_k(0)$ for vanishing homogeneous background field $\Phi = 0$ are shown in Fig. 3.15. One can see, that below k_s (which is the scale at which the TLR procedure is initiated) the inverse propagator is negative. As the running scale is lowered, the value of G^{-1} increases, while the value of $\rho_k(0)$ decreases until the running scale k reaches a finite scale $k' < k_s$. At the scale k', the propagator becomes vanishing and the amplitude of the spinodal instability abruptly jumps to zero. This refers to the fact, that below the scale k', no further tree-level renormalization occurs and neither does the periodic condensate survive the IR limit. The flow of ρ_k is qualitatively the same as it was found in the Case Y study of the restored symmetry phase. There, the periodic configuration emerges below the scale k_s but it is washed out at some non-vanishing scale k'.

It has also been observed, that for any given value of $\tilde{Y}$, the effective potential is quasi-universal in the sense, that it does not depend on at which point $(v_1(\Lambda),\ v_2(\Lambda))$ the RG trajectories have been started. This suggested me, to compute the mean values $\overline{v_1(0)}$ and $\overline{v_2(0)}$ of the couplings $v_1(0)$ and $v_2(0)$ with their variances by averaging them over all evaluated RG trajectories, which belong to a given value of $\tilde{Y}$. Table 3.2 summarizes the results. It shows, that the dimensionful mass squared decreases with increasing values of $\tilde{Y}$ linearly as

$$\overline{v_1(0)}(\tilde{Y}) \quad = \quad [\overline{v_1(0)}]_{\tilde{Y}\to 0}(1 - \tilde{Y}) \tag{3.36}$$

(see Fig. 3.16). The small non-vanishing value of $\overline{v_2(0)}$ is accompanied by an error, with magnitude as big as the mean itself. Thus, we can state, that the coupling of the quartic term vanishes in the infrared limit. Similarly to the latter, all the higher-order couplings $\tilde{v}_{n>2}(0)$ vanish. One should remember to the fact, that the theory in the limit $\tilde{Y} \to 0$ is energetically unbounded from below.

The following idea came after the publication of the work about Case Y. Namely, it is not an impossible scenario, that the loop corrections become significant for scales $k < k'$ again, since no more tree-level correction occurs there. To this end, I inserted the values of the couplings $\tilde{v}_n(k')$ $(1 \leq n \leq 10)$ obtained by the TLR procedure as initial

$\tilde{Y}$	$\overline{v_1(0)} \pm \Delta v_1(0)$	$\overline{v_2(0)} \pm \Delta v_2(0)$
.0	$.92 \pm .03$	$-.016 \pm .036$
.3	$.69 \pm .01$	$-.010 \pm .016$
.5	$.50 \pm .01$	$-.007 \pm .016$
.7	$.25 \pm .05$	$.002 \pm .050$
1.0	$.025 \pm .007$	$-.016 \pm .018$

Table 3.2: Mean IR values of the dimensionful couplings of the quadratic and quartic terms of the effective potential with their errors in phase II for various values of the higher-derivative coupling $\tilde{Y}$.

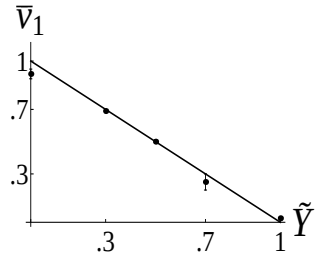

Figure 3.16: The dimensionful mass squared $\bar{v}_1(0)$ against the higher-derivative coupling $\tilde{Y}$ in phase II.

conditions into the WH RG equation for $k < k'$. It has been established numerically, that the loop-corrections can be accounted for less than 0.1 per cent change in the value of $v_1(k')$ and ~ 30 per cent change in $v_2(k')$ on any particular RG trajectory. It has been argued above, that the non-vanishing values of $v_n(k')$ for $n \geq 2$ is caused by numerical inaccuracies. This is why I conclude, that the TLR result obtained at the scale k' is stable against further loop-corrections in the region $0 \leq k < k'$.

3.5.4 Phase III

Phase III is present for $\tilde{Y} > 1$. Initially, it was divided into two subregions in the parameter plane $(\tilde{v}_1, \tilde{v}_2)$ specified by the singularity scale $k_s = \Lambda$ in the region with $-1 \leq \tilde{v}_1 \leq -1+\tilde{Y}$ and $k_s = k_c < \Lambda$ for $-1+\tilde{Y} < \tilde{v}_1 < \tilde{v}_u$, where $\tilde{v}_u$ is the phase boundary III-I. It has been found, that phase III is characterized by spontaneous breaking of $O(2)$ symmetry and a quasi-universal dimensionless effective potential. It is quasi-universal in the sense, that it depends only on the particular value of $\tilde{Y}$. It is given by

$$\tilde{U}_{k\to 0}(\tilde{\Phi}) \quad = \quad -\frac{1}{2}(-1+\tilde{Y})\tilde{\Phi}^2, \tag{3.37}$$

providing the Maxwell-cut like universal dimensionful effective potential of the symmetry breaking phase of the ordinary $O(2)$ model. Fig. 3.17 shows an example of the blocking of the dimensionful potential along with the IR limit of the amplitude of the spinodal

instability. Numerical data of the TLR procedure is summarized in Table 3.3. It contains the value $\tilde{v}_1(0)$, which can be compared with its theoretical value $1-\tilde{Y}$.

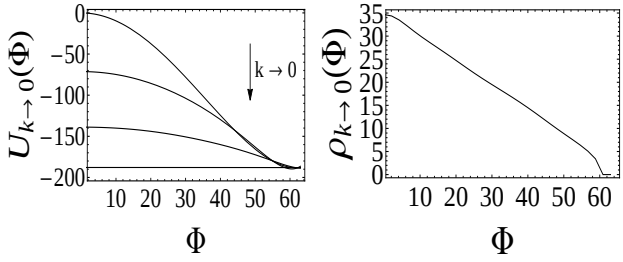

Figure 3.17: The dimensionless blocked potential $\tilde{U}_k(\Phi)$ (left) and the amplitude $\rho_0(\Phi)$ of the spinodal instability (right) against the homogeneous background field Φ for $\tilde{Y}=1.5$ in phase III.

The dimensionless effective potential (3.37) being a downside facing parabola with curvature $1-\tilde{Y}<0$ is the generalization of that with curvature -1 in the symmetry breaking phase of the ordinary $O(2)$ model without higher order derivative terms. The latter case is recovered as a limiting one for $\tilde{Y}=2$. The presence of the higher-derivative coupling $\tilde{Y}>1$ decreases the magnitude of the curvature. Similarly to the ordinary $O(2)$ model, the amplitude of the spinodal instability was found to survive the IR limit and depend linearly on the homogeneous background field Φ,

$$\rho_{k\to 0}(\Phi) \quad = \quad \beta(-\Phi+\Phi_c(0)). \tag{3.38}$$

The values of the slope β are computed numerically for various values of $\tilde{Y}$. They are compared in Table 3.3. These values do not show dependence on $\tilde{Y}$ and yield the mean $\bar{\beta}=-.53\pm.01$. According to this result and assuming, that the limit $\tilde{Y}\to 2$ is continuous, it is sensible to suggest, that the exact value is $\beta=1/2$. However, our TLR procedure has some systematic error.

The scaling of the dimensionless couplings in the deep IR region has also been determined. Referring to this, Fig. 3.18 shows the RG flow of $\tilde{v}_1$, $\tilde{v}_2$ and $\tilde{v}_3$ on double logarithmic plots, computed by the TLR procedure.

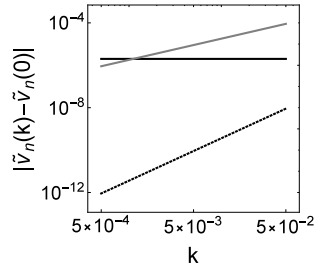

Figure 3.18: Scaling of the dimensionless couplings $\tilde{v}_1(k)$ (solid black line), $\tilde{v}_2(k)$ (solid gray line) and $\tilde{v}_3(k)$ (dashed black line) for $\tilde{Y} = 1.5$ in phase III.

According to Fig. 3.18, there clearly exists an IR scaling region in which the couplings $\tilde{v}_n(k)$ with $n \geq 2$ scale down to zero according to the power law $\tilde{v}_{n\geq 2} \sim k^{\alpha_n}$, while $\tilde{v}_1(k) - \tilde{v}_1(0) \sim k^{\alpha_1}$ remains essentially zero in the same region. The numerical values of the scaling exponents α_n turned out to be independent of $\tilde{Y}$, as shown in Table 3.3. This shows, that all the dimensionful couplings reach their constant IR values with the power law $v_n(k) - v_n(0) \sim k^2$.

$\tilde{Y}$	$\tilde{v}_1(0)$	$\tilde{v}_2(0)$	α_1	α_2	α_3	α_4	β
1.3	$-.281$	$< 10^{-5}$	0	1	2	3	.534
1.5	$-.469$	$< 10^{-5}$	0	1	2	3	.531
1.8	$-.75$	$< 10^{-5}$	0	1	2	3	.521
2	$-.94$	$< 10^{-5}$	0	1	2	3	.531

Table 3.3: The IR limiting values of the first two couplings of the dimensionless potential, the coefficient β of the amplitude in Eq. (3.38) along with the first few scaling exponents α_n for phase III.

3.5.5 On the phase transitions

A finite jump of the free energy $\mathcal{G}$, i.e., the presence of latent heat in phase transitions means a first order phase transition, while those with continuous $\mathcal{G}$ but singularities in the derivatives of $\mathcal{G}$ are called continuous phase transitions. The transition from phase III to phase I in the present case is rather straightforward to identify, it is continuous. One determines the behavior of the correlation length $\xi \sim 1/k_c$ in the vicinity of the boundary of phases I and III from the side of phase III. This approach, however, can only be applied at the phase boundary III-I, because the singularity scale k_c can be detected by solving the WH RG equation (3.22). This scale lies above the UV cutoff Λ for phase II, which means, that we cannot make such calculations at the phase boundaries II-I and II-III. The reduced temperature $t = \tilde{v}_u - \tilde{v}_1(\Lambda)$ is identified as the 'distance' of the starting point of the RG trajectories from the phase boundary $\tilde{v}_u$. Pursuing the goal, to compute the dependence of the correlation length ξ on the reduced temperature t, I have

solved the WH RG equation (3.22) for several initial conditions $\tilde{v}_{1i}(\Lambda) = \tilde{v}_u - i \cdot 10^{-4}$ $(i = 1, 2, \ldots, 500)$ for $\tilde{v}_2(\Lambda) = 0.01,\ 0.1$ and $\tilde{Y} = 1.2,\ 1.5,\ 2.0$. It has been found, that the correlation scales according to the power law

$$\xi \sim 1/k_c \quad \sim \quad t^{-\nu}, \tag{3.39}$$

near the phase boundary for any fixed values of $\tilde{Y}$, Fig. 2.2 shows an example of the qualitative behavior of ξ at several t values. This signals, that the phase transition III $\rightarrow$ I is continuous, just as the phase transition in the ordinary $O(2)$ model. The critical exponent ν is found to be insensitive to the bare parameters $\tilde{Y}$ and $\tilde{v}_2(\Lambda)$, its mean value is $\bar{\nu} = 0.46 \pm 0.03$. The ϕ^4 model can be considered as the textbook example of the RG technique. Therefore, it is widely investigated in various dimensions and in various levels of truncations [17, 57, 58, 15, 59, 60, 61, 62, 63]. Let us remember, that the purpose of this work was not to precisely calculate ν (which is $\nu = 0.67$ in the ordinary 3-dimensional $O(2)$ symmetric model), rather than that, it was to explore the phase structure and phase transitions of Case $\tilde{Y}$.

Let us now move on to the transitions II $\rightarrow$ I and III $\rightarrow$ II. The difficulty of the identification of these transitions has already been elaborated. Let us turn to an other way to study the continuity of these phase transitions. One can compute the jump of the free-energy density (or latent heat) per unit volume directly. To be more precise, the jump of the minimum of the effective potential passing from one phase to another through the phase boundary. In order to do this, I determined the IR limit of the constant term $v_0^A(0)$ of the effective potential in phases A =I, II, III at both sides of the phase boundary and compared them. For the comparison one has to consider RG trajectories on which the bare potential has the same minimum value. Otherwise, the jump can be accounted to the correction of the IR values $v_0^A(0)$ by the minimum value of the bare potential $(U_\Lambda^A)_{min}$, i.e., by the replacement $v_0^A(0) \longrightarrow (v_0^A)_{corr} = v_0^A(0) - (U_\Lambda^A)_{min}$.

When bare potentials with equal minimum values in A and B are selected, the transition from phase B to phase A is going to be accompanied by a jump of the potential (Euclidean action per volume) $\Delta v^{A\rightarrow B} = (v_0^B)_{corr} - (v_0^A)_{corr}$. The non-vanishing or vanishing value of $\Delta v^{A\rightarrow B}$ signals, whether the phase transition is a first order one or a continuous one, respectively. In the present setting, $(U_\Lambda^A)_{min}$ is non-vanishing only for RG trajectories belonging to the bare potential of a double-well form (those starting close to the phase boundaries III-I and III-II in phase III, and close to the phase boundary II-III in phase II). For the numerical computation of $\Delta v^{\mathrm{II}\rightarrow\mathrm{I}}$, I have selected RG trajectories which start at the 'distance' $t = 0.001$ from the phase boundary, i.e., very close to it. When evaluating $\Delta v^{\mathrm{III}\rightarrow\mathrm{I}}$, I took RG trajectories with the values of $v_1(\Lambda)$ increased in steps $t = 0.001$ and by this, the phase boundary is crossed. Lastly, $\Delta v^{\mathrm{III}\rightarrow\mathrm{II}}$ has been calculated from the comparison of RG trajectories for $\tilde{Y} = 1.1$ and 0.9 and various values of $\tilde{v}_1(\Lambda)$. All calculations have been conducted with the setting $\tilde{v}_2(\Lambda) = 0.01$. Fig. 3.19 shows the results. In the plot on the left, one can notice, that there is a jump of the free-energy density of 2 orders of magnitude larger for $0 < \tilde{Y} < 1$ than for $1 < \tilde{Y} < 2$. Along with the finding on the correlation length, this enables one to conclude, that the phase transition III$\rightarrow$ I is continuous, while II$\rightarrow$ I is of first order. The plot to the right in Fig. 3.19 shows that the phase transition III$\rightarrow$II is a first order one, with a latent heat per unit volume decreasing to zero, when the triple point is approached.

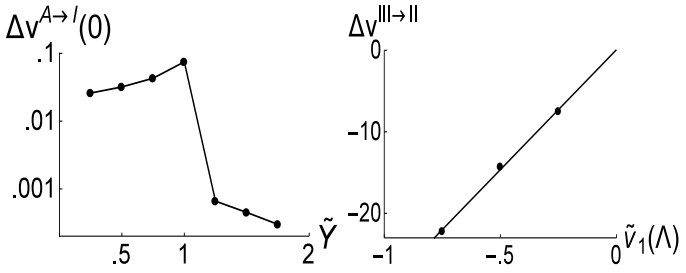

Figure 3.19: The jump of the 'free-energy density' $\Delta v^{A\to B}$ for B =I, A =II ($0 < \tilde{Y} < 1$) and A =III ($1 < \tilde{Y} < 2$) (left), and for A =III, B =II (right).

Chapter 4

Modified effective average action renormalization group method applied to the $O(1)$ ghost model with periodic condensate

This chapter is based on [**D**]. The work presented here is the continuation of Chapter 3, they share the motivation. However, it deserves an own chapter for the following reasons. I moved on from Wegner and Houghton's scheme to the effective average action approach, pursuing the goal to examine the ghost condensation in the higher orders of the gradient expansion. Namely, the numerical calculations were conducted in the NLO order of the GE. In the present chapter I consider the 3-dimensional, Euclidean scalar $O(1)$ ghost model, where the usual quadratic gradient term has the wrong sign, i.e., the wave function renormalization $Z = -1$ is negative and the positive quartic gradient term with the coupling $Y > 0$ ensures the boundedness of the action from below. It is a rather simple model in which a periodic vacuum state may occur. The $O(1)$ symmetric model has been chosen over the $O(2)$ symmetric one of the previous section, because of its simplicity: the formulas derived are very involved even in the $O(1)$ symmetric case and become increasingly more difficult when an $O(N)$-vector field is considered. In the 3-dimensional, Euclidean ordinary $O(2)$ models, the phase structure does not alter qualitatively compared to the $O(1)$ case, both models exhibit a symmetric and a symmetry broken phase. The critical behavior of the system changes, since different critical exponents correspond to the Wilson-Fisher fixed point, however the heart of this work is the study of the periodic condensates rather than the critical behavior. The introduction of [**D**] summarizes neatly the scheme we used in the work presented in this chapter: "We developed a modified version of the EAA RG approach [12] in order to

investigate the possibility of spatially periodic vacuum states in 3-dimensional Euclidean $O(1)$ ghost model and discussed the methodology in detail in [5]. Numerical results are obtained for the characteristics of the WF FP and the phase structure of the model in LPA and in NLO of the GE. The field-dependence of the derivative couplings is neglected for the sake of simplicity. However, the flow equations are expanded around the nontrivial minimum of the local potential (if there is any), which provides reliable results when the functional RG is applied to the ordinary $O(N)$ models, see Appendix A of [**A**]. In the $O(1)$ ghost model the opposite signs of the quadratic and quartic derivative terms ensure that at any value of the gliding scale k, there may exist Fourier-modes of the field with a particular momentum P_k. Then it may happen that for a field configuration with periodic condensate of momentum P_k, the value of the Euclidean action gets smaller than that for any homogeneous field configurations. The purpose of this work is to apply the modified EAA RG framework and study the scale-dependence of the periodic condensate. The basic idea of the modification is that the dynamical symmetry breaking - caused by the appearing of the periodic condensate - can be mimicked by explicit breaking of translation symmetry of the EAA. Mimicking dynamical symmetry breaking by an explicit one is a widely used approach in ordinary $O(1)$ scalar models when the Z_2 symmetric double-well potential is approximated by its truncated Taylor-expansion around one of its minimums [17, 6], and has also been successfully used in the case of the ordinary $O(N)$ scalar models, when spontaneous breaking of $O(N)$ symmetry has been partially mimicked by the inclusion of explicit symmetry breaking gradient terms into the EAA [**A**]. In a phase with a periodic condensate in the vacuum, the EAA should have its minimum at the corresponding periodic field configuration. Therefore we shall try to expand the EAA around the periodic field configuration minimizing it. It seems to be a too involved task to determine the exact form of the field configuration minimizing the EAA. Therefore, we shall look for it in a restricted subspace of field configurations, namely among the ones characterized by the particular momentum P_k at the gliding scale k and being periodic in the single spatial direction of the unit vector e_μ. The higher harmonics of the fundamental momentum P_k correspond to condensate modes of smaller wavelengths and are supposed to be gradually suppressed by the dynamics with decreasing scale k. Therefore, one expects that even the approximation containing only the fundamental Fourier mode with amplitude $\sigma_k(\Phi)$ and momentum P_k may provide physically reliable results for the low-energy behavior of the model. Therefore, we restrict ourselves to the one-mode approximation, where the homogeneous background Φ (the zero-mode) and the fundamental periodic mode of the background are taken into account. The modified EAA includes extra derivative terms and potentials induced by the periodic condensate which describe a kind of a back-reaction of the periodic condensate on the quantum fluctuating component of the scalar field. They do this in a self-consistent manner, because the induced terms are functionals of the total field, the sum of the background and the fluctuating piece. Whenever the Fourier-amplitude $\sigma_k(\Phi)$ vanish at some scale $k_{\rm fr}$, the corresponding induced terms are assumed to freeze out for $k < k_{\rm fr}$. As a further simplification we neglect the effect of the condensate induced on the derivative terms." The periodic condensation is a more general phenomenon, the condensates of ghost models may be periodic, but the periodic condensates are not restricted to ghosts. I have contributed in the derivation of the formulas as well as in the establishing of the algorithm for solving the equations. I have implemented a numerical code for this algorithm and performed the numerical computations. After this, I have also contributed

to the analysis of the numerical data.

4.1 Fourier-Wetterich renormalization group approach

This section elaborates the method used to achieve the RG-equations as well as the specific treatment one has to use to solve these equations.

4.1.1 Structure of the RG equation

In the process of applying the EAA RG approach to the one-component scalar field ϕ_x, one splits the EAA $\bar{\Gamma}_k[\phi] = \Gamma_k[\phi] + \Delta\Gamma_k[\phi]$ into the reduced EAA (rEAA) $\Gamma_k[\phi]$ and the regulator term

$$\Delta\Gamma_k[\phi] \quad = \quad \frac{1}{2}\int_{x,y} \phi_x \mathcal{R}_{k\ x,y}\phi_y, \tag{4.1}$$

where

$$\mathcal{R}_{k\ x,y} \quad = \quad R_k(-\Delta_\perp, -\partial_\parallel^2)\delta(x-y), \tag{4.2}$$

with a field-independent infrared (IR) cutoff function $R_k(u_\perp, u_\parallel)$. Throughout this chapter, the differential operators act always on the spatial coordinates x_μ ($\mu = 1,2,3$), with the parallel coordinate $x_\parallel = x_1 = x_\mu e_\mu$ and the transverse vector $x_\perp = (x_2, x_3)$ and k stands for the running cutoff, while $\partial_\parallel = \partial_{x_\parallel}$. Lastly, $\Delta_\perp = \sum_{\mu=2}^{3} \partial_{x_\mu}^2$ denote the Laplacian in the 2-dimensional plane perpendicular to the symmetry axis (x_1-axis). The WE for the rEAA Γ_k is

$$\dot{\Gamma}_k \quad = \quad \frac{1}{2}\mathrm{Tr}\left([\Gamma_k^{(2)} + \mathcal{R}_k]^{-1}\dot{\mathcal{R}}_k \right), \tag{4.3}$$

where the $\dot{}$ shows the scale-derivative $k\partial_k$, $\Gamma_k^{(2)}$ is a shorthand notation for the second functional derivative matrix $\Gamma^{(2)}_{k,x,y} = \frac{\delta^2\Gamma_k[\phi]}{\delta\phi_x\delta\phi_y}$. The trace operation is over a complete set of field configurations. Let us now make an ansatz for the rEAA, also keeping the gradient terms up to the quartic ones. The application of the usual GE technique involves the division of the field $\phi_x = \phi_{Bx} + \eta_x$ into the background piece ϕ_{Bx} and the inhomogeneous fluctuating field η_x. The background field $\phi_{Bx} = \Phi + \chi_x$ consists of the homogeneous background Φ and the periodic background

$$\chi_x \quad = \quad \sum_{n=1}^{N_m} 2\sigma_{n\ k}(\Phi)\cos(nP_k x_1) \tag{4.4}$$

representing the periodic condensate. For the rEAA, our general general ansatz is

$$\Gamma_k[\phi] \;=\; \frac{1}{2}\int_{x,y}\sum_{n=0}^{N_m}\phi_x D^{-1}_{n\ x,y}\phi_y\cos(nP_kx_1)+\int_x\sum_{n=0}^{N_m}U_{n\ k}(\phi_x)\cos(nP_kx_1), \tag{4.5}$$

where for each of the n-th modes, the kernels

$$D^{-1}_{n\ x,y}(-\Delta_\perp,-\partial_\parallel^2) \;=\; \mathcal{Z}_{n\ k}(-\Delta_\perp,-\partial_\parallel^2)\delta_{x,y} \tag{4.6}$$

have been introduced with the momentum-dependent but field-independent wave function renormalizations $\mathcal{Z}_{n\ k}(-\Delta_\perp,\,-\partial_\parallel^2)$. The Fourier-amplitudes $\sigma_{n\ k}(\Phi)$ and the momentum P_k are the ones that minimize the EAA at any given scale k for a given homogeneous background Φ.

The one-mode approximation stands for the truncation $N_m = 1$, when

$$\chi_x \;=\; 2\sigma_k(\Phi)\cos(P_kx_1) \tag{4.7}$$

and the notation can be shortened to $\mathcal{Z}_{0\ k}=\mathcal{Z}_k$, $\mathcal{Z}_{1\ k}=\mathcal{E}_k$, $U_{0\ k}=U_k$, $U_{1\ k}=V_k$, and $\sigma_{1\ k}=\sigma_k$. We keep the terms containing $\mathcal{E}_k$ in the general formulas for the flow equations, but our numerical results are obtained by setting $\mathcal{E}_k\equiv 0$, due to the complexity of the set of flow equations otherwise. The potentials and the amplitude of the periodic condensate are chosen to be polynomials,

$$U_k(\phi)=\sum_{n=2}^{M}\frac{g_n(k)}{n!}\phi^n,\qquad V_k(\phi)=\sum_{n=2}^{M-1}\frac{v_n(k)}{n!}\phi^n,\qquad \sigma(\phi)=\sum_{n=0}^{M-2}\frac{\sigma_n(k)}{n!}\phi^n. \tag{4.8}$$

The lowest-order derivatives $U_k''(\phi)$ and $V_k'''(\phi)$ of the potentials present in the propagator (the prime denoted differentiation with respect to the variable Φ) select the first nonvanishing terms. The flow of the ordinary potential U_k with the accuracy up to the term $\mathcal{O}(\phi^M)$ means, that the induced potential and the amplitude $\sigma_k(\phi)$ should be given the accuracy up to the term $\mathcal{O}(\phi^{M-1})$ and $\mathcal{O}(\phi^{M-2})$, respectively. The truncation $M=4$ is used in this chapter. It is assumed, that the ordinary potential displays Z_2 symmetry, $U_k(\phi)=U_k(-\phi)$, i.e., $g_3=0$ and $g_4>0$ for a physically reliable theory. When $g_2<0$, the ordinary potential exhibits nontrivial minimums at $\Phi=\pm\Phi_*$ for homogeneous field configurations. In this case, the expansion around the nontrivial minimum $\phi=\Phi_*$ yields

$$U_k(\phi)=\sum_{n=1}^{M}\frac{u_n(k)}{n!}\psi^n,\quad V_k(\phi)=\sum_{n=1}^{M-1}\frac{w_n(k)}{n!}\psi^n, \tag{4.9}$$

where $\Phi=\phi-\Phi_*$ and $\Phi_*=\sqrt{-6g_2/g_4}$, $u_1=0$, $u_2=-2g_2$, $u_3=g_4\Phi_*$, $u_4=g_4$ and $w_1=\frac{1}{2}v_3\Phi_*^2$, $w_2=v_3\Phi_*$, $w_3=v_3$. In this way, our calculations can be conducted in terms of Φ_*, u_4 and w_3.

In the one-mode approximation the momentum-dependence of the wave function

renormalization is chosen as

$$\mathcal{Z}_k(-\Delta_\perp,-\partial_\parallel^2) \;=\; -Z_{\perp\ k}\Delta_\perp - Z_{\parallel\ k}\partial_\parallel^2 + Y_{\perp\ k}\Delta_\perp^2 + 2Y_{X\ k}\Delta_\perp\partial_\parallel^2 + Y_{\parallel\ k}\partial_\parallel^4 \tag{4.10}$$

and a similar assumption is made for the momentum-dependence of $\mathcal{E}_k$. The ansatz (4.10) takes the axial symmetry into account, induced by the periodic condensate, but it respects the reflection symmetry $x_1 \leftrightarrow -x_1$. At the UV scale, the initial conditions are set to be $Z_{\perp\Lambda} = Z_{\parallel\Lambda} = -1$, $Y_{\perp\ \Lambda} = Y_{\parallel\ \Lambda} = Y_{X\ \Lambda} > 0$ (that ensure boundedness of the bare Euclidean action from below) and $\mathcal{E}_\Lambda = 0$.

The truncation of the functional Taylor-expansion at the quadratic term of the order $\mathcal{O}(\eta^2)$ results in the left-hand side of the WE taking the form

$$\dot\Gamma_k[\phi_B+\eta] \;=\; \dot\Gamma_k[\phi_B] + \int_x \dot F_{k\ x}\eta_x + \frac{1}{2}\int_{x,y}\eta_x\dot A_{k\ x,y}\eta_y, \tag{4.11}$$

while the expansion of the second functional derivative of the EAA is

$$\Gamma^{(2)}_{k\ x,y}[\phi_B+\eta] \;=\; A_{k\ x,y} + (\eta B)_{k\ x,y} + \frac{1}{2}(\eta C\eta)_{k\ x,y}, \tag{4.12}$$

where

$$F_{k\ x} \;=\; \left.\frac{\delta\Gamma_k}{\delta\phi_x}\right|_{\phi=\phi_B} \tag{4.13}$$

$$A_{k\ x,y} \;=\; \Gamma^{(2)}_{k,x,y}[\phi_B], \tag{4.14}$$

$$(\eta B)_{k\ x,y} \;=\; \int_z \eta_z \left.\frac{\delta^3\Gamma_k}{\delta\phi_x\delta\phi_y\delta\phi_z}\right|_{\phi=\phi_B}, \tag{4.15}$$

$$(\eta C\eta)_{k\ x,y} \;=\; \int_{z,u}\eta_z \left.\frac{\delta^4\Gamma_k}{\delta\phi_x\delta\phi_y\delta\phi_z\delta\phi_u}\right|_{\phi=\phi_B}\eta_u. \tag{4.16}$$

The terms linear in η on the left-hand side of the WE should vanish, i.e., $F_k = 0$, because the amplitude $\sigma_k(\Phi)$ and the characteristic momentum P_k of the periodic background χ_x are determined via minimizing the rEAA $\Gamma_k[\phi_B]$ for given scale k and homogeneous background Φ. The first few functional derivatives of the rEAA were derived explicitly in the one-mode approximation. Every term proportional to $\cos(P_k x_1)$ including the ones from the product $\cos(P_k x_1)\cos(2P_k x_1)$ were kept. After that, the left-hand side of the WE was expanded in the powers of the fluctuating field η_x at the background configuration ϕ_{Bx}, while keeping the terms up quadratic in the fluctuating field η_x. The latter is a technical tool to divide the flow of the potentials from the ones of gradient terms in the EAA. We supposed, that η_x does not contain Fourier-modes $\eta_Q = \int_x e^{iQx}\eta_x$ with zero momentum and with the longitudinal momenta P_k and its upper harmonics, implying that the terms linear in η_Q vanish exactly on both sides of the WE. The induced derivative piece with $\mathcal{E}_k(-\Delta_\perp,-\partial_\parallel^2)$ when not zero, would violate Z_2 symmetry of the rEAA. Therefore, we set $\mathcal{E}_k(-\Delta_\perp,-\partial_\parallel^2) = 0$. The left-hand side of the WE after the

lengthy but straightforward analytic manipulations is

$$\begin{aligned}\dot{\Gamma}_k[\phi_B+\eta] &= \dot{\Gamma}_k[\phi_B]+\gamma_k^{(1)}(\eta_{P_k e}+\eta_{-P_k e}) \\ &\quad +\int_Q \gamma_k^{(2)0}(Q_\perp^2,Q_\parallel^2)\eta_Q\eta_{-Q}+\sum_{\tau=\pm}\int_{Q,Q'}\gamma_k^{(2)1}(Q_\perp^2,Q_\parallel^2)\delta_{Q+Q'+\tau P_k e,0}\eta_Q\eta_{Q'}\end{aligned} \tag{4.17}$$

where the rEAA at the background configuration ϕ_{Bx} is

$$\begin{aligned}\Gamma_k[\phi_B]V^{-1} &= \sigma_k^2\mathcal{Z}_k(0,P_k^2)+\frac{1}{2}\Phi\sigma_k\mathcal{E}_k(0,P_k^2)+U_k(\Phi)+\sigma_k V_k'(\Phi) \\ &\quad +\sigma_k^2U_k''(\Phi)+\frac{1}{2}\sigma_k^3V_k'''(\Phi)+\frac{1}{4}\sigma_k^4U_k''''(\Phi),\end{aligned} \tag{4.18}$$

and the integral kernels are given as

$$\gamma_k^{(1)} = \sigma_k\dot{\mathcal{Z}}_k(0,P_k^2)+\frac{1}{4}\Phi\dot{\mathcal{E}}_k(0,P_k^2)+\frac{1}{2}\dot{V}_k'(\Phi)+\sigma_k\dot{U}_k''(\Phi)+\frac{3}{4}\sigma_k^2\dot{V}_k'''(\Phi)+\frac{1}{2}\sigma_k^3\dot{U}_k''''(\Phi), \tag{4.19}$$

$$\gamma_k^{(2)0}(Q_\perp^2,Q_\parallel^2) = \frac{1}{2}\dot{\mathcal{Z}}_k(Q_\perp^2,Q_\parallel^2)+\frac{1}{2}\dot{U}_k''(\Phi)+\frac{1}{2}\sigma_k\dot{V}_k'''(\Phi)+\frac{1}{2}\sigma_k^2\dot{U}_k''''(\Phi), \tag{4.20}$$

and

$$\gamma_k^{(2)1}(Q_\perp^2,Q_\parallel^2) = \frac{1}{4}\dot{\mathcal{E}}_k(Q_\perp^2,Q_\parallel^2)+\frac{1}{4}\dot{V}_k''(\Phi)+\frac{1}{2}\sigma_k\dot{U}_k'''(\Phi)+\frac{3}{8}\sigma_k^2\dot{V}_k''''(\Phi). \tag{4.21}$$

The scale-derivative $\dot{\Gamma}_k[\phi_B]$ of the rEAA at the given configuration ϕ_B should be evaluated by taking the scale-derivatives of the couplings in the expression (4.18) at given $\sigma_k(\Phi)$ and momentum P_k since the latter are parameters in ϕ_B.

The Z_2 symmetry is realized as follows. The ordinary Z_2 symmetric potential is an even function, $U_k(\Phi)=U_k(-\Phi)$. The symmetry of the rEAA demands $\sigma_k(\Phi)$ to be even accordingly (see the ordinary gradient piece in the right-hand side of Eq. (4.18).) The terms containing the induced potential in Eq. (4.18) are symmetric if and only if $V_k(\Phi)$ is an odd function, $V_k(\Phi)=-V_k(-\Phi)$. Moreover, the induced gradient term would only be symmetric if $\mathcal{E}_k(0,P_k^2)$ would change its sign under the transformation $\Phi\to-\Phi$, but for background-independent induced derivative piece this implies $\mathcal{E}_k(0,P_k^2)=0$ as the sole option. Hence, we are going to assume, that the induced gradient piece in the one-mode approximation vanishes, although we shall write down formally, how the RG flow equation could be derived for it.

The trace on the right-hand side of the WE (4.3) is sorted into terms by increas-

ing powers of η_x,

$$\mathrm{Tr}\bigg([\Gamma^{(2)}+\mathcal{R}_k]^{-1}\dot{\mathcal{R}}_k\bigg) \;=\; T_0+T_1+T_{2B}+T_{2C}, \tag{4.22}$$

with

$$\begin{aligned} T_0 &= \mathrm{Tr}[\mathcal{G}\cdot\dot{\mathcal{R}}_k], && (4.23)\\ T_1 &= -\mathrm{Tr}[\mathcal{G}\cdot(\eta B)\cdot\mathcal{G}\cdot\dot{\mathcal{R}}_k], && (4.24)\\ T_{2B} &= \mathrm{Tr}[\mathcal{G}\cdot(\eta B)\cdot\mathcal{G}\cdot(\eta B)\cdot\mathcal{G}\cdot\dot{\mathcal{R}}_k], && (4.25)\\ T_{2C} &= -\frac{1}{2}\mathrm{Tr}[\mathcal{G}\cdot(\eta C\eta)\cdot\mathcal{G}\cdot\dot{\mathcal{R}}_k]. && (4.26) \end{aligned}$$

Here $\mathcal{G}$ is the IR regulated full propagator described Appendix B.1. The matrices B and C are obtained explicitly, by the Fourier-transformation of the third and fourth functional derivatives of the rEAA at the field configuration ϕ_B. We need the values of the matrices B and C only at $\phi=\Phi_*$ in the flow equations for the derivative terms, because we are restricted to field-independent derivative couplings,

$$B_{p,q,r}|_{\Psi=0} = b_0\delta_{p+q+r,0}+b_1\sum_{\tau=\pm1}\delta_{p+q+r+\tau Pe,0}, \tag{4.27}$$

$$C_{p,q,r,s}|_{\Psi=0} = c_0\delta_{p+q+r+s,0}+c_1\sum_{\tau=\pm1}\delta_{p+q+r+s+\tau Pe,0}, \tag{4.28}$$

with $\Psi=\Phi-\Phi_*$

$$\begin{aligned} b_0 &= U_k'''(0)+\sigma_k(0)V_k''''(0) = u_4\Phi_*,\\ b_1 &= \frac{1}{2}\bigg(V_k'''(0)+\sigma_k(0)U_k''''(0)\bigg) = \frac{1}{2}\bigg(w_3+\sigma_0u_4\bigg),\\ c_0 &= u_4, \quad c_1=0, && (4.29) \end{aligned}$$

the prime $'$ denotes the differentiation with respect to the variable Ψ. The traces contributing to the flow equations are listed in Appendix B.2.

We assumed, that the RG transformations integrate out the various modes η_Q of the fluctuating field gradually in cylindrical momentum shells of thickness dk at momenta Q with $Q_\perp=|\vec{Q}_\perp|=k/\sqrt{2}$ and $Q_\parallel=\pm k/\sqrt{2}$. This choice is made in order to reconcile with the axial symmetry of the system implied by the periodic condensate. A Litim-type regulator is used and adjusted to the cylindrical symmetry of the system. The traces contain the loop-integrals

$$\int_p f(p_\perp^2,p_\parallel) \;=\; \alpha_3\int_{-k/\sqrt{2}}^{k/\sqrt{2}}dp_\parallel\int_0^{k/\sqrt{2}}dp_\perp p_\perp f(p_\perp^2,p_\parallel) \tag{4.30}$$

in cylindrical momentum coordinates with $\alpha_3=(2\pi)(2\pi)^{-3}=(4\pi^2)^{-1}$. Appendix B.1 is about the propagator and its regularization in greater detail.

4.1.2 Parameters of the periodic condensate

One needs two parameters P_k and $\sigma_k(\Phi)$ to describe the periodic condensate in the one-mode approximation. The former is the characteristic momentum, while the latter is the amplitude of the aforementioned condensate. The rEAA $\Gamma_k[\phi_B]$ given by Eq. (4.18) should be considered as the function of and minimized with respect to the parameters P and σ at any given scale k and homogeneous background Φ. The full set of the necessary conditions of the extremums are

$$\partial\Gamma_k[\phi_B]/\partial P^2 = 0, \tag{4.31}$$

$$\partial\Gamma_k/\partial\sigma = 0, \tag{4.32}$$

with their solutions being

$$P_k^2 = -\frac{Z_{\|k}}{2Y_{\|k}}, \tag{4.33}$$

$$0 = V_k'(\Phi) + 2\sigma_k(\Phi)\left(U_k''(\Phi) - \frac{Z_{\|k}^2}{4Y_{\|k}}\right) + \frac{3}{2}\sigma_k^2(\Phi)V_k'''(\Phi) + \sigma_k^3(\Phi)U_k''''(\Phi). \tag{4.34}$$

The equation for σ is solved by using Cardano's formulas. The solution either has one or three real roots. At every value of the running scale k, the root providing the deepest minimum for the rEAA is used. This is achieved by substituting into the different roots and comparing the resulting value of the rEAA.

4.1.3 Strategy for solving the RG equations

The flow equations for the potentials and the wave function renormalizations are exploited by equating the terms of the order $\mathcal{O}(\eta^0)$ and those of $\mathcal{O}(\eta^2)$ on both sides of the WE, respectively. The setting $\sigma_k = 0$ in the flow equation for the potentials allows one to obtain the flow equation for the ordinary potential $U_k(\Phi)$. The original equation for the potentials with $\sigma_k(\Phi)$ corresponding to the (deepest) minimum of the EAA is considered to be the flow equation for the induced potential $V_k(\Phi)$. The couplings of the potentials are determined by the expansion of the both sides of the flow equation for U_k and that for V_k in powers of $\Psi = \Phi - \Phi_*$. The flow equations for the wave function renormalizations $Z_\|$ and $Z_\perp$ are obtained by equating the second partial derivatives with respect to the momenta $Q_\|$ and $\vec{Q}_\perp$ on both sides of the flow equation for the wave function renormalization when $\Phi = \Phi_*$ is set. The explicit flow equations for the various couplings were generated by a computer algebraic code, written by me. The RG flow of the various couplings can be computed numerically, by iterating the list of steps below, starting from the UV scale $k = \Lambda$ with given initial conditions for the couplings and with a given resolution $\delta k = \Delta k/k$ =const. (Δk is step in k in every iteration). An example step, taken after the scale k is given as

1. Calculate the couplings of the ordinary potential $U_{k-\Delta k}$ at the lower scale $k - \Delta k$ from the flow equation for the ordinary potential (with $\sigma_k = 0$).

2. Determine P_k and $\sigma_k(\Phi)$, by solving Eqs. (4.33) and (4.34) and finding the root minimizing the EAA at the scale k.

3. Insert $\sigma_k(\Phi)$ into the flow equation for the induced potential and into the flow equation for the wave function renormalizations and determine the couplings of $V_{k-\Delta k}$, $Z_\perp(k-\Delta k)$ and $Z_\parallel(k-\Delta k)$ at the lower scale $k-\Delta k$. If the amplitude $\sigma_k(\Phi)$ calculated in the second step happens to be zero, then do not change the induced potential and compute the values $Z_\perp(k-\Delta k)$ and $Z_\parallel(k-\Delta k)$ of the wave function renormalizations for $\sigma_k = 0$.

4.2 Numerical results

4.2.1 On our numerical approach

The phase structure of the Euclidean 3-dimensional $O(1)$ ghost model in various approximations of the Fourier-Wetterich RG framework is explored by numerical means in a successive manner. The LPA of the zero-mode approximation (LPA0) was examined first, then the LPA of the one-mode approximation (LPA1). As for the next step, we moved on to the NLO, where the NLO of the zero-mode approximation (NLO0), and the NLO of the one-mode approximation (NLO1) were studied. The zero-mode approximation is basically the ordinary EAA approach. For NLO1, the flow equations of the wave function renormalizations include several terms proportional to different (up to third) powers of the induced vertex $\mathfrak{V}$. The induced vertex $\mathfrak{V}$ is introduced in the expression of the full propagator via the resummation of elementary interaction processes between the fluctuating field η_x and the periodic background field χ_x, in which interactions an intermediate shift of the longitudinal momentum with $\pm P_k$ occurs (see Appendix B.1). In the present case, the backreaction of the periodic condensate of the gradient terms of the EAA is neglected, i.e., $\mathcal{E}_k = 0$ is chosen. Hence, the induced vertex becomes independent of the momenta. Furthermore, the induced vertices are nonvanishing in the flow equations for the wave function renormalizations $Z_\parallel$ and $Z_\perp$, if the field-dependencies are expanded around the nontrivial minimum Φ_* of the ordinary potential U_k.

The phase diagram is spanned in the space $\{\tilde{c}_i\}$ of the dimensionless couplings. In order to determine it, several RG trajectories - with different initial conditions - have been computed numerically and their infrared behaviors have been compared. The trajectories lie in the same phase, when their infrared behavior is qualitatively the same. In the scenario when the local potential has nontrivial minimums, the space of the couplings in LPA0 is $\{\tilde{\Phi}_*, \tilde{u}_4\}$, in NLO0 it is $\{\tilde{\Phi}_*, \tilde{u}_4, Z_\parallel, Z_\perp\}$, while in the case of a trivial minimum it is $\{\tilde{g}_2, \tilde{g}_4\}$ for LPA0 and $\{\tilde{g}_2, \tilde{u}_4, Z_\parallel, Z_\perp\}$ for NLO0. In the one-mode approximation these spaces also include the coupling $\tilde{v}_3$. The final results below are presented in terms of the coupling $\tilde{g}_2$ (which is just the coupling proportional to Φ^2), rather than $\tilde{\Phi}_*$ for the sake of transparency.

Generally, the initial conditions were set to be $Z_{\parallel\,\Lambda} = Z_{\perp\,\Lambda} = 1$ and $\tilde{Y}_\parallel = \tilde{Y}_X = \tilde{Y}_\perp = \tilde{Y} \in (0, 2]$ and $\tilde{v}_3(\Lambda) = 0$ corresponding to a Z_2 symmetric model at the UV scale $\Lambda = 1$, only $\tilde{u}_4(\Lambda)$ and $\tilde{\Phi}_*$ were varied in order to explore the phase structure of

the model.I implemented the fourth order explicit Runge-Kutta method to solve the RG equations with the numerical resolution set to $\delta k = 5 \times 10^{-3}$.

In LPA0 and LPA1 the fixed points were calculated with the usage of the Newton-Rhapson method. In NLO1, we were keen on the effect of the periodic condensate on the RG flow of the wave function renormalizations and due to this, we did not absorb $Z_{\parallel}$ or $Z_{\perp}$ into the definitions of the dimensionless couplings. This makes the location fixed points from the vanishing of the beta-functions impossible, since the wave function renomalizations do not display constant, plateau-type scaling in the vicinity of the fixed points. Therefore, the initial conditions were fine-tuned numerically to get RG trajectories approaching a fixed point sufficiently close. The LPA0 at $Z_{\parallel\,\Lambda} = Z_{\perp\,\Lambda} = 1$, where the wave function renormalizations do not exhibit nontrivial RG-flow, has two fixed points,

$$\tilde{u}_4^{\mathrm{G}} = 0, \qquad \tilde{\Phi}_*^{\mathrm{G}} = \frac{1}{2\pi}\left[\frac{3}{\sqrt{2}}\frac{2\tilde{Y}-1}{(\tilde{Y}-1)^2}\right]^{\frac{1}{2}}, \tag{4.35}$$

$$\tilde{u}_4^{\mathrm{WF}} = \frac{9\pi^2}{\sqrt{2}}\frac{(\tilde{Y}-1)^3}{2\tilde{Y}-1}, \qquad \tilde{\Phi}_*^{\mathrm{WF}} = \frac{1}{\pi}\left[\frac{1}{3}\frac{2\tilde{Y}-1}{(\tilde{Y}-1)^2}\right]^{\frac{1}{2}}, \tag{4.36}$$

the Gaussian and the Wilson-Fisher fixed points, respectively, where $\tilde{g}_4 = \tilde{u}_4$ and $\tilde{g}_2 = -\frac{1}{6}\tilde{\Phi}_*^2\tilde{u}_4$. The LPA1 results are very similar, there the above results are extended with the fixed point values $\tilde{v}_3^{\mathrm{G}} = \tilde{v}_3^{\mathrm{WF}} = 0$ and the vanishing amplitude of the periodic condensate. Therefore in LPA we can state, that the critical theory has no periodic condensate. Furthermore in the $\tilde{Y} \in (0, 2]$ range, the WF fixed point is only present for $1 < \tilde{Y} < 2$ with $\tilde{g}_2^{\mathrm{WF}} < 0$ and for $0 < \tilde{Y} < \frac{1}{2}$ with $\tilde{g}_2^{\mathrm{WF}} > 0$. In the NLO1 approximation, we clearly found the IR repulsive Gaussian fixed point, which can clearly be identified on the planar slices on Fig. 4.1. The existence of the WF fixed point is also established in NLO1, however it behaves differently in the cases with $\tilde{g}_2^{\mathrm{WF}} > 0$ and $\tilde{g}_2^{\mathrm{WF}} < 0$, see the rightmost figure in Fig. 4.3 and Fig. 4.4, respectively. The difference can be explained with the contributions of the induced vertex $\mathfrak{V}$: (1) for $\tilde{g}_2^{\mathrm{WF}} > 0$ one has to use the expansion around the trivial minimum of the ordinary potential, because the critical potential is a parabola with a trivial minimum. In this case, the induced vertex vanish $\mathfrak{V}(\tilde{\Phi} = 0) = 0$; (2) for $\tilde{g}_2^{\mathrm{WF}} < 0$ one has to use the expansion around the nontrivial minimum of the ordinary potential. In this scenario, the critical potential is the 'Mexican-hat' type potential with two nontrivial minimums. The induced vertex does not vanish now $\mathfrak{V}(\tilde{\Phi} = \tilde{\Phi}^*) \neq 0$. In the (1) case, the periodic condensate assumes complex values in a short interval, when the trajectory is sufficiently close to the WF fixed point. The imaginary part of $\tilde{\sigma}$ is found to be of the same order of magnitude as its real part, thus it should be a systematic error of the employed method, rather than a numerical one. When the imaginary part becomes nonvanishing, we switch to the usage of $\tilde{\sigma}_k = 0$ and freeze the evolution of $\tilde{v}_3$, the latter frozen value tends to zero on trajectories, which pass the WF fixed point closer and closer. This is agrees with the findings of the LPA1, that the critical theory has no periodic condensate in it.

4.2.2 The phase structure

The phase diagram projected on the $(\tilde{g}_2, \tilde{Y})$ plane at $\tilde{g}_4 = 0$ in the NLO1 approximation is shown on the top on Fig. 4.1. This is supplemented with various planar slices on the $(\tilde{g}_2, \tilde{g}_4)$ plane at fixed, constant $\tilde{Y}$. The subscripts in the roman numbers denote, whether the trajectories in that given phase had to be computed with the expansion around the trivial minimum of the local potential (1) or with the nontrivial one (2). The NLO1 approximation has non-negligible effect on the behavior of several phases compared to the LPA1. Furthermore in NLO1, the induced vertices $\mathfrak{V}$ (compared to no vertices included) further affect the behavior of some phases. The vertical line at $\tilde{g}_2 = 0$ on the top figure of Fig. 4.1 stand for the Gaussian fixed line. On the horizontal line at $\tilde{Y} = 1$ the momentum dependence of the inverse propagators cancel, while on the line $\tilde{Y} = \frac{1}{2}$ the quantum corrections vanish in the flow equations due to the factor $1 - 2\tilde{Y}$. Also, the straight line $\tilde{g}_2 = 1 - \tilde{Y}$ is shown for $\tilde{Y} \in [0, 1]$. These lines represent phase boundaries in the plane $\tilde{g}_4 = 0$. The intersection of these lines are the multicritical points, connecting 3 to 4 phases. The typical RG-flow of the coupling of the induced potential $\tilde{v}_3$, the anomalous dimensions $\eta_A = -\beta_{Z_A}/Z_A$ $(A = \|, \perp)$, and the dimensionless amplitude of the periodic condensate $\tilde{\sigma}_0 = \tilde{\sigma}_k(\Phi = 0)$ are shown in every phase and subspace.

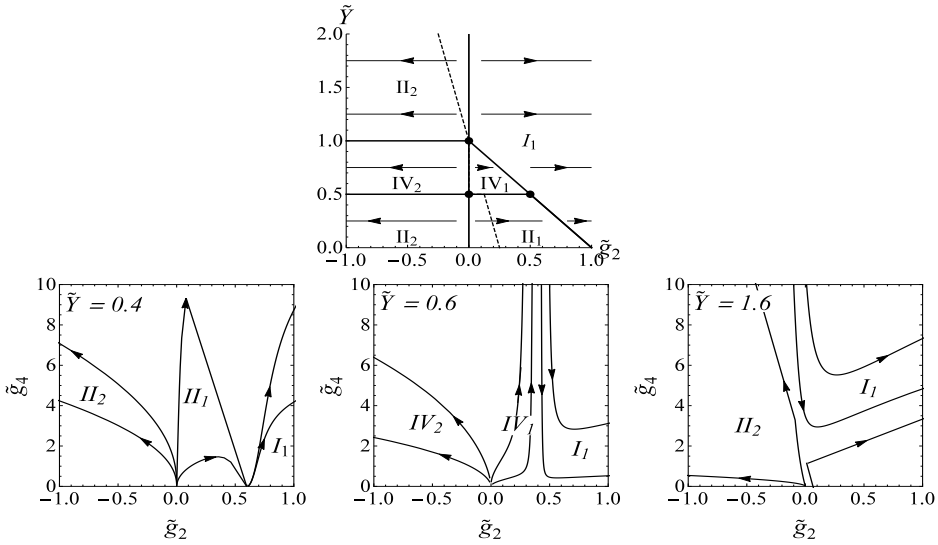

Figure 4.1: The phase diagram on the $(\tilde{g}_2, \tilde{Y})$ plane at $\tilde{g}_4 = 0$ (top) and various planar slices on the $(\tilde{g}_2, \tilde{g}_4)$ plane in the NLO1 approximation. The full lines denote the phase boundaries, the arrows show the flow of the RG trajectories in the given phase, the dots correspond to the multicritical points. The dashed line is the projection of the WF fixed point onto the $(\tilde{g}_2, \tilde{Y})$ plane. Lastly, the different phases are labeled with roman numbers.

Symmetric Phase I_1

This phase is present for all $\tilde{Y}$ in the range $(0, 2]$ and is characterized by the following three attributes: *(i)* the couplings $\tilde{g}_2$ and $\tilde{g}_4$ tend to positive infinities in the infrared scaling region, with tree-level scaling laws $\tilde{g}_2 \sim k^{-2}$ and $\tilde{g}_4 \sim k^{-1}$, so the dimensionful ordinary potential is convex in the IR limit; *(ii)* the periodic condensate dies at an intermediate scale and this freezes the evolution of $\tilde{v}_3$, see Fig. 4.2; *(iii)* the wave function renormalizations $Z_{\parallel}$ and $Z_{\perp}$ saturate at constant values after a rather short intermediate scaling. The symmetric phase stays unaltered beyond LPA1. Trajectories, which belonging to this phase can also be found for $\tilde{Y} > 1$ and for some values $\tilde{g}_2(\Lambda) < 0$, when one has to use the expansion around the nontrivial minimum of the local potential. In that scenario, the symmetric phase is identified by trajectories which reach $\tilde{\Phi}_* = 0$ at finite k' scales. Whenever $\tilde{\Phi}_* = 0$ occurs, one has to turn to the expansion around the trivial minimum of the potential to continue the RG flow below k'.

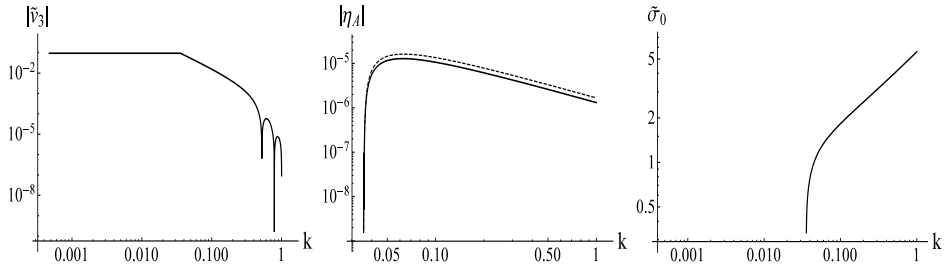

Figure 4.2: A typical RG flow of $\tilde{v}_3$, η_A $(A = \|, \perp)$ and $\tilde{\sigma}_0$ in Phase I_1 at $\tilde{Y} = 1.6$. The dashed and the continuous lines correspond to $\eta_{\|}$ and $\eta_{\perp}$, respectively.

Symmetry breaking Phases II_1 and II_2

Two subspaces II_1 and II_2 show the characteristics of a symmetry breaking phase, although they behave differently in the IR. Subspace II_1 can be found at $\tilde{g}_2 > 0$ and $0 < \tilde{Y} < \frac{1}{2}$, see the bottom left figure on Fig. 4.1. In subspace II_1, the expansion around the trivial minimum of the potential had to be used. The WF fixed point controls the RG flow in subspace II_1. It deflects the RG flow of the trajectories to ultimately terminate in the point $\tilde{g}_2 = 1 - \tilde{Y}$ and $\tilde{g}_4 = 0$, this way, the dimensionful ordinary potential becomes convex and universal and its dimensionful counterpart vanishing in the IR limit. Subspace II_2 is present for $\tilde{g}_2 < 0$ and $0 < \tilde{Y} < \frac{1}{2}$ and $1 < \tilde{Y} < 2$ as can be seen on the bottom left and right figures on Fig. 4.1. The trajectories there end up assuming their tree-level infrared scaling laws, with $\tilde{g}_2 \sim -k^{-2}$, $\tilde{g}_4 \sim k^{-1}$ and $\tilde{v}_3 \sim -k^{3/2}$, with the IR dimensionful ordinary potential being concave. This has to be the fault of the approximations used by us. The WF fixed point can only be found in Phase II_2 for $1 < \tilde{Y} < 2$ as the dashed line on the top figure of Fig. 4.1 shows the position of the WF fixed line on the $(\tilde{g}_2, \tilde{Y})$ plane. Wherever the WF fixed point can be found, there is a separatrix on the plane $(\tilde{g}_2, \tilde{g}_4)$ connecting the Gaussian and the WF fixed points and separating the phases II_1 and I_1 for $0 < \tilde{Y} < \frac{1}{2}$ and II_2 and I_1 for $1 < \tilde{Y} < 2$. Wherever possible, we have

investigated the behavior of the scaling of the amplitude of the periodic condensate in the vicinity of the Wilson-Fisher fixed point along fine-tuned trajectories flowing in the close neighborhood of the separatrix. In Phase II_1 the results show, that the periodic condensate is present in trajectories passing very close to the WF fixed point, with both the dimensionless $\tilde{\sigma}$ and its dimensionful counterpart diverging in the IR scaling regime as $\tilde{g}_4 \to 0$ (see Fig. 4.3). Contrarily, in Phase II_2 (for $< \tilde{Y} < 2$) the periodic condensate dies out for trajectories sufficiently close to the WF fixed point and it revives when the RG trajectory flows away from the WF fixed point (see Fig. 4.4). The dimensionless amplitude $\tilde{\sigma}$ assumes a constant value in the IR scaling region, so that the dimensionful amplitude vanishes as $k \to 0$. As for phase II_2 for $0 < \tilde{Y} < \frac{1}{2}$, one can find no WF fixed point, however the IR scaling laws of the couplings and that of the amplitude of the periodic condensate are exactly the same as the ones for phase II_2 for $1 < \tilde{Y} < 2$.

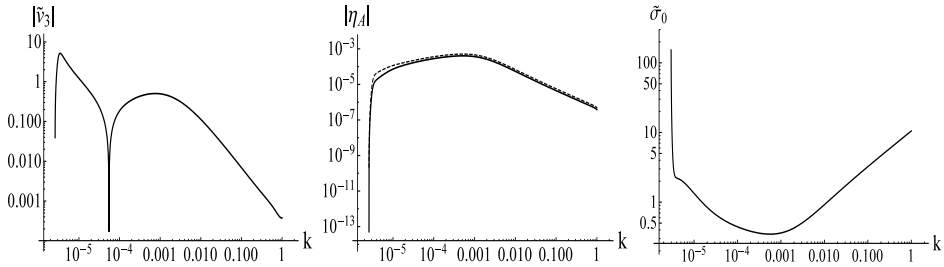

Figure 4.3: A typical RG flow of $\tilde{v}_3$, η_A $(A = \|, \perp)$ and $\tilde{\sigma}_0$ in Phase II_1 at $\tilde{Y} = 0.4$. The dashed and the continuous lines correspond to $\eta_\|$ and $\eta_\perp$, respectively.

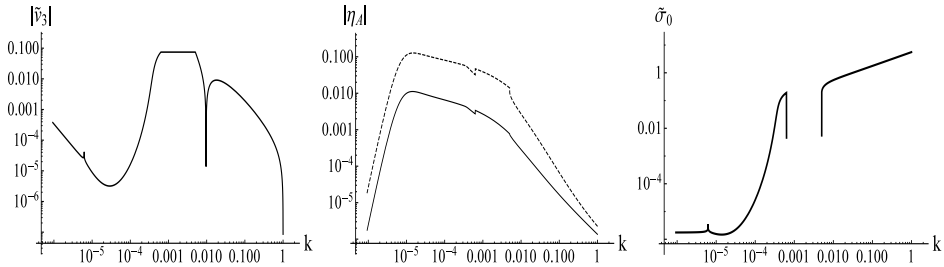

Figure 4.4: A typical RG flow of $\tilde{v}_3$, η_A $(A = \|, \perp)$ and $\tilde{\sigma}_0$ in Phase II_2 at $\tilde{Y} = 1.6$. The dashed and the continuous lines correspond to $\eta_\|$ and $\eta_\perp$, respectively.

Phase III

This phase cannot be found on the phase diagrams, shown on Fig. 4.1. Phase III can only be observed in LPA0 for $\tilde{g}_2 < 0$ and $0 < \tilde{Y} < \frac{1}{2}$. The coupling $\tilde{g}_4$ here has the infrared scaling $\tilde{g}_4 \sim k^1$, i.e. it dies out in the IR limit. Moving beyond LPA0, in LPA1 and NLO1, this phase turns into Phase II_2, which means, that the couplings assume the following scaling laws $\tilde{g}_2 \sim -k^{-2}$, $\tilde{g}_4 \sim k^{-1}$ and $\tilde{v}_3 \sim -k^{3/2}$.

Phases $\mathbf{IV}_1$ and $\mathbf{IV}_2$

Phases IV_1 and IV_2 are located in the range $\frac{1}{2} < \tilde{Y} < 1$. The subspaces IV_1 and IV_2 are similar regarding their qualitative behavior. The corresponding quantities are shown on Fig. 4.5 for Phase IV_1 and in Fig. 4.6 for Phase IV_2. The trajectories are computed by using the expansion around the trivial and nontrivial minimum of the local potential, respectively. This phase is characterized by the blowing up of $\tilde{g}_4$ in subspace IV_1 and that of the wave function renormalizations in subspace IV_2 hand-in-hand with the abrupt vanishing of the dimensionless amplitude of the periodic condensate in both cases. The blowing up also means the termination of the RG flow at some intermediate scale.

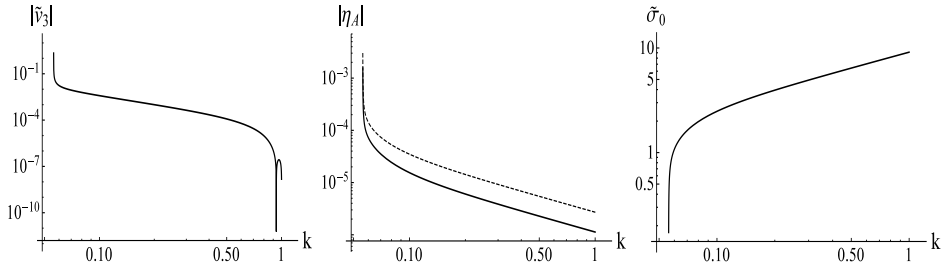

Figure 4.5: A typical RG flow of $\tilde{v}_3$, η_A ($A = \|, \perp$) and $\tilde{\sigma}_0$ in Phase IV_1 at $\tilde{Y} = 0.6$. The dashed and the continuous lines correspond to $\eta_{\|}$ and $\eta_{\perp}$, respectively.

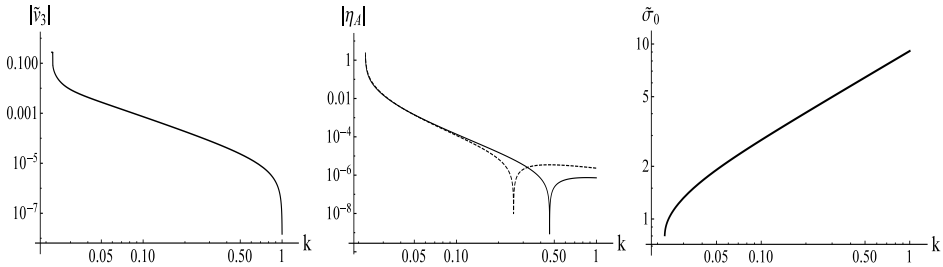

Figure 4.6: A typical RG flow of $\tilde{v}_3$, η_A ($A = \|, \perp$) and $\tilde{\sigma}_0$ in Phase IV_2 at $\tilde{Y} = 0.6$.The dashed and the continuous lines correspond to $\eta_{\|}$ and $\eta_{\perp}$, respectively.

Chapter 5

Conclusions

This chapter summarizes the content and the results of the present PhD thesis in English language.

Chapter 1 introduces the reader to the Functional Renormalization Group together with a brief reminder on the features of the 3-dimensional, $O(N)$ symmetric models.

Chapter 2 is about mastering the methodology of the gradient expansion in the context of Wetterich's RG equation. The employed ansatz, alongside the approximations provide results in the fourth order of gradient expansion (NNLO) for the critical exponents of the $O(N)$ models. Firstly, the $O(1)$ model has been investigated. I have determined the stability of the polynomial expansion by computing the truncation dependence of ν, η and the first subleading scaling correction ω. The $d = 4-\epsilon$ expansion has been performed and the results agree very well with the literature and I have established as a new result, that the dimensionless quartic gradient coupling scales as $\bar{Y} \sim \epsilon^3$. In continuous dimensions $2 < d < 4$, I have determined the dimension dependence of ν and η and the trends of these functions are in excellent accordance with the literature. The effect of the NNLO on the critical exponents compared to the second order of the gradient expansion (NLO) was found to never exceed 5%, the magnitude of this effect varies in the literature. I deducted, that this variation possibly originates from the choice of regulator function and whether the field dependence of the wave function renormalization is neglected or not. I have compared the results of our highest level approximation in $d = 3$ with that of the literature. I have found, that my result $\nu = 0.634$ is rather close to FRG's most accurate $0.630^{+0.002}_{-0.005}$. My result for the anomalous dimension $\eta = 0.059$ exceeds the FRG's most accurate $0.034^{+0.005}_{-0.003}$ by about 60%. The reason behind this deviation is argued to be the same as the one behind the variation of the magnitude of the NNLO effect in different schemes. I have established, that the quartic gradient coupling $\tilde{Y}$ assumes zero fixed point value at the Wilson-Fisher fixed point WFFP at $d \approx 8/3$ and falls to negative ones for lower dimensions $2 < d < 8/3$. On one hand, this causes the action to be unbounded from below. On the other hand, it is argued to be caused by the emergence of a new, multicritical point. For the first time in the literature, I have calculated the critical exponents ν and η of the $O(N)$ models for $N > 1$ in NNLO in dimension $d = 3$. The RG evolution

of the wave function renormalizations for the Goldstone modes and the radial mode was found to be different on trajectories, which are close to the separatrix. I have followed the principle of minimal symmetry breaking, i.e., computed the results at fixed ratio $\hat{z} = 1$ of the wave function renormalizations and have arrived to results, that are consistent with the literature in NLO. The difference between the evolution of the Goldstone and radial modes' wave function renomalizations is the most prominent on trajectories, which are close to criticality. There, in the vicinity of the WFFP, the β-function of their ratio $\hat{z}$ should tend to zero, however it has the magnitude $\mathcal{O}(\eta)$, which is small ($< 10^{-1}$), in the case of the 3-dimensional $O(N > 1)$ models. The NNLO corrections for the critical exponents in the range $100 > N > 1$ were found to be the following. $\delta\eta$ is the relative NNLO correction of the radial mode's anomalous dimension and it never exceeds 1%, while $\delta\bar{\eta}$ corresponding to the Goldstone modes never exceeds 0.2%. Lastly, the relative NNLO correction for ν, $\delta\nu$ was found to be tiny and asymptotically vanishing for large N. I have also provided data on the N-dependence of the first three scaling corrections in NNLO. As my personal contribution to the paper, which is the basis of this chapter, I have contributed to the derivation of the flow equations, I have written computer programs for the numerical calculations and have provided the numerical data and contributed to its analysis and I have also made the figures in the paper [**A**], which is the basis of this chapter.

In chapter 3, the motivation was to study the so called periodic condensation in terms of the FRG. Models with periodic groundstates are relevant in many fields of physics. Such periodic condensation can be observed in models where the sign of the gradient terms alternate. Such a model is presently studied ghost $O(2)$-model. This chapter elaborates the phase structure and the infrared behavior of the 3-dimensional ghost $O(2)$ model in two different approaches in the local potential approximation (LPA), using Wegner and Houghton's RG equation and the tree-level renormalization procedure. I denote the first approach with Case Y, where the dimensionful higher derivative coupling, corresponding to the quartic gradient term in the action is kept constant. Where the dimensionless counterpart of Y is kept constant is denoted with Case $\tilde{Y}$. The phase structure of the model turned out to be richer in Case $\tilde{Y}$ with three phases, than in Case Y with two phases. Thus, it remains an open question, whether the model exhibits two or three phases. The ambiguity of keeping constant either the dimensionful or the dimensionless higher-derivative coupling is an essential feature of the LPA and cannot be avoided in the WH RG approach. Articles [**B**] and [**C**] exemplify, that such an ambiguity may heavily affect the physical results, when higher-derivative terms are included into the model. This ambiguity is lifted beyond the LPA in the gradient expansion. As a first step of the work, I have implemented a program for the numerical computation of the tree-level renormalization, which was used to study the deep-infrared scaling of the RG-trajectories and ultimately to identify phases. This has been tested on the 3-dimensional ordinary $O(1)$ models and the 2-dimensional sine-Gordon model with success. I have reproduced the known infrared scaling laws of the couplings of those models. Nextly, we have moved on to the actual subject of the investigation, the 3-dimensional ghost $O(2)$ model. In Case Y, I have found two phases. A symmetric one, where no ghost condensation occurs and a phase with 'restored' symmetry. In the latter the periodic condensate was present at intermediate scales but washed out in the low energy limit. It has also been established, that the correlation length remains finite when the phase boundary is approached in the

phase with restored symmetry, this suggests the presence of a first order phase transition. In Case $\tilde{Y}$, I have identified three phases (I, II and III) with an emergent triple point and have also identified the types of phase transitions. Phase I is present for any positive $\tilde{Y}$, it is similar to the symmetric phase of the ordinary O(2) model. Phase II is present, when $0 \leq \tilde{Y} \leq 1$. The dimensionful effective potential in phase II is quasi-universal, it depends on $\tilde{Y}$, yet it is independent of the other bare couplings. Phase II has no analogue in the ordinary O(2) model, however it has the same properties as the symmetry restored phase, found in [**B**]. Its existence is based on the ghost-condensation mechanism available in the model with $Z < 0$ and $\tilde{Y} > 0$. Phase III can be found in the range $1 < \tilde{Y} \leq 2$. Here, the dimensionful effective potential is universal. It exhibits the Maxwell cut, which is accompanied with the non-vanishing amplitude of the periodic spinodal instability for scales $k \to 0$. Phase III is the one, where spontaneous symmetry breaking occurs similarly to the symmetry breaking phase of the ordinary $O(2)$ model. The phase boundaries III-I and III-II intersect in a triple line. It has been found, that phase transitions $II \to I$ and $III \to II$ are of first order, while $III \to I$ is a continuous one. My personal contribution to this part of the work have been the following: I have written computer programs for the numerical calculations, have provided the numerical data and have contributed to its analysis and I have also made the figures for papers [**B**, **C**].

Chapter 4 is based on [**D**]. There, I employed a modified version of the EAA RG method, called by the authors the Fourier-Wetterich RG scheme. The method is not elaborated in this chapter due to its length, but can be found on the arXiv [5]. This scheme has been developed in order to study condensates displaying spatial periodicity in terms of FRG, but at higher levels of the gradient expansion. The 3-dimensional, Euclidean $O(1)$ ghost model was studied in detail, in the action of which the usual $\mathcal{O}(\partial^2)$ kinetic term appears with the 'wrong' sign and also a positive definite quartic $\mathcal{O}(\partial^4)$ derivative term has been included. This alternating sign of the gradient terms in this ghost model may cause the formation of a periodic condensate. It is assumed, that the condensate can be approximated with a truncated Fourier-series with N_m modes, among them the zero-mode with N_0 includes the homogeneous background Φ, while the first mode of the scale-dependent wave number P_k and the amplitude $\sigma_k(\Phi)$ is the fundamental mode. The scheme allows one to take upper harmonics into account, but their role is argued to be suppressed for decreasing running scale k. The parameters of the periodic condensate are determined by the minimization of the EAA at each value of the scale k during the solution of the RG flow equations. The periodic condensate is supposed to reveal periodicity in one spatial direction, meaning that the system exhibits cylindrical symmetry. Hence, the direction parallel to the condensate's axis and those perpendicular to it should be distinguished in the kinetic terms of the EAA. In the NLO of the GE, this manifests as wave function renormalizations $Z_{\parallel}$ and $Z_{\perp}$, differing in the longitudinal and transverse directions. In order to close the set of the flow equations for the truncation N_m of the Fourier series, additional potentials and additional derivative terms are incorporated into the ansatz for the EAA. These represent the terms induced by the various Fourier-modes of the periodic condensate. The zero-mode approximation ($N_m = 0$) corresponds to the ordinary EAA RG approach, when the periodic condensate is neglected. The proposed Fourier-Wetterich RG scheme allows one to study, when the periodic condensate occurs and how it evolves during the RG flow and to show in which of the phases the condensate survives the IR limit. I performed numerical calculations

to determine the characteristics of the WF FP and the phase structure of the model in the one-mode approximation in the NLO of the GE. The phase diagram has been studied at constant values of $\tilde{Y} \in (0, 2]$ and depicted on the plane, spanned by the couplings $\tilde{g}_2$ and $\tilde{g}_4$ corresponding to the dimensionless mass squared and the quartic coupling of the ordinary potential, respectively. Although whenever it was possible, we expanded our equations around the nontrivial minimum of the local potential, and used the dimensionless couplings $\tilde{\Phi}_* = \sqrt{-6\tilde{g}_2/\tilde{g}_4}$ and $\tilde{g}_4$ in our numerical work. In the scenario of the potential having nontrivial minima, this provides physically more reliable results than the expansion around the vanishing background field. Moreover, in this case, all the terms and contributions corresponding to the induced vertex $\mathfrak{V}$ are taken into account. Due to this, the RG flow of the wave function renormalizations is very strong, compared to my previous, preliminary numerical analysis [5] and it indeed affects the phase structure. The calculations show the existence of five phases: A symmetric one called Phase I_1 present for $\tilde{Y} \in (0, 2]$, with no periodic condensate in the IR. In the IR scaling region $\tilde{g}_2$ and $\tilde{g}_4$ show their tree-level scaling laws; Two symmetry breaking breaking phases II_1 and II_2 for $0 < \tilde{Y} < \frac{1}{2}$ and $1 < \tilde{Y} < 2$, where the $O(1)$ symmetry is spontaneously broken. The symmetry breaking is governed in both cases by the WF fixed point, but the phase behaves differently when $\tilde{g}_2^{\mathrm{WF}} > 0$ or $\tilde{g}_2^{\mathrm{WF}} < 0$. In the $\tilde{g}_2^{\mathrm{WF}} > 0$ case (II_1), the dimensionless amplitude of the periodic condensate assumes nonvanishing value in the close vicinity of the WF fixed point and both the dimensionless and dimensionful amplitudes blow up in the IR. In the $\tilde{g}_2^{\mathrm{WF}} < 0$ case (II_2), the dimensionless amplitude of the periodic condensate vanishes in the close neighborhood of the WF fixed point but becomes nonvanishing and saturates at a constant value in the IR. Hence, the dimensionful amplitude vanishes in the IR; Finally, two nonperturbative phases. The Phase IV has no counterpart for ordinary $O(N)$ models. It is present for $\frac{1}{2} < \tilde{Y} < 1$ and characterized by the blowing up of either the coupling $\tilde{g}_4$ (IV_1) or the wave-function renormalizations (IV_2) at an intermediate scale, which also causes the dimensionless amplitude of the periodic condensate to vanish abruptly. Further possible improvements of this scheme are elaborated in [5]. Among those, the one with the highest impact would be taking the momentum dependence of the induced vertex into account, because the inclusion of that vertex - even without the momentum dependence taken into account - affects the phase structure severely. In this work, I contributed to the derivation of the formulas, written computer programs for the numerical calculations, provided the numerical data and contributed to its analysis and I also made the figures for paper [**D**]

Chapter 6

Összefoglaló

Ez a fejezet magyar nyelven foglalja össze a jelen, angol nyelven íródott doktori disszertáció tartalmát és eredményeit.

Az 1. fejezet bemutatja az olvasónak a funkcionális renormálási csoportot, illetve felidézi az euklideszi, 3-dimenziós $O(N)$ szimmetrikus modellek tulajdonságait.

A második fejezet fő célja a gradienskifejtés alkalmazásának elsajátítása a Wetterich-séma keretein belül. Az ansatz, az általam alkalmazott közelítésekkel a gradienskifejtés negyedik rendjét figyelembe vevő (a továbbiakban NNLO) eredményeket szolgáltat az euklideszi $O(N)$-modellek kritikus exponenseire. Első lépésként az $O(1)$-modellt vizsgáltam. Megbizonyosodtam a polinomiális kifejtés stabilitásáról azáltal, hogy kiszámoltam a ν, η kritikus exponensek és a Wilson-Fisher-fixponthoz tartozó ω vezető skálázási korrekciók értékeinek függését a polinomiális sor csonkolásának a rendjétől. Elvégeztem a $d = 4 - \epsilon$ kifejtést, melynek eredményei remekül egyeznek a szakirodalommal. Ezen belül új eredményként kiszámoltam, hogy a dimenziótlan, magasabb rendű gradienshez tartozó tag csatolása $\bar{Y} \sim \epsilon^3$ módon skálázik. Meghatároztam ν és η dimenziófüggését a $2 < d < 4$ tartományban, ezen függvények trendje kiválóan egyezik a szakirodalommal. Azt találtam, hogy a gradienskifejtés második rendjét figyelembe vevő közelítéshez (NLO) képest az NNLO közelítés kritikus exponenseken vett hatásának a nagysága nem haladja meg az 5%-ot, ám ennek a korrekciónak az értéke változó a szakirodalomban. Arra jutottam, hogy ennek az oka a regulátorfüggvény explicit alakja, illetve a hullámfüggvény renormálás térfüggésének elhanyagolása/figyelembe vétele lehet. Összehasonlítottam a legpontosabb $d = 3$-ban vett eredményeimet a szakirodalommal és a következőket találtam. Az általam számolt korrelációs hossz kritikus exponense $\nu = 0.634$ meglehetősen közel van a funkcionális renormálási csoport módszerével számolt legpontosabb értékhez $0.630^{+0.002}_{-0.005}$. Az anomális dimenzióra az $\eta = 0.059$ értéket kaptam, ez körülbelül 60%-al meghaladja a funkcionális renormálási csoport legpontosabbját $0.034^{+0.005}_{-0.003}$-et. Más szakirodalmi eredményeket megnézve, arra jutottam, hogy ennek a fő oka az lehet, hogy a sémánkban elhanyagoltuk a hullámfüggvény renormálás térfüggését. Érdekesség, hogy számolásaimban a magasabb rendű gradienshez tartozó csatolás értéke a Wilson-Fisher-fixpontban nullává válik $d \approx 8/3$-nál és negatív értékeket vesz fel alatta. Ettől megszűnik

a hatás alulról korlátossága. Érvelésem szerint ezt, az alkalmazott közelítések mellett, egy új, $d \approx 8/3$-nál megjelenő multikritikus pont okozhatja. A szakirodalomban először számoltam ki az euklideszi, 3-dimenziós $O(N)$-modellek ($N > 1$) kritikus exponenseit NNLO szinten. Azt találtam, hogy a radiális és Goldstone módusok hullámfüggvény renormálása máshogyan skálázik a közel kritikus trajektóriákon. A Wilson-Fisher-fixponthoz közel eső trajektóriákon, az arányukhoz, $\hat{z}$-hez tartozó β-függvénynek nullához kellene tartani, de ez az eltérő skálázás miatt nem történik meg. Számolásaim során a $\hat{z}$ arány értékét rögzítettem 1-re, ezzel a minimális szimmetriasértés elvét szem előtt tartva. Ekkor a fixpontegyenletek teljesültek a Wilson-Fisher-fixpontban, kivéve $\beta_{\hat{z}} = 0$ egyenletet, ez utóbbi legkisebb értéke a fixpontban $\beta_{\hat{z}} \approx -\mathcal{O}(\eta)$. Az η értéke az $O(N)$ szimmetrikus modellek esetében kicsi, kevesebb mint 10^{-1}. Az euklideszi $O(N)$-modellek ($100 > N > 1$) esetében az NNLO korrekciók értékére a következőket kaptam. A radiális módus anomális dimenziójára eső relatív NNLO korrekció nem haladja meg az 1%-ot, míg ugyan ez a Goldstone módus esetében nem haladja meg a 0.2%-ot. A korrelációs hossz kritikus exponensére vett NNLO korrekcióra csekély értéket kaptam, amely aszimptotikusan eltűnik nagy N értékekre. Az ezen fejezetben taglalt munkához való hozzájárulásomként részt vettem a folyási egyenletek levezetésében, programkódokat írtam a numerikus számolásokhoz, illetve én biztosítottam a numerikusan számolt adatokat. Ezeken felül részt vettem az adatok elemzésében és értelmezésében, továbbá én készítettem a második fejezet alapjául szolgáló cikkben [**A**] az ábrákat.

A harmadik fejezet motivációja a periodikus kondenzáció vizsgálata a funkcionális renormálási csoport keretein belül. A periodikus alapállapottal rendelkező modellek fontos szerepet játszanak a fizika számos területén. Ismert, hogy olyan modellekben, ahol a kinetikus energiában szereplő különböző gradienstagok előjele váltakozik, felléphet ilyen periodikus kondenzáció. Ebben a fejezetben egy ilyen modellt vizsgálok negatív másodrendű és pozitív negyedrendű gradienstaggal, az előbbi miatt az ilyen modelleket szellemteres modelleknek nevezzük. Az euklideszi 3-dimenziós szellemteres $O(2)$-modell fázisszerkezetét és infravörös viselkedését vizsgálom a lokálispotenciál-közelítés szintjén a Wegner-Houghton-egyenlettel és a faszintű renormálás alkalmazásával. Két szemléletmódot vizsgálok ki: Y eset és $\tilde{Y}$ eset. Az Y esetben a magasabb rendű gradienshez tartozó dimenziós csatolást, Y-t tartom állandó értéken. Az $\tilde{Y}$ esetben az Y-nak megfelelő dimenziótlan csatolást rögzítem állandó értéken. A két szemléletmód által szolgáltatott fázisszerkezet eltérőnek adódott. Az $\tilde{Y}$ eset gazdagabbnak bizonyult az Y esetnél. Ezért még nem tisztázott, hogy a modellnek valójában milyen a fázisszerkezete. A lokálispotenciál közelítés szintjén a két szemléletmód közül nem lehet egyértelműen kiválasztani a 'helyeset', továbbá ezt a kettősséget nem lehet megkerülni a Wegner-Houghton-sémában. A jelen fejezet alapjául szolgáló cikkek [**B**] és [**C**] jól példázzák, hogy ez milyen mélyen befolyásolhatja egy modell fázisszerkezetét. A különbség viszont megszűnik a gradienskifejtés magasabb rendjeiben. A munka első részeként a faszintű renormálás procedúrájátt kivitelező programot implementáltam és teszteltem az euklideszi, 3−dimenziós normál $O(1)$-modellen és az euklideszi, 2−dimenziós sine-Gordon-modellen. A teszt sikeres volt, a szakirodalmi eredményeket nagy pontossággal reprodukáltam. Ezek után az euklideszi, 3−dimenziós szellemteres $O(2)$-modellt kezdtem vizsgálni a két fenti esetben. Az Y esetben két fázist találtam. Egy szimmetrikust, ahol nem jelentkezik a szellemtér kondenzációja, illetve egy olyan fázist, ahol átmeneti skálákon fellép a szellemtér kondenzációja, de kihal az infravörös, alacsonyenergiás skálán. Az utóbbi fázist ezért visszaállt szim-

metriájú fázisnak neveztem el. Megbizonyosodtam róla, hogy a visszaállt szimmetriájú fázisban a korrelációs hossz véges marad a fázishatárhoz tetszőlegesen közel is. Ebből arra következtettem, hogy elsőrendű fázisátmenet van a két fázis között. Az $\tilde{Y}$ esetben három fázist találtam, egy hármasponttal. Az I. fázis a szimmetrikus fázis, amely ugyan olyan tulajdonságokkal bír mint a normál $O(2)$-modell szimmetrikus fázisa, ez minden $\tilde{Y}$ értéknél jelen van. A II. fázis csak akkor fordul elő, ha $0 \leq \tilde{Y} \leq 1$. Ezen fázis tulajdonságai hasonlóak a visszaállt szimmetriájú fáziséhoz. A dimenziós effektív potenciál kvázi univerzális, függ $\tilde{Y}$-tól, de független a csupasz csatolások értékétől. Ennek a fázisnak nincs normál $O(2)$-modellbeli megfelelője. A fázis jelenléte azon alapul, hogy a szellemtér kondenzációja akkor léphet fel, ha $Z < 0$ és $\tilde{Y} > 0$ teljesül. A III. fázis a $1 < \tilde{Y} \leq 2$ tartományban lelhető fel és a normál $O(2)$-modell szimmetria sértő fázisához hasonló tulajdonságokkal bír. A dimenziós effektív potenciál univerzális, mutatja a Maxwell-vágást és a periodikus spinodális instabilitás amplitúdója túléli az infravörös limeszt $k \to 0$. A III-I és a III-II fázishatárok metszete adja a hármas vonalat. Utolsó lépésként megállapítottam a fázisátmenetek fajtáit. A számolásaim azt mutatják, hogy a $II \to I$ és $III \to II$ fázisátmenetek elsőrendűek, míg $III \to I$ folytonos. A személyes hozzájárulásom a munka ezen részéhez a következő volt: programkódot írtam a numerikus számolásokhoz és én szolgáltattam a numerikus adatokat, részt vettem ezeknek az adatoknak a feldolgozásában és értelmezésében, továbbá én készítettem a harmadik fejezet alapjául szolgáló cikkek [**B**, **C**] ábráit.

A negyedik fejezet a [**D**] cikken alapszik. A Wetterich-séma egy módosított változatát, az általunk Fourier-Wetterich-sémának nevezett módszert alkalmaztam. A módszert nem részletezem ebben a fejezetben a hossza miatt, ám kifejlesztésében döntő szerepet játszottam. A részletes elemzés megtalálható az arXiv-on [5]. A módszert térbeli periodicitást mutató kondenzátumok tanulmányozására fejlesztettük ki. Pontosabban egy FRG módszert, amely alkalmazható a gradienskifejtés magasabb rendjeiben. Részletesen tanulmányoztam az euklideszi 3-dimenziós szellemteres $O(1)$-modellt, amelynek a hatásában a kinetikus energia szokásos $\mathcal{O}(\partial^2)$-rendű tagjának 'rossz' az előjele, ugyanakkor tartalmaz egy pozitív definit $\mathcal{O}(\partial^4)$-rendű deriváltas tagot is. A gradienstagok váltakozó előjele ebben a szellemteres modellben is előidézheti a periodikus kondenzátum megjelenését. Azt feltételezzük, hogy a kondenzátum közelíthető egy csonkolt Fourier-sorral amely N_m módust tartalmaz. Ebben a zérómódus a Φ homogén hátteret tartalmazza, az egymódus - amely a fundamentális módus - pedig a P_k skálafüggő hullámszámot és a $\sigma_k(\Phi)$ amplitúdót foglalja magába. A kifejlesztett séma ugyan lehetővé teszi a magasabb harmonikusok figyelembe vételét, ám ezek szerepe nagyban csükken, csökkenő k skálával. Az effektív átlagos hatás (EAA) minden k skálán való minimalizálásával határozzuk meg a periodikus kondenzátum paramétereit. Azt feltételezzük periodikus kondenzátum térbeli periodicitást mutat egy térbeli irányba, amely azt jelenti, hogy a rendszer hengerszimmetriával rendelkezik. Ez azt jelenti, hogy az EAA kinetikus tagjaiban meg kell különböztetni a kondenzátum tengelyével párhuzamos és az arra merőleges irányokat. Ez azt jelenti a gradienskifejtés NLO rendjében, hogy két futó hullámfüggvény renormálás jelenik meg $Z_\parallel$ és $Z_\perp$, melyek az előbb említett párhuzamos és merőleges irányokban különböznek. Annak érdekében, hogy zárttá tegyük a folyási egyenleteket N_m csonkolásra, további úgynevezett indukált potenciálokat és deriváltas tagokat adunk az EAA-ra tett ansatzhoz. Ezen tagokat a periodikus kondenzátum Fourier-módusai gerjesztik. A zérómódus közelítés a hagyományos EAA sémát jelenti, ahol nincs periodikus kondenzátum.

A Fourier-Wetterich séma alkalmazása lehetővé teszi, hogy a periodikus kondenzátum kialakulásának a körülményeit, RG-folyását - különös tekintettel az infravörös viselkedésére - vizsgáljuk. Numerikus számolásokat végeztem abból a célból, hogy a Wilson-Fisher-fixpont és a fázisszerkezet jellemzőit feltárjam az egymódus közelítésben, NLO rendben. A fázisdiagramot a $\tilde{Y}$ csatolás konstans $\tilde{Y} \in (0, 2]$ értékeinél vizsgáltam és a $\tilde{g}_2$ és $\tilde{g}_4$ csatolások által kifeszített síkon ábrázoltam. Az előbbi a dimenziótlan tömegnégyzet, míg az utóbbi a negyedrendű önkölcsönhatás csatolása a hagyományos potenciálnak. Amikor csak lehetséges volt a számolások során, az egyenleteket az U_k hagyományos potenciál $\tilde{\Phi}_* = \sqrt{-6\tilde{g}_2/\tilde{g}_4}$ nem triviális minimuma körül fejtettem ki. Abban esetben, ha az U_k potenciálnak van nem triviális minimuma, ez a kifejtés fizikailag megbízhatóbb eredményeket szolgáltat, mint az eltűnő háttér körüli kifejtés. Továbbá, ebben az esetben, minden járulék, amit a $\mathfrak{V}$ indukált kölcsönhatási vertex okoz figyelembe van véve. Ez azt is jelenti, hogy egyrészt a hullámfüggvény-renormálás sokkal nagyobb szerepet kap, mint a [5]-ban szereplő előzetes vizsgálatomban (ahol végig eltűnő háttér mellett fejtettem ki az egyenleteket), másrészt $\mathfrak{V}$ figyelembe vétele nem elhanyagolható hatással van a fázisszerkezetre. A számítások öt fázis létét fedték fel. Van egy szimmetrikus fázis I_1, amely $\tilde{Y} \in (0, 2]$ esetén van jelen. Itt az infravörös skálázási tartományban kihal a periodikus kondenzátum, a $\tilde{g}_2$ és $\tilde{g}_4$ csatolások pedig faszintű skálázást mutatnak. Két szimmetriasértő fázist II_1 és II_2 is találtam a $0 < \tilde{Y} < \frac{1}{2}$ és $1 < \tilde{Y} < 2$ tartományon. Mind a két fázisban spontán sérül az $O(1)$ szimmetria. A szimmetriasértésre a Wilson-Fisher-fixpont jelenléte utal, ugyanakkor $\tilde{g}_2^{\mathrm{WF}} > 0$ és $\tilde{g}_2^{\mathrm{WF}} < 0$ más kvalitatív viselkedést jelent. Ezt a két esetet olyan trajektóriákon keresztül mutatom be, amelyek nagyon közel kerülnek a Wilson-Fisher-fixponthoz RG-folyásuk során ezen két tartományon. Abban az esetben, amikor $\tilde{g}_2^{\mathrm{WF}} > 0$ (II_1) a periodikus kondenzátum dimenzótlan amplitúdója véges (és nem nulla) marad a Wilson-Fisher-fixpont közvetlen környezetében, de a dimenziós megfelelőjével együtt felrobban az infravörös limeszben. Abban az esetben, amikor $\tilde{g}_2^{\mathrm{WF}} < 0$ (II_2) a periodikus kondenzátum dimenzótlan amplitúdója eltűnik a Wilson-Fisher-fixpont közvetlen környezetében, ugyanakkor alacsonyabb k skálákon újra megjelenik és állandó értékre áll be az infravörös skálázás során, így a dimenziós amplitúdó eltűnik a $k \to 0$ határesetben. A IV fázisnak nincs megfelelője a klasszikus $O(N)$ modellekben. Ez a fázis $\frac{1}{2} < \tilde{Y} < 1$ esetén van jelen és a dimenziótlan $\tilde{g}_4$ csatolás (IV_1) vagy a hullámfüggvény-renormálások (IV_2) felrobbanása jellemzi amely mindkét esetben a periodikus kondenzátum hirtelen eltűnését is okozza. A séma tovább javítható néhány közelítés feloldásával, vagy enyhítésével, ezeket részleteztem [5]-ben. Ezek közül a legnagyobb hatással az indukált vertexek impulzusfüggésének a figyelembevétele van, ugyanis amint láthattuk a indukált vertexek - még impulzusfüggés nélkül is - komolyan befolyásolják a fázisszerkezetet. A jelen fejezetben taglalt munkában a hozzájárultam a formulák levezetéséhez, programkódokat írtam a numerikus számolásokhoz, valamint én végeztem el azokat.

Appendices

Appendix A

Tree-level renormalization and the Wegner-Houghton equation

A.1 Tree-level renormalization of Euclidean one-component scalar field theory with polynomial potential

This appendix is a short summary ho the tree-level renormalization technique (TLR) works in the one-component scalar field theory with ordinary kinetic term. A more in-depth discussion on TLR can be found in Ref. [47]. For scales $k < k_c$, the spinodal instability occurs when the logarithm in the right-hand side of Eq. (3.4) fulfills the inequality

$$Z + \tilde{v}_1(k_c) + \frac{3}{2}\tilde{v}_2(k_c)\tilde{\Phi}^2 \quad \leq \quad 0. \tag{A.1}$$

Since the last term in the left-hand side of the inequality (A.1) is always positive, the critical scale is given via the equation

$$Z + \tilde{v}_1(k_c) \quad = \quad 0. \tag{A.2}$$

One can estimate the interval $\Phi \in [-\Phi_c(k), \Phi_c(k)]$, in which instability shows up for scales $k < k_c$ from inequality (A.1) as

$$\tilde{\Phi}_c(k) = \sqrt{-\frac{2[Z + \tilde{v}_1(k)]}{3\tilde{v}_2(k)}}, \quad \Phi_c(k) = \sqrt{k}\tilde{\Phi}_c(k). \tag{A.3}$$

For scales $k < k_c$ and background fields $\Phi \in [-\Phi_c(k), \Phi_c(k)]$, one turns to the tree-level blocking relation (3.8) and inserting the ansatz (3.9) into it and obtains the following

recursion relation

$$U_{k-\Delta k}(\Phi) \quad = \quad \min_{\{\rho\}}\left(U_k(\Phi) + Zk^2\rho^2 + \sum_{n=1}^{M} \frac{\rho^{2n}}{(n!)^2}\partial_\Phi^{2n} U_k(\Phi)\right) \tag{A.4}$$

for the blocked potential. For given scale k with given couplings $v_n(k)$ and for given homogeneous field $\Phi \in [-\Phi_c(k), \Phi_c(k)]$, one calculates the value $\rho_k(\Phi)$, which minimizes the right-hand side of Eq. (A.4). Then one iterates this process for several values of Φ and determines the corresponding $U_{k-\Delta k}(\Phi)$ potential. Lastly, these discrete values of $U_{k-\Delta k}(\Phi)$ are fitted by the polynomial (3.9) in the interval $\Phi \in [-\Phi_c(k), \Phi_c(k)]$ in order to acquire the new couplings $v_n(k-\Delta k)$. This way, the behavior of the RG trajectories can be investigated in the deep IR region. This numerical procedure converges for sufficiently small values of the ratio $\Delta k/k$. It is shown in Ref. [47], that for $Z = 1$, the amplitude $\rho_k(\Phi)$ of the spinodal instability is a linear function of the homogeneous background Φ, $2\rho_k(\Phi) = -\Phi + \Phi_c(k)$. Outside of the interval $-\Phi_c(k) \le \Phi \le \Phi_c(k)$ the dimensionful blocked potential $U_{k-\Delta k}(\Phi)$ is just $U_{k_c}(\Phi)$. In the IR limit $k \to 0$ and in the interval $-\Phi_c(0) \le \Phi \le \Phi_c(0)$ the tree-level blocking results in the downside facing parabola $\tilde{U}_{k\to 0}(\tilde{\Phi}) = -\frac{1}{2}\tilde{\Phi}^2$ for the dimensionless blocked potential corresponding to $\tilde{v}_1(0) = -1$, $\tilde{v}_n(0) = 0$ for $n \ge 2$. Therefore, the dimensionful potential flattens, taking a constant value in the interval $-\Phi_c(k) \le \Phi \le \Phi_c(k)$ that represents the so-called Maxwell cut.

A.2 Wegner-Houghton equations for ϕ^4 models with $O(2)$ symmetry

The Wegner-Houghton equation for the $O(2)$ symmetric scalar field theory is derived here by using the ansatz for the blocked action (3.21). The blocking relation

$$e^{-S_{k-\Delta k}[\underline{\phi}]} \quad = \quad \int \mathcal{D}\underline{\phi}' e^{-S_k[\underline{\phi}+\underline{\phi}']} \tag{A.5}$$

is the straightforward generalization of the relation (1.6) for the 2-component scalar field. The Wegner-Houghton equation can only be applied in the LPA, the lowest order of the gradient expansion, therefore it is sufficient to Taylor-expand the action $S_k[\underline{\phi}+\underline{\phi}']$ in the exponent of the integrand around the homogeneous field configuration $\underline{\phi}(x) = \underline{\Phi}$,

$$S_k[\underline{\Phi}+\underline{\phi}'] \quad = \quad S_k[\underline{\Phi}] + \frac{1}{2}\int d^dx \underline{\phi}'^T \underline{\underline{S_k^{(2)}}}[\underline{\Phi}]\underline{\phi}' + \mathcal{O}((\phi')^3), \tag{A.6}$$

where the matrix of the second functional derivative of the blocked action is given by

$$\begin{aligned}\underline{\underline{S_k^{(2)}}}[\underline{\Phi}] &= \left.\begin{pmatrix} \frac{\delta^2 S[\underline{\Phi}+\underline{\phi'}]}{\delta\underline{\phi'}_1(x)\delta\underline{\phi'}_1(y)} & \frac{\delta^2 S[\underline{\Phi}+\underline{\phi'}]}{\delta\underline{\phi'}_1(x)\delta\underline{\phi'}_2(y)} \\ \frac{\delta^2 S[\underline{\Phi}+\underline{\phi'}]}{\delta\underline{\phi'}_2(x)\delta\underline{\phi'}_1(y)} & \frac{\delta^2 S[\underline{\Phi}+\underline{\phi'}]}{\delta\underline{\phi'}_2(x)\delta\underline{\phi'}_2(y)} \end{pmatrix}\right|_{\underline{\phi'}=0} \\ &= \begin{pmatrix} S_{11} & S_{12} \\ S_{21} & S_{22} \end{pmatrix}\delta(x-y). \end{aligned} \tag{A.7}$$

By abandoning the terms of order $\mathcal{O}(\phi'^3)$ and higher, we can carry out the Gaussian path integral and reduce Eq. (A.5) to the blocking relation for the blocked action

$$S_{k-\Delta k}[\underline{\Phi}] = S_k[\underline{\Phi}] + \frac{\hbar}{2}\mathrm{tr}\ln\underline{\underline{S_k^{(2)}}}[\underline{\Phi}]. \tag{A.8}$$

In the limit $\Delta k/k \to 0$ the neglected terms, corresponding to higher orders in ϕ' give vanishing contributions. Taking this into account, one arrives to the exact Wegner-Houghton equation

$$\partial_k S_k[\underline{\Phi}] = -\lim_{\Delta k\to 0}\frac{\hbar}{2\Delta k}\mathrm{tr}\ln\underline{\underline{S_k^{(2)}}}[\underline{\Phi}]. \tag{A.9}$$

In order to cast Eq. (A.9) into a more explicit form, one has to evaluate the trace log in its right-hand side. The matrix $\underline{\underline{S_k^{(2)}}}[\underline{\Phi}]$ is diagonal in the momentum space, consisting of 2×2 block matrices in the internal space. For the purpose of the determination of the elements of those block matrices for given momentum p let us impose the LPA ansatz

$$S[\underline{\phi}] = \frac{1}{2}\sum_{a=1}^{2}\int\frac{d^dp}{(2\pi)^d}\phi_{a,-p}\Omega(p^2)\phi_{a,p} + \int d^dx U_k(\underline{\phi}^T\underline{\phi}) \tag{A.10}$$

for the blocked action. The elements of the matrix are

$$\begin{aligned} S_{11} &= \Omega(p^2) + U_k'(r) + \Phi_1^2 U_k''(r), \\ S_{22} &= \Omega(p^2) + (U_k'(r) + \Phi_2^2 U_k''(r)), \\ S_{12} &= \Phi_1\Phi_2 U_k''(r) = S_{21}, \end{aligned} \tag{A.11}$$

with $U_k'(r) = \partial_r U_k(r)$ and $U_k''(r) = \partial_r^2 U_k(r)$ and $r = \frac{1}{2}\underline{\Phi}^T\underline{\Phi} = \frac{1}{2}(\Phi_1^2+\Phi_2^2)$. The eigenvalues s_+ and s_- of the block matrices of $\underline{\underline{S_k^{(2)}}}[\underline{\Phi}]$ can be determined from the vanishing of the determinant of the corresponding eigenvalue equations $s^2 - s(S_{11}+S_{22}) + S_{11}S_{22} - S_{12}^2 = 0$ and are

$$\begin{aligned} s_+(p) &= \Omega(p^2) + U_k'(r) + 2rU_k''(r), \\ s_-(p) &= \Omega(p^2) + U_k'(r). \end{aligned} \tag{A.12}$$

The trace log of the matrix $\underline{\underline{S_k^{(2)}}}[\underline{\Phi}]$ consists of the sum of the logarithms of the eigenvalues of the matrix. The trace operation in the right-hand side of Eq. (A.9) can be performed

by summing over the degrees of freedom of the internal space and integrating over the modes in the infinitesimally thin momentum shell $|p| \in [k - \Delta k, k]$. Thus, the resulting Wegner-Houghton equation is

$$k\partial_k U_k(r) \quad = \quad -\alpha k^d \ln[s_+(k)s_-(k)]. \tag{A.13}$$

From this formula, one obtains the Wegner-Houghton equation (3.22).

Appendix B

Fourier-Wetterich approach

B.1 Regulated full propagator

The full propagator $\mathcal{G}_{p,q}$ in the one-mode approximation is given through the relation

$$\mathcal{G}^{-1}_{p,q} \quad = \quad \Gamma^{(2)}_{k\ p,q}|_{\phi_B} = G^{-1}(p^2_\perp, p^2_\parallel, \Phi)\delta_{p+q,0} + \mathfrak{V}_{\ p,q}, \tag{B.1}$$

where

$$G^{-1}(p^2_\perp, p^2_\parallel, \Phi) \quad = \quad \mathcal{Z}_k(p^2_\perp, p^2_\parallel) + U'_k(\Phi) + \sigma V'''(\Phi) + \sigma^2 U''''(\Phi) \tag{B.2}$$

means the inverse of the reduced propagator and $\mathfrak{V}$ represents the interaction vertex induced by the periodic condensate,

$$\mathfrak{V}_{p,q} \quad = \quad \mathfrak{V}(p^2_\perp, p^2_\parallel, q^2_\perp, q^2_\parallel, \Phi) \sum_{\tau=\pm 1} \delta_{p+q+\tau Pe,0} \tag{B.3}$$

with

$$\mathfrak{V}(p^2_\perp, p^2_\parallel, q^2_\perp, q^2_\parallel, \Phi) = \tag{B.4}$$

$$\frac{1}{2}\left(\frac{1}{2}\mathcal{E}_k(p^2_\perp, p^2_\parallel) + \frac{1}{2}\mathcal{E}_k(q^2_\perp, q^2_\parallel) + V'_k(\Phi) + 2\sigma U'''_k(\Phi) + \frac{3}{2}\sigma^2 V''''_k(\Phi)\right). \tag{B.5}$$

The reduced propagator can be understood as a kind of particle propagator with the momentum-independent self-energy piece $\sigma V'''(\Phi) + \sigma^2 U''''(\Phi)$ acquired by the particle, because of the presence of the periodic condensate with the amplitude $\sigma = \sigma_k(\Phi)$ and the induced potential V_k. The induced vertex Eq. (B.3) is the momentum-dependent piece of the self-energy and comes from elementary processes when the propagating particle pick up the longitudinal momentum shift P, these are the 'Umklapp' processes in solid-state physics terms. It is worth to mention, that the factor Eq. (B.4) of the induced vertex Eq. (B.3) loses its momentum-dependence when Z_2 symmetry of the model is strictly

demanded, i.e., the backreaction of the periodic condensate on the derivative terms is neglected by setting $\mathcal{E}_k = 0$. Furthermore, one has to set $\phi = \Phi_*$ in the flow equations for the wave function renormalizations, which means that when the ordinary potential has its minimum at $\Phi_* = 0$, the factor $\mathfrak{V}$ vanishes and zero contributions come from the 'Umklapp' process.

The full propagator can be obtained in the one-mode approximation - by the inversion of $\mathcal{G}^{-1}_{p,q}$ - in a closed form by resumming the Neumann-series,

$$\mathcal{G}_{p,q} = \mathcal{G}(p_\perp^2, p_\parallel, \Phi)\Big[\delta_{p+q,0} - G(q_\perp^2, q_\parallel^2, \Phi)\mathfrak{V}(p_\perp^2, p_\parallel^2, q_\perp^2, q_\parallel^2, \Phi)\sum_{\tau=\pm}\delta_{p+q+\tau Pe,0}\Big] \quad \text{(B.6)}$$

with

$$\begin{aligned}\mathcal{G}(p_\perp^2, p_\parallel, \Phi) = \\ \Big(1 - G(p_\perp^2, p_\parallel^2, \Phi)\sum_{\tau=\pm} G(p_\perp^2, (p_\parallel + \tau P)^2, \Phi) \times \mathfrak{V}^2(p_\perp^2, p_\parallel^2, p_\perp^2, (p_\parallel + \tau P)^2, \Phi)\Big)^{-1} \\ \times G(p_\perp^2, p_\parallel^2, \Phi). \end{aligned} \quad \text{(B.7)}$$

The full propagator includes a Dyson-type resummation of the contributions of the successive repetition of Umklapp processes

$$G(p_\parallel^2)\Big(\sum_{\tau=\pm}\mathfrak{V}(p_\parallel^2, (p_\parallel + \tau P)^2)G((p_\parallel + \tau P)^2)\mathfrak{V}((p_\parallel + \tau P)^2, (p_\parallel^2)\Big)G(p_\parallel^2). \quad \text{(B.8)}$$

The dependencies on the transverse momenta and the homogeneous background have been suppressed for better transparency. In this elementary amplitude, the first vertex $\mathfrak{V}$ shifts the longitudinal momentum $p_\parallel$ with τP and after an intermediate propagation, the second vertex $\mathfrak{V}$ resets the longitudinal momentum to its original value.

The right-hand side of the WE is expressed in terms of the IR regulated full propagator $\mathcal{G}_{\text{reg } p,q} = (\Gamma_k^{(2)}[\phi_B]) + \mathcal{R})^{-1}_{p,q}$. The comparison with Eq. (B.1) shows that one has to regulate the reduced propagator $G(p_\perp^2, p_\parallel^2, \Phi)$ by adding the corresponding regulator function to its inverse, i.e., perform the replacement of $G(p_\perp^2, p_\parallel^2, \Phi)$ given in Eq. (B.2) via

$$G_{\text{reg}}(p_\perp^2, p_\parallel^2, \Phi) = \Big(\mathcal{Z}(p_\perp^2, p_\parallel^2) + U''(\Phi) + \sigma^2 U''''(\Phi) + \sigma V'''(\Phi) + R_k(p_\perp^2, p_\parallel^2)\Big)^{-1} \quad \text{(B.9)}$$

For the sake of simplicity, below we shall not indicate the regulation of the propagators in the notation explicitly, i.e., $\mathcal{G}$ and G shall stand for the regulated expressions.

As for the regulator function, a generalization of Litim's optimized regulator is employed, which is adapted to the cylindrical symmetry of the periodic condensate. Litim's regulator [58, 92, 93] acts only below the running momentum scale k by compensating the momentum-dependence of the inverse propagator. For ordinary fields (i.e., those with $Z_k > 0$) it has to satisfy the criterion of nonnegativity. For nonshifted longitudinal

momenta, it is chosen as

$$
\begin{aligned}
&R_k(p_\perp^2, p_\parallel^2) = \\
&\left[Z_{\perp\ k}\left(\frac{1}{2}k^2 - p_\perp^2\right) + Z_{\parallel\ k}\left(\frac{1}{2}k^2 - p_\parallel^2\right) + Y_{\perp\ k}\left(\frac{1}{4}k^4 - p_\perp^4\right) + 2Y_{X\ k}\left(\frac{1}{4}k^4 - p_\perp^2 p_\parallel^2\right)\right. \\
&\left. + Y_{\parallel\ k}\left(\frac{1}{4}k^4 - p_\parallel^4\right)\right] \times \Theta(\frac{1}{2}k^2 - p_\perp^2)\Theta(\frac{1}{2}k^2 - p_\parallel^2),
\end{aligned} \tag{B.10}
$$

while for shifted longitudinal momenta $p_\parallel \pm P_k$ it is

$$
\begin{aligned}
&R_k^{[\pm]}\big(p_\perp^2, (p_\parallel \pm P_k)^2\big) = \\
&\left\{ Z_{\perp\ k}\left(\frac{1}{2}k^2 - p_\perp^2\right) + Z_{\parallel\ k}\left[\left(\frac{k}{\sqrt{2}} + P_k\right)^2 - (p_\parallel \pm P_k)^2\right] + Y_{\perp\ k}\left(\frac{1}{4}k^4 - p_\perp^4\right)\right. \\
&\left. + 2Y_{X\ k}\left[\frac{k^2}{2}\left(\frac{k}{\sqrt{2}} + P_k\right)^2 - p_\perp^2(p_\parallel \pm P_k)^2\right] + Y_{\parallel\ k}\left[\left(\frac{k}{\sqrt{2}} + P_k\right)^4 - (p_\parallel \pm P_k)^4\right]\right\} \\
&\times \Theta(\frac{1}{2}k^2 - p_\perp^2)\Theta(\frac{1}{2}k^2 - p_\parallel^2).
\end{aligned} \tag{B.11}
$$

B.2 Traces contributing to the flow equations

The regulated propagators lose their dependencies on the loop-momenta at zero fluctuating momentum $Q_A = 0$. One can exploit this and introduce simplifying notations, such as

$$
\begin{aligned}
G(p_\perp^2, p_\parallel) &\equiv G, \\
G(p_\perp^2, p_\parallel - \tau P) &\equiv G(\tau P), \\
G((p_\perp - Q_\perp)^2, p_\parallel - Q_\parallel) &\equiv G(Q), \\
G((p_\perp - Q_\perp)^2, p_\parallel - Q_\parallel - \tau P) &\equiv G(Q + \tau P).
\end{aligned} \tag{B.12}
$$

This can be generalized trivially for the full propagator $\mathcal{G}$. Applying this notation and the fact, that the scale derivative of the regulator $\dot{R}$ and the induced vertex $\mathfrak{V}$ are independent

of the loop momentum, one can identify five types of integral

$$\zeta_0 = \int_p 1, \tag{B.13}$$

$$\zeta_1 = \int_{Q,Q',p} \mathcal{G}(Q), \tag{B.14}$$

$$\zeta_2 = \int_{Q,Q',p} [\mathcal{G}(Q+P) + \mathcal{G}(Q-P)], \tag{B.15}$$

$$\zeta_3 = \int_{Q,Q',p} \mathcal{G}(Q)[G(Q+P) + G(Q-P)], \tag{B.16}$$

$$\zeta_4 = \int_{Q,Q',p} G(Q)[\mathcal{G}(Q+P) + \mathcal{G}(Q-P)], \tag{B.17}$$

Accommodating these notations, we can finally write the traces in a transparently. The trace

$$T_0 = \frac{1}{8\sqrt{2}\pi^2}\dot{R}\mathcal{G}\zeta_0 \tag{B.18}$$

contributes to the flow equations of the potentials U_k and V_k. The trace $T_{2B} = \sum_{n=0}^{3} T_{2B}^{[n]}$ contributes to the flow equations of $Z_\parallel$ and $Z_\perp$. Its pieces are

$$T_{2B}^{[0]} = b_0^2\dot{R}\mathcal{G}^2\zeta_1 + b_1^2\dot{R}\mathcal{G}^2\zeta_2, \tag{B.19}$$

$$\begin{aligned} T_{2B}^{[1]} &= -b_0 b_1 \mathfrak{V}(\Phi)\dot{R}\mathcal{G}\Big(G\mathcal{G}(P) + G(P)\mathcal{G}\Big)\Big(2\zeta_1 + \zeta_2\Big) \\ &\quad -b_0 b_1 \mathfrak{V}(\Phi)\dot{R}\mathcal{G}^2\Big(\zeta_3 + \zeta_4\Big), \end{aligned} \tag{B.20}$$

$$\begin{aligned} T_{2B}^{[2],0} &= b_0^2\dot{R}\mathfrak{V}^2\mathcal{G}\Big\{GG(P)\mathcal{G}(P)\zeta_2 + G\mathcal{G}(P)\zeta_3 + \mathcal{G}G(P)\zeta_4\Big\} \\ &\quad +b_1^2\dot{R}\mathfrak{V}^2\mathcal{G}\Big\{2G\mathcal{G}G(P)\zeta_2 + 2G[G(P)]^2\zeta_3 + 2G\mathcal{G}(P)\zeta_4\Big\}, \end{aligned} \tag{B.21}$$

$$T_{2B}^{[3],0} = -b_0 b_1 \dot{R}\mathfrak{V}^3\mathcal{G}G\Big\{2\mathcal{G}(P)G(P)\zeta_3 + 2\mathcal{G}(P)G(P)\zeta_4\Big\}. \tag{B.22}$$

The factors b_0 and b_1 are given in Eqs. (4.29) The pure loop integral $\int_p$, when performed yields a k-dependent factor $(8\sqrt{2}\pi^2)^{-1}k^3$.

Bibliography

[**A**] Z. Péli, S. Nagy, K. Sailer, Eur. Phys. J. A **54**, 20 (2018).
[**B**] Z. Péli, S. Nagy, K. Sailer, Phys. Rev. D **94**, 065021 (2016), hep-th/1605.07836.
[**C**] Z. Péli, S. Nagy, K. Sailer, Phys. Rev. D **94**, 065037 (2016), hep-th/1608.02080.
[**D**] Z. Péli, S. Nagy, K. Sailer, Ann. Phys. **Accepted at Int. J. Mod. Phys. A.** (2018).
[5] Z. Péli, S. Nagy, and K. Sailer, arXiv:hep-th/1803.10116
[6] J. Berges, N. Tetradis, and C. Wetterich, Phys. Rept. **363**, 223 (2002), hep-ph/0005122.
[7] L. P. Kadanoff, Physics Vol. **2**, No. 6, pp. 263-272, (1966).
[8] K. G. Wilson, Rev. Mod. Phys. **47**, 773 (1975).
[9] K. G. Wilson, Phys. Rev. B **4**, 3174 (1971).
[10] F. J. Wegner, A. Houghton, Phys. Rev. A **8**, 401 (1973).
[11] J. Polonyi, Cent. Eur. J. Phys. **1**, 1 (2003), hep-th/0110026.
[12] C. Wetterich, Phys. Lett. B **301**, 90 (1993).
[13] B. Delamotte, Lecture Notes in Physics **852**, 49 (2012), cond-mat/0702365
[14] D. F. Litim, Nucl. Phys. B **631**, 128 (2002), hep-th/0203006.
[15] L. Canet, B. Delamotte, D. Mouhanna, and J. Vidal, Phys. Rev. B **68**, 064421 (2003), hep-th/0302227.
[16] L. Canet, B. Delamotte, D. Mouhanna, and J. Vidal, Phys. Rev. D **67**, 065004 (2003), hep-th/0211055.
[17] N. Tetradis, C. Wetterich, Nucl. Phys. B **422**, 541 (1994), hep-ph/9308214.
[18] D. F. Litim, E. Marchais, Phys. Rev. D **95**, 025026 (2017), hep-th/1607.02030
[19] A. Jüttner, D. F. Litim, E. Marchais, Nucl. Phys. B **921**, 769 (2017), hep-th/1701.05168
[20] S. Nagy, K. Sailer, Int. J. of Mod. Phys. A **28**, 1350130 (2013), hep-th/1012.3007.
[21] D. F. Litim, D. Zappalá, Phys. Rev. D **83**, 085009 (2011), hep-th/1009.1948
[22] D. F. Litim, L. Vergara, Phys. Lett. B **581**, 263 (2004), hep-th/0310101.
[23] S. El-Showk, M. F. Paulos, D. Poland, S. Rychkov, D. Simmons-Duffin, A. Vichi, J. Stat. Phys. **157**, 869 (2014), hep-th/1403.4545.
[24] A. Pelissetto, E. Vicari, Phys. Rept. **368**, 549 (2002), cond-mat/0012164.
[25] H. Kleinert, V. Schulte-Frohlinde, *C*ritical Properties of Φ^4-Theories (Singapore, World Scientific, 2001).
[26] H. Ballhausen, J. Berges, C. Wetterich, Phys. Lett. B **582**, 144 (2004), hep-th/0310213.
[27] K. Wilson, J. Kogut, Phys. Rept. **12C**, 75 (1974).
[28] R. Guida, J. Zinn-Justin, J. Phys. A **31**, 8103 (1998), cond-mat/9803240.
[29] S. Yabunaka, B. Delamotte, Phys. Rev. Lett. **119**, 191602 (2017), cond-mat.stat-mech/1707.04383

[30] N. Clisby, B. Dünweg, Phys. Rev. E **94**, 052102 (2016).
[31] F. Kos, D. Poland, D. Simmons-Duffin, A. Vichi, JHEP **08**, 036 (2016), hep-th/1603.04436
[32] M. Campostrini, M. Hasenbusch, A. Pelissetto, E. Vicari, Phys. Rev. B **74**, 144506 (2006), cond-mat/0605083.
[33] M. Campostrini, M. Hasenbusch, A. Pelissetto, E. Vicari, Phys. Rev. B **65**, 144520 (2002), cond-mat/0110336.
[34] M. Hasenbusch, J. Phys. A **34**, 8221 (2001), cond-mat/0010463.
[35] S. A. Antonenko, A. I. Sokolov, Phys. Rev. E **51**, 1894 (1995).
[36] M. Moshe, J. Zinn-Justin, Phys. Rept. **385**, 69 (2003), hep-th/0306133.
[37] F. Benitez, J.-P. Blaizot, H. Chaté, B. Delamotte, R. Mendez-Galain, N. Wschebor, Phys. Rev. E **80**, 030103 (2009),cond-mat.stat-mech/0901.0128
[38] F. Benitez, J.-P. Blaizot, H. Chaté, B. Delamotte, R. Mendez-Galain, N. Wschebor, Phys. Rev. E **85**, 026707 (2012), cond-mat.stat-mech/1110.2665
[39] E. Marchais, P. Mati, D. F. Litim, Phys. Rev. D **95**, 125006 (2017), hep-th/1702.05749
[40] W. A. Bardeen, M. Moshe, Phys. Rev. D **28**, 1372 (1983).
[41] W. A. Bardeen, M. Moshe, M. Bander, Phys. Rev. Lett. **52**, 1188 (1984).
[42] E. D'Hoker, R. Jackiw, Phys. Rev. D **26** (1982), 3517-3542; Phys. Rev. Lett. **50** (1983).
[43] A. H. Chamseddine, M. Reuter, Nucl. Phys. B **317**, 757-771 (1989).
[44] M. Reuter, C. Wetterich, Nucl. Phys. B **506** (1997), 483-520, hep-th/9605039.
[45] S. W. Hawking, Proceedings of the Les Houches Summer School (1983).
[46] B. S. DeWitt, R. Stora, Eds., North Holland, Amsterdam, (1984).
[47] J. Alexandre, V. Branchina, J. Polonyi, Phys. Lett. B **445**, 351 (1999), cond-mat/9803007
[48] J. Alexandre, J. Polonyi, Tree-level Renormalization, hep-th/9906017
[49] S. Nagy, K. Sailer, Int. J. of Mod. Phys. A **28**, 1350130 (2013), hep-th/1012.3007
[50] I. Nándori, J. Polonyi, K. Sailer, Phys. Rev. D **63**, 045022 (2001), hep-th/9910167
[51] S. Nagy, I. Nándori, J. Polonyi, K. Sailer, Phys. Lett. B **647**, 152 (2007), hep-th/0611061
[52] S. Nagy, I. Nándori, J. Polonyi, K. Sailer, Phys.Rev. D**77**, 025026 (2008), hep-th/0611216
[53] J. Fingberg, J. Polonyi, Nucl. Phys. B **486**, 315 (1997), hep-lat/9602003.
[54] V. Branchina, H. Mohrbach, J. Polonyi, Phys. Rev. D **60**, 045006 (1999), hep-th/9612110.
[55] M. D. Fournier, J. Polonyi, Phys. Rev. D **61**, 065008 (2000), hep-lat/9903020.
[56] G. Basar, G. V. Dunne, M. Thies, Phys. Rev. D **79**, 105012 (2009), hep-th/0903.1868.
[57] S.-B. Liao, J. Polonyi, M. Strickland, Nucl. Phys. B **567**, 493 (2000), hep-th/9905206.
[58] D. F. Litim, Phys. Rev. D **64**, 105007 (2001), hep-th/0103195.
[59] J. Zinn-Justin, Phys. Rept. **344**, 159 (2001), hep-th/0002136.
[60] T. R. Morris, Nucl. Phys. B**495**, 477 (1997), hep-th/9612117.
[61] D. F. Litim, Dario Zappalá, Phys. Rev. D**83**, 085009 (2011), hep-th/1009.1948.
[62] C. Bervillier, J. Phys. Cond. Mat. **17**, S1929 (2005), hep-th/0501087.
[63] P. Mati, Phys. Rev. D **91**, 125038 (2015), hep-th/1601.00450.
[64] A.I. Larkin and Yu.N. Ovchinnikov, Zh. Eksp. Teor. Fiz. **47**, 1136 (1964) Sov. Phys. JETP **20**, 762 (1965).
[65] P. Fulde and R. A. Ferrell, Phys. Rev. **135**, 550 (1964).

[66] M. Kutschera, W. Broniowski, and A. Kotlorz, Phys. Lett. B **237**, 159 (1990), Nucl. Phys. A **516**, 566 (1990).
[67] M. Sadzikowski and W. Broniowski, Phys. Lett. B **488**, 63 (2000), hep-ph/0003282.
[68] T. Holstein, H. Primakoff, Phys. Rev.,**58**, 1098 (1940).
[69] S. Nagy, J. Polonyi, and K. Sailer, Phys. Rev. D **70**, 105023 (2004), hep-th/0405156.
[70] A. Pais and G. E. Uhlenbeck, Phys. Rev. **79**, 145 (1950).
[71] K.S. Stelle, Gen. Rel. Grav. **9**, 353 (1978).
[72] K.S. Stelle, Phys. Rev. D **16**, 953 (1977).
[73] A. Salvio and A. Strumia, JHEP **1406**, 080 (2014), hep-ph/1403.4226.
[74] M.B. Einhorn and D.R.T. Jones, JHEP **1503**, 047 (2015), hep-ph/1410.8513.
[75] J.F. Donoghue, *A conformal model of gravitons,* hep-th/1609.03524.
[76] A. Salvio and A. Strumia, Eur. Phys. J. C **76**, 227 (2016), hep-th/1512.01237.
[77] M.M. Ivanov and A.A. Tokareva, JCAP **12**, 018 (2016), hep-th/1610.05330.
[78] F.R. Urban and A.R. Zhitnitsky, Phys. Rev. D **80**, 063001 (2009), astro-ph/0906.2165.
[79] F.R. Urban and A.R. Zhitnitsky, JCAP **0909**, 018 (2009), astro-ph/0906.3546.
[80] F.R. Urban and A.R. Zhitnitsky, Nucl. Phys. B **835**, 135 (2010), astro-ph/0909.2684.
[81] F.R. Urban and A.R. Zhitnitsky, Phys. Rev. D **82**, 123532 (2011), astro-ph/1011.2425.
[82] E. Ebrahimi and A. Sheykhi, Int. J. Mod. Phys. D **20**, 2369 (2011), hep-th/1106.3504.
[83] Chao-Jun Feng, Xin-Zhou Li, and Ping Xi, JHEP **1205**, 046 (2012), astro-ph/1204.4055.
[84] Chao-Jun Feng, Xin-Zhou Li, and Xian-Yong Shen, Phys. Rev. D **87**, 023006 (2013), astro-ph/1202.0058.
[85] M. Khurshudyan and A. Khurshudyan, *Interacting varying Ghost Dark energy models in General Relativity*, pp. 14, gr-gc/1307.7859v2.
[86] R. Caldwell, Phys. Lett. B **545**, 23 (2002).
[87] M.G. Brown, K. Freese, and W.H. Kinney, JCAP **0803**, 002 (2008).
[88] B. Feng, X.L. Wang, and X.M. Zhang, Phys. Lett. B **607**, 35 (2005), astro-ph/0404224.
[89] B. Feng, M. Li, Y.S. Piao, and X. Zhang, Phys. Lett. B **634**, 101 (2006), astro-ph/0407432.
[90] O. Lauscher, M. Reuter, C. Wetterich, Phys. Rev. D **62**, 12 (2000), hep-th/0006099.
[91] A. Bonanno, M. Reuter, Phys. Rev. D **87**, 8 (2013), hep-th/1302.2928.
[92] D. F. Litim, JHEP **0111**, 059 (2001), hep-th/0111159.
[93] D. F. Litim, Nucl.Phys. B **631**, 128 (2002), hep-th/0203006.
[94] P. Fischer and D. F. Litim, Phys.Lett.B **638**, 497 (2006), hep-th/0602203.
[95] N. Christiansen, D. F. Litim, Jan M. Pawlowski, and A. Rodigast, Phys. Lett. B **728**, 114 (2012), hep-th/1209.4038..
[96] C. Bervillier, A. Juttner, and D. F. Litim, Nucl.Phys. B **783,** 213 (2007), hep-th/0701172.
[97] S. Nagy, Phys. Rev. D **86**, 085020 (2012), hep-th/1201.1625.